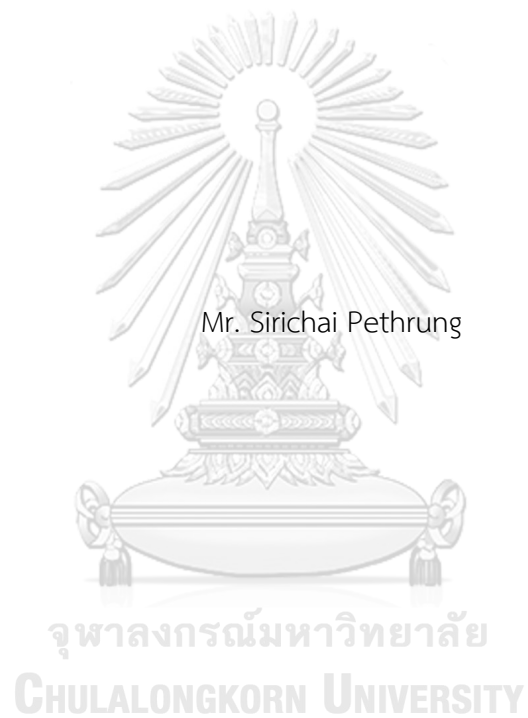


SHEAR WAVE VELOCITY MEASUREMENT OF BANGKOK CLAY UNDER TRIAXIAL
TESTING WITH VARIOUS STRESS PATHS



A Dissertation Submitted in Partial Fulfillment of the Requirements
for the Degree of Doctor of Philosophy in Civil Engineering

Department of Civil Engineering

FACULTY OF ENGINEERING

Chulalongkorn University

Academic Year 2019

Copyright of Chulalongkorn University

การวัดความเร็วคลื่นเฉือนของดินเหนียวกรุงเทพฯภายใต้การทดสอบสามแกนที่ต่างทางเดินความเค้น



วิทยานิพนธ์นี้เป็นส่วนหนึ่งของการศึกษาตามหลักสูตรปริญญาวิศวกรรมศาสตรดุษฎีบัณฑิต
สาขาวิชาวิศวกรรมโยธา ภาควิชาวิศวกรรมโยธา
คณะวิศวกรรมศาสตร์ จุฬาลงกรณ์มหาวิทยาลัย
ปีการศึกษา 2562
ลิขสิทธิ์ของจุฬาลงกรณ์มหาวิทยาลัย

สิริชัย เพชรรุ่ง : การวัดความเร็วคลื่นเฉือนของดินเหนียวกรุงเทพฯภายใต้การทดสอบสามแกนที่ต่างทางเดินความเค้น. (SHEAR WAVE VELOCITY MEASUREMENT OF BANGKOK CLAY UNDER TRIAXIAL TESTING WITH VARIOUS STRESS PATHS)
 อ.ที่ปรึกษาหลัก : ศ.สุพจน์ เตชวรสินสกุล

แนวเส้นทางความเร็วคลื่นเฉือนสำหรับดินเหนียวภายใต้การทดสอบภายใต้การทดสอบแบบสามแกน ในลักษณะหลายรูปแบบการทดสอบขึ้นอยู่กับปัจจัยที่มีความซับซ้อน เช่น ทิศทางของความเค้น อัตราส่วนของช่องว่างระหว่างดิน และสัมประสิทธิ์ของความดันดิน เป็นต้น อย่างไรก็ตาม มีผู้ที่ทำการศึกษาเป็นจำนวนมากได้ทำการแนะนำให้ใช้ค่าหน่วยแรงประสิทธิผลในการเปรียบเทียบเคียงค่าโมดูลัสแรงเฉือนสำหรับดิน ซึ่งมีเหมาะสมเป็นอย่างดี ในการศึกษาครั้งนี้ ผู้วิจัยได้เสนอการจำแนกความเร็วคลื่นเฉือนภายใต้การทดสอบแบบสามแกนในหลายรูปแบบ อาทิเช่น การทดสอบแบบสามแกน-ไม่ระบายน้ำ ในลักษณะอัดแรงและถอนแรงเป็นวงรอบ การทดสอบแบบสามแกน-ระบายน้ำอัดแรงทางเดียว การทดสอบแรงอัดแบบสามแกน-ระบายน้ำ ในลักษณะอัดแรงและถอนแรงเป็นวงรอบ การทดสอบแบบสามแกนควบคุมความเค้น การทดสอบแรงดึงสามแกน-ระบายน้ำ และการทดสอบแรงดึงสามแกน-ไม่ระบายน้ำ ร่วมกับการตรวจวัดด้วยเบนเดอร์อิลิเมนต์ ผลการวิจัยพบว่า ความเค้นในแนวตั้งและความเค้นในแนวนอนสามารถจำแนกแนวเส้นทางความเร็วคลื่นเฉือนในสภาวะระบายน้ำได้ ในขณะที่หน่วยแรงประสิทธิผลในทุกรูปแบบของการทดสอบแบบสามแกนสามารถบ่งชี้ทิศทางการของแนวเส้นทางความเร็วคลื่นเฉือน โดยเฉพาะอย่างยิ่งเมื่อความเร็วคลื่นเฉือนซึ่งถูกทำให้ปรับให้เป็นมาตรฐานด้วยฟังก์ชันช่องว่างระหว่างดิน ผลของการปรับแก้พบว่า ความเร็วคลื่นเฉือนในรูปแบบของการทดสอบที่ระดับความเครียดต่ำถึงความเครียดระดับสูง แนวเส้นทางความเร็วคลื่นเฉือนมีแนวโน้มเป็นเส้นตรง จากข้อมูลการทดลองนี้ แนวโน้มเส้นตรงซึ่งสามารถสร้างจากความสัมพันธ์ระหว่างหน่วยแรงประสิทธิผลกับความเร็วคลื่นเฉือน-โมดูลัสเฉือนได้ถูกนำเสนอเพื่อจำแนกแนวเส้นทางความเร็วคลื่นเฉือน โมดูลัสเฉือนนำไปสู่การเสนอสมการใหม่เพื่อใช้ประเมินความแข็งของดินเหนียวกรุงเทพฯ

สาขาวิชา วิศวกรรมโยธา

ลายมือชื่อนิสิต

ปีการศึกษา 2562

ลายมือชื่อ อ.ที่ปรึกษาหลัก

5771473921 : MAJOR CIVIL ENGINEERING

KEYWORD: SHEAR WAVE VELOCITY, ELASTIC SHEAR MODULUS, BENDER
ELEMENTS, BANGKOK CLAY

Sirichai Pethrung : SHEAR WAVE VELOCITY MEASUREMENT OF BANGKOK
CLAY UNDER TRIAXIAL TESTING WITH VARIOUS STRESS PATHS. Advisor:
Prof. SUPOT TEACHAVORASINSKUN, D.Eng.

Orientation paths of shear wave velocity for clayey soil subjected to multiple triaxial loading tests are dependent on complicated factors direction of stresses, void ratio, coefficient of earth pressure at rest, etc. However, most suggested the mean effective stress could provide a suitable correlation as well. In the present study, an identify the shear wave velocity under triaxial undrained small loading-unloading test , monotonic triaxial drained compression test , triaxial drained loading-unloading test , triaxial stress control test , drained triaxial extension , and undrained triaxial extension measured using the bender elements was presented. These results are indicated that the vertical stress and horizontal stress were found to be more favorable in only drained conditions while the mean effective stress for entire experimental triaxial testing could clarify the orientation paths of shear wave velocity and elastic shear modulus, especially when shear wave velocity were properly normalized by void ratio function. The shear wave velocity during drained and undrained mode shearing at small strain to large strain levels were almost linear. Based on tests data, straight trend lines from the relationship between the mean effective stress with shear wave velocity and elastic shear modulus could be established. The proposed identification of shear wave velocity and elastic shear modulus with various stress paths could well provide a new empirical expression to evaluate the stiffness Banekok clay.

Field of Study: Civil Engineering Student's Signature

Academic Year: 2019 Advisor's Signature

ACKNOWLEDGEMENTS

The author wishes to instant his deep appreciation and sincere gratitude to his advisor, Professor Supot Teachavorasinskun, D.Eng. for the guidance, assistant constant support throughout his study in Chulalongkorn University. Grateful acknowledgements are due to Associate Professor Tirawat Boonyatee, D.Eng, Professor Suched Likitlersuang, D.Phil, and Associate Professor Boonchai Ukritchon, Sc.D. for their invaluable comments and recommendations. Special thanks are also extended to those who have helped directly and indirectly tin the presentation of this thesis.

Sirichai Pethrung



TABLE OF CONTENTS

	Page
.....	iii
ABSTRACT (THAI)	iii
.....	iv
ABSTRACT (ENGLISH)	iv
ACKNOWLEDGEMENTS	v
TABLE OF CONTENTS	vi
LIST OF TABLES	x
LIST OF FIGURES.....	xi
CHAPTER I INTRODUCTION.....	1
1.1 Introduction	1
1.2 Objectives of the Research.....	2
1.3 Scope of the Research.....	2
1.4 Research outcome.....	3
CHAPTER II LITERATURE REVIEW.....	4
2.1. Introduction	4
2.2 The theory approach.....	5
2.2.1 Mohr coulomb theory	5
2.3 Strain Localization in clay	8
2.4 Measurement elastic shear modulus method.....	9
2.4.1 Elastic shear modulus method at large strain levels	10

2.4.2 Elastic shear modulus method at small strain levels and very small strain levels.....	10
2.5 Factors affecting elastic shear modulus.....	11
2.5.1 Void ratio function.....	15
2.6.1 Bender Elements.....	16
2.6.2. Types of Bender Elements.....	17
2.6.3. Determining of effective length.....	18
2.6.4. Determination of Travel Time.....	19
2.6.5. Driving waveform.....	22
2.7 Some of the previous work.....	25
CHAPTER III RESEARCH METHODOLOGY.....	31
3.1. Clayey soil Materials.....	31
3.2 Testing equipment.....	32
3.3. Bender Element Test.....	35
3.3.1 Bender Element setup.....	35
3.3.2 Bender measurement system.....	37
3.4 Testing Procedure.....	39
3.4.1. Preparation of Specimens.....	39
3.4.2 Triaxial preparation setup on triaxial apparatus.....	40
3.4.3 Triaxial de-air and suction Technique.....	40
3.4.4 Saturation of specimens.....	41
3.4.5 Consolidation of Specimens.....	42
3.4.6 Shearing mode of specimens.....	43
3.5 Travel time and shear wave velocities determination.....	50

3.6 Summary of Testing Program	52
4.1 Dependency of stress-strain responses from triaxial tests.....	53
4.2 Shear wave velocity of Bangkok clay from triaxial tests	58
4.2.1 Shear wave velocity under monotonic drain triaxial tests (CID-mono).....	60
4.2.2 Shear wave velocity under load-unloading drained triaxial tests (CID-UL)	62
4.2.2 Shear wave velocity under load-unloading undrained triaxial tests (CID- UL) and triaxial stress control tests (CIDS)	66
4.2.3 Shear wave velocity under drained triaxial extension (CIDE)and undrained triaxial extension (CIDE).....	71
4.3 Dependency of the elastic shear modulus of Bangkok clay from triaxial tests .	76
4.3.1 Dependency of elastic shear modulus subjected to monotonic drained triaxial compression tests (CID-mono).....	76
4.3.2 Dependency of elastic shear modulus subjected to drained triaxial loading-unloading tests (CID-LU)	79
4.3.3 Dependency of elastic shear modulus subjected to undrained triaxial small loading-unloading tests (CIU-LU).....	83
4.3.4 Dependency of elastic shear modulus under stress control tests (CIDS) .	87
4.3.6 An identification elastic shear modulus for Bangkok clay.....	98
4.4 G-bender element and G-secant of Bangkok clay	101
4.4.1 Undrained G-bender element with G-secant	101
4.4.2 Drained G-bender element with G-secant.....	104
4.5 Relationship between G-Bender undrained and G-Bender drained	110
4.6 Application of proposed methodology in calibrating shear modulus undrained condition into the drained condition.....	113
CHAPTER V CONCLUSIONS AND RECOMMENDATIONS	115

5.1 Conclusions..... 115

REFERENCES..... 118

VITA 123



LIST OF TABLES

Table 2.1 The small strain magnitude method	9
Table 2.2 The void ratio function using to interpret of shear modulus proposed by(Mitchell & Soga, 2005)	15
Table 2.3 Summary of waveform, magnitude, and frequency of applied voltage and soil type used by previous researchers (After Leong et al, 2005)	24
Table 3.1 Properties of soft Bangkok clay	31
Table 3.2 Suction step in triaxial apparatus	41



LIST OF FIGURES

Figure 2.1 Normalized stiffness degradation curve (modified after Atkinson and Sallfors (1991) and Mair (1993).	4
Figure 2.2 (a) and (b) Mohr-Coulomb solution to shear orientation (Pongvithayapanu, 2010)	6
Figure 2.3 Shear band thickness dependent post peak behavior ((Thakur, 2007))	8
Figure 2.4 Relationship between the vertical stress and shear wave velocity of angular shape (D16), Low to medium sphericity with angular shape (D40).....	14
Figure 2.5 (a) schematic representation of a bender element, (b) directivity: both P- and S-waves are generated (Lee & Santamarina, 2005).....	16
Figure 2.6 (a) X-poled bender Element Poled for Series Operation (2 wires).....	18
Figure 2.7 Relationship between travel time and specimen length (Viggiani & Atkinson, 1995)	19
Figure 2.8 The travel time of arrived signal (t_0) and the time between first peak to peak (t_{pp}) with Of S-wave and (a) with P-wave (b) (Kumar and Madhusudhan, 2010) .	20
Figure 2.9 The time of arrival using cross-correlation method (t_{cc}) with of S-wave and (a) with P-wave (b) (Kumar and Madhusudhan, 2010).....	22
Figure 2.10 (a) square pulse, (b) sine pulse, and (c) continuous sine wave (Blewett et al, 2000).....	23
Figure 2.11 stress rate effect on stiffness of bangkok soft clay using triaxial cyclic compression tests as mean effective 50 kPa (Teachavorasinsakun and Thongchimp (2002)	25
Figure 2.12 Variation of elastic shear modulus during undrained shearing.....	26
Figure 2.13 Variation of elastic shear modulus during loading and reloading cycle.....	27
Figure 2.14 Relation between G_{max} and void ratio e	28

Figure 2.15 (a) and (b) evaluation of $G_{v/h \max}$ along isotropic stress paths (Dano & Hicher, 2002)	29
Figure 2.16 Effect of stress path and ESP of Bangkok clay	30
Figure 3.1 The schematic detail of the triaxial strain control test with bender element measurement system	33
Figure 3.2 The schematic detail of the triaxial stress control test with the bender element measurement system	33
Figure 3.0.3 The triaxial strain control test with bender element measurement system	34
Figure 3.4 The triaxial stress control test with bender element measurement system	34
Figure 3.5 The bender element detail installed in the top cap and in the pedestal of the triaxial apparatus	35
Figure 3.6 Wiring and coating of bender elements (a) Receiver (b) Transmitter	36
Figure 3.7 The installation detail of parallel- or series-type for bender element	37
Figure 3.8 Bender element tests set-up	38
Figure 3.9 Vertical filter paper (a) Vertical filter paper attached to the specimen (b) size of vertical filter paper proposed by Sivakumar, V. et al. (2010)	39
Figure 3.10 Value control in triaxial apparatus	40
Figure 3.11 Control diagram of undrain triaxial small loading-unloading test	43
Figure 3.12 Control diagram of drained triaxial small loading-unloading test	45
Figure 3.13 An idea diagram for confining stress control	47
Figure 3.14 The diagram of stress control test	48
Figure 3.15 Oscilloscope signals from the transmitter and receiver bender elements	50

Figure 3.16 (a) Bender elements signals from square pulse +10 voltage excitation, (b) bender elements signals from square pulse -10 voltage excitation, and (c) Cross check signal from the bender elements.....	51
Figure 3.17 Schematic diagram of testing procedure.....	52
Figure 4.1 The stress-strain relation of undrain loading-unloading condition tests with 150, 225, and 300 kPa isotropic confining pressure	54
Figure 4.2 The stress-strain relation of drain loading condition tests with 150, 225, and 300 kPa isotropic confining pressure.....	55
Figure 4.3 The stress-strain relation of drain load-unloading condition tests with 150, 225, and 300 kPa stress-controlled.....	55
Figure 4.4 The stress-strain relation of drain loading condition tests with 150, 225, and 300 kPa stress-controlled.....	56
Figure 4.5 The stress-strain relation of undrain triaxial extension tests with 50, 150, and 225 kPa.....	56
Figure 4.6 The stress-strain relation of drain triaxial extension tests with 50, 150, and 225 kPa	57
Figure 4.7 The relationship between mean effective stress and shear wave velocity of CID-mono	61
Figure 4.8 The relationship between vertical stress and $V_s/F(e)$ of clay for CID-mono.....	61
Figure 4.9 The relationship between mean effective stress and shear wave velocity of CID-LU	64
Figure 4.10 The relationship between vertical stress and $V_s/F(e)$ of clay for CID-UL ...	64
Figure 4.11 The relationship between mean effective stresses and shear wave velocity of CID-mono and CID-LU.....	65

Figure 4.12 (a) shows the relationship between vertical stress, σ_v' , and V_s normalized of CIU-LU and (b) shows the relationship between horizontal stress, σ_h' , and V_s normalized.....	68
Figure 4.13 (a) shows the relationship between vertical stress, σ_v' , and V_s normalized of CIU-LU and (b) shows the relationship between horizontal stress, σ_h' , and V_s normalized.....	69
Figure 4.14 The relationship between mean effective stress and shear wave velocity of CIU-LU.....	70
Figure 4.15 The relationship between mean effective stress and shear wave velocity of CIDS	70
Figure 4.16 (a) shows relationship between vertical stress, σ_v' , and V_s normalized of CIUE and (b) shows relationship between horizontal stress, σ_h' , and V_s normalized.....	72
Figure 4.17 The relationship between mean effective stress and shear wave velocity of drained triaxial extension (CIDE) and undrained triaxial extension (CIUE).....	73
Figure 4.18 Shows the paths of shear wave velocity various mean effective stress of clay soil under CID-mono, CID-LU, CIU-LU, CIUE, CIDE and CIDS triaxial testing.....	75
Figure 4.19 The results of CID-mono test on clay soil specimens: (a) and (b) vertical effective stress and elastic shear modulus normalized.....	78
Figure 4.20 The results of CID-LU test on clay soil specimens: (a) and (b) vertical effective stress and elastic shear modulus normalized.....	80
Figure 4.21 The results of CID-mono and CID-LU test on clay soil specimens: mean effective stress and elastic shear modulus	82
Figure 4.22 The results of CID-mono and CID-LU test on clay soil specimens: mean effective stress and elastic shear modulus normalized.....	82
Figure 4.23 The results of CID-LU test on clay soil specimens: (a) vertical effective stress with elastic shear modulus normalized, and (b) horizontal effective stress with elastic shear modulus normalized.	85

Figure 4.24 The results of CIU-LU test on clay soil specimens: mean effective stress and elastic shear modulus	86
Figure 4.25 The results of CIU-LU test on clay soil specimens: mean effective stress and elastic shear modulus normalized.....	86
Figure 4.26 The results of CIDS test on clay soil specimens: (a) relationship vertical stress with elastic shear modulus normalized and (b) horizontal stress with elastic shear modulus normalized	89
Figure 4.27 The results of CIDS test on clay soil specimens: mean effective stress and elastic shear modulus.....	90
Figure 4.28 The results of CIDS test on clay soil specimens: mean effective stress and elastic shear modulus normalized	90
Figure 4.29 The results of CIUE test on clay soil specimens: (a) relationship vertical stress with elastic shear modulus normalized and (b) horizontal stress with elastic shear modulus normalized	94
Figure 4.30 The results of CIDE test on clay soil specimens: (a) relationship vertical stress with elastic shear modulus normalized and (b) horizontal stress with elastic shear modulus normalized	95
Figure 4.31 The results of CIUE and CIDE on clay soil specimens: mean effective stress and elastic shear modulus.....	96
Figure 4.32 The results of CIUE and CIDE on clay soil specimens: mean effective stress and elastic shear modulus normalized	97
Figure 4.33 Relationship between mean effective stress and elastic shear modulus of entire experiments.....	99
Figure 4.34 Relationship between mean effective stress and elastic shear modulus normalized of entire experiments	100
Figure 4.35 Relationship between G_{BE} and G_{sec} various shear strain under undrained tests.....	102

Figure 4.36 Relationship between η and various shear strain of undrained tests ...	103
Figure 4.37 Comparison between G_{BE} , G_{sec} and G_{cal} various shear strain of undrained tests.....	103
Figure 4.38 Comparison between G_{BE} and G_{sec} various shear strain of drained tests	106
Figure 4.39 Relationship between η and various shear strain of drained monotonic tests.....	106
Figure 4.40 Comparison between G_{BE} , G_{sec} and G_{cal} various shear strain of drained tests.....	107
Figure 4.41 Comparison between G_{BE} and G_{sec} various shear strain of drained loading- Unloading tests.....	108
Figure 4.42 Relationship between η and various shear strain of loading- Unloading tests.....	108
Figure 4.43 Comparison between G_{BE} , G_{sec} and G_{cal} various shear strain of drained loading- Unloading tests.	109
Figure 4.44 The relationship of ratio between G_{BE} drained and G_{BE} undrained various shear strain.....	111
Figure 4.45 Comparison between G_{max-BE} and $G_{max-cal}$ various shear strain of drained tests.....	112

CHAPTER I

INTRODUCTION

1.1 Introduction

Shear wave velocity is one of the significant tools in estimating the stiffness of clay. It is especially useful for geomechanics designs or to assess the path of an elastic shear modulus due to vibration events, which can come from various sources, such as earthquakes, moving vehicles, and vibrations from wind turbines. A number of studies related to the correlation of soils using bender element techniques together with triaxial tests have been reported in the past (Hardin & Richart Jr, 1963), (Patel & Singh, 2009), (Escribano & Nash, 2015). It is conventionally and practically adopted to determine the shear wave velocity of clay.

In general, the shear wave velocity of soil is classified into two categories: induced undrained and induced drained, following the concepts adopted by many researchers, e.g. (Bartake, Patel, & Singh, 2008), and (Oh, Bang, Cho, & Park, 2017). The estimation of undrained shear strength is determined by using shear wave velocity. The undrained shear strength, void ratio, and shear wave velocity are entirely related. As presented in previous literature, researchers developed an empirical expression model under a variation of mean effective stress, p' , and void ratio, which was proposed by (Hardin & Richart Jr, 1963), (T. Iwasaki & Tatsuoka, 1977), (Senetakis, Anastasiadis, & Pitilakis, 2012). Very recently, (Escribano & Nash, 2015) proposed that both stresses in the particle motion directions and wave propagation are the primary components affecting the shear wave velocity, as the elastic shear modulus function as stress acts orthogonally to the wave motion plane. Notable previous research has studied the characteristics of shear wave velocity of sand soil behaviors under drained triaxial compression, i.e., (Teachavorasinskun & Pongvithayapanu, 2016). This work focused only on the shear wave velocity empirical expression correlation function for sand. However, while an empirical expression function is also appropriate for determined shear wave velocity paths, it is not adequate for clayed soil.

The main purpose of this research is to demonstrate the results of various stress paths of the shear wave velocity in clayed soil subjected to multiple triaxial loading tests in both drained and undrained isotropic conditions for shearing specimens. An identification of the shear wave velocity paths under triaxial undrained compression test with small loading-unloading, CIU-LU, triaxial drained monotonic compression test, CID-mono, triaxial drained compression test with small loading-unloading, CID-LU, triaxial stress control test, CIDS, triaxial undrained extension test, CIUE, and triaxial drained extension test, CIDE, measured using the bender elements was carried out. An empirical model to correlate and identify the shear wave velocity paths of different stress paths is proposed for clayed soil.

1.2 Objectives of the Research

The main topics of this study comprised of three main topics follow;

- (a) To study the characteristic of shear wave velocity and shear modulus of Bangkok clay under drained triaxial testing and undrained triaxial testing.
- (b) To adopt a methodology in converting shear modulus from the degradation curve.
- (c) To propose a methodology in calibrating shear modulus undrained condition into the drained condition

1.3 Scope of the Research

In this study, this research will be clarified all literature studied. The main topics of this study comprised of five topics follow;

- a) The triaxial testing with strain control test.
- b) The triaxial testing with stress control test.
- c) The triaxial testing with bender element technique.
- d) The factors effecting shear wave velocity in clayey soil.
- e) An identify the factors affecting shear wave velocity in clayey soil.

1.4 Research outcome

- 1) The paths of shear wave velocity of Bangkok clay with various stress paths from multiple triaxial loading tests.
- 2) An empirical equation to correlate shear wave velocity and shear modulus for Bangkok clay under various mode shearing form triaxial loading tests.
- 3) The method to calibrate shear modulus undrained condition into drained condition



CHAPTER II

LITERATURE REVIEW

2.1. Introduction

Current knowledge of shear wave velocity, V_s has importance for determining the stiffness of soil. The elastic shear modulus, G_{max} parameter of soil at a small strain level can be computed by shear wave velocity. These parameters have been widely used to apply the problem in geotechnical engineering. Many researchers have performed researches to study the nonlinear behavior of soil stiffness. Consequently, the way to determine the stiffness of soil is important to predict the ground movement. The normalized elastic shear modulus at any strain level is shown in

Figure 2.1

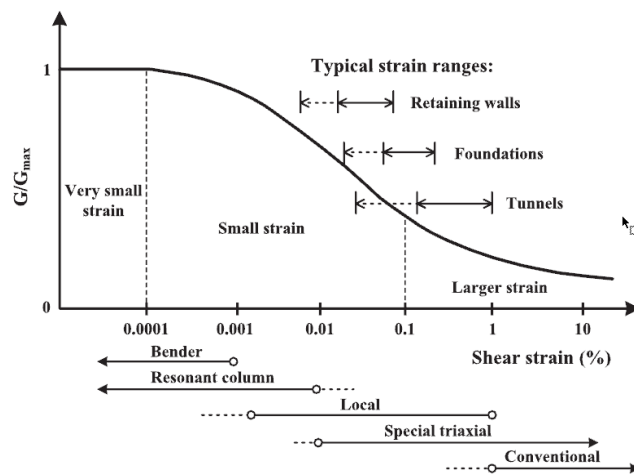


Figure 2.1 Normalized stiffness degradation curve (modified after Atkinson and Sallfors (1991) and Mair (1993)).

At very small shear strain ($\gamma < 0.001\%$), the elastic shear modulus, G_{max} can be determined by using wave propagation. Therefore, many researchers selected the bender element or resonant column to determine soil stiffness at a small strain level.

This bender element technique was first conducted to soil testing by (Shirley & Hampton, 1978), and developed by (Dyvik & Madshus, 1985).

The previously mentioned bender element transducers can be used to transmit and receive shear waves only. However, a new transducer called bender-extender element can transmit and receive both compression wave (P - wave) and shear wave (S - wave). Consequently, a pair of elements can be used easily to identify the Young's modulus E_{max} , and the shear modulus G_{max} in the small strain domain simultaneously (Lings & Greening, 2001), (Dano, Hareb, & Hicher, 2003).

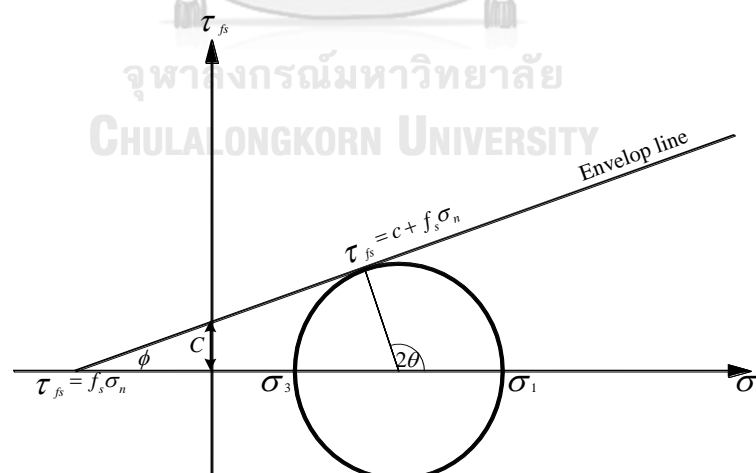
2.2 The theory approach

2.2.1 Mohr coulomb theory

Coulomb criterion can be represented as more circle as shown in Figure 2.2a which is shown the relationship between shear stress, normal stress, and frictional coefficient as express in equation (2.1) with basic law and equation 2.2 respectively, modify low by including roch's cohesion.

$$\tau_{fs} = f_s \sigma_n \quad (2.1)$$

$$\tau_{fs} = c + f_s \sigma_n \quad (2.2)$$



(a)

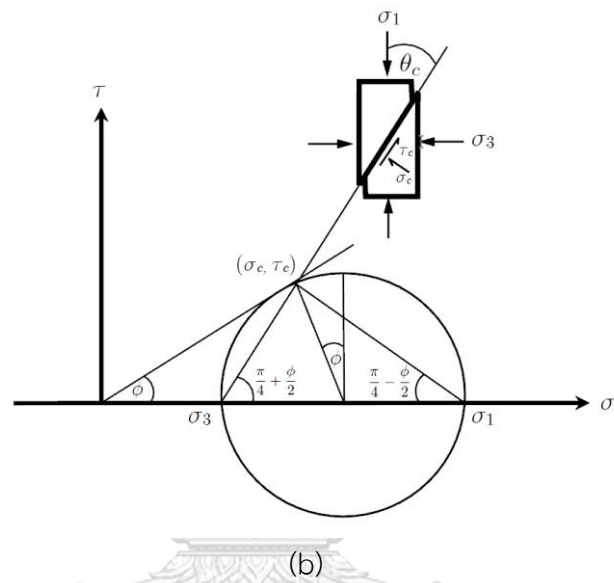


Figure 2.2 (a) and (b) Mohr-Coulomb solution to shear orientation

จุฬาลงกรณ์มหาวิทยาลัย (Pongvithayapanu, 2010)

CHULALONGKORN UNIVERSITY

Mohr coulomb criterion diagram in Figure 2.2b is interesting in the failure of enveloping cohesion and internal angle of friction. For the stage of the stress of the material, plotting with a diameter of $(\sigma_1 - \sigma_3)$ failure will occur when the circle intersects with the failure envelope. The angle of θ is the angle between a plan and principal stress as shown in equation 2.3

$$\sin(2\theta) = \frac{2\sigma_s}{(\sigma_1 - \sigma_3)} \quad (2.3)$$

The Mohr-Coulomb theory states that the shear band plane of strain localization will parallel to the surface which passes through the failure stresses (σ_c, τ_c) on the Mohr - Coulomb failure envelope. The calculation of this classical theory can be displayed as in equation 2.4

$$\theta_c = \frac{\pi}{4} - \frac{\phi}{2} \quad (2.3)$$

Where θ_c is the angle between the major principal stress direction and shear band is the value of the mobilized friction angle at failure. By definition, the mobilized friction angle, ϕ , is calculated from the major and minor principle stress, σ_1 and σ_3

2.3 Strain Localization in clay

Strain localization failure in clay is one of the significant matters in geotechnical engineering problems. When loading increased. It is nearly to fail, the strain localization or zone of shear bands occur. The stress discontinuity within soil mass will present and result in the change in the physical properties of soil such as the low density of soil particles and relatively high strain within the zone of shear band. Therefore, the strain of soft clay exhibits a decrease in shear resistance with the increasing strain after the peak shear stress. Since the materials are usually depicted two possible failure modes. One is the diffuse failure where strain softening occurs in each material point within the domain and other is the localized failure where strain-softening only occurs within a shear band shown in Figure 2.3

Figure 2.3 shows that an example of a sample constrained with plane strain conditions may exhibit a different mode of failures. The post-peak behavior of the force-displacement plot depends on the thickness of the shear band (t_{sb}). Thinner shear bands exhibit higher softening modulus in the post-peak regime

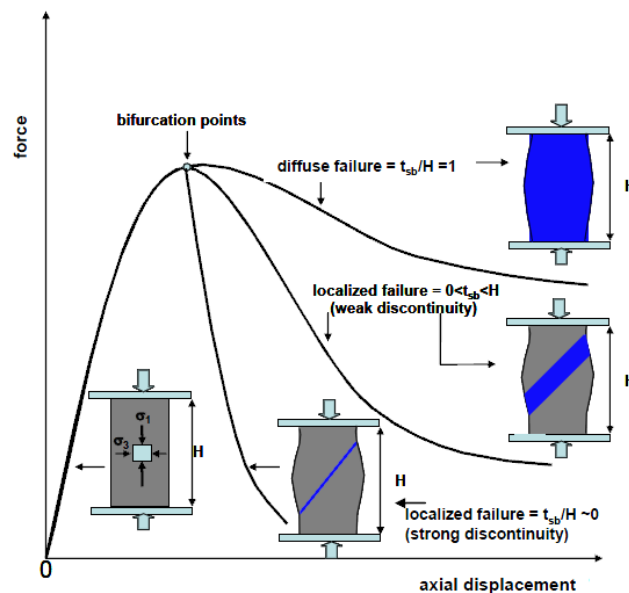


Figure 2.3 Shear band thickness dependent post peak behavior ((Thakur, 2007))

2.4 Measurement elastic shear modulus method

The measurement method of elastic shear modulus is dependent on a period of stress-strain level. Usually, the medium-large strain stiffness is obtained by using secant modulus which is calculated by the stress-strain curve. At the small strain level, many researchers who suggested resonant column test, resonant column test, and ultrasonic shear wave velocity measurements to evaluate the stiffness of soil. For very small strain, the bender element technics, relay wave velocity survey, seismic refraction survey, cross-hole test, and seismic Cones were used to determine the elastic shear modulus of soil.

Table 2.1 The small strain magnitude method

Magnitude of strain		10^{-6}	10^{-5}	10^{-4}	10^{-3}	10^{-2}	10^{-1}
Phenomena		Wave Propagation, Vibration		Cracks, differential settlement		Slide, Compaction, liquefaction	
Mechanical characteristics		Elastic		Elastic - plastic		Failure	
Effect of load repetition		↔					
Effect of rate of loading		↔					
Constants		Shear modulus, Poisson's ratio damping				Angle of internal Friction, cohesion	
In-situ measurement	Seismic wave method	↔					
	In-situ Vibration test	↔					
	Repeated Loading test	↔					
Laboratory Measurement	Wave Propagation, Precise test	↔					
	Resonant Column Precise test	↔					
	Repeated Loading test	↔					

2.4.1 Elastic shear modulus method at large strain levels

Estimation of the shear modulus at large strain levels can be determined by the experimental laboratory test i.e. the triaxial test and the unconfined compression test. The result which is obtained the stress-strain curve can be used to compute the modulus. The methods of measuring the modulus depend on the strain level at which the modulus is required for solving the geotechnical problem.

Baldy, High, and Thomas (1988) as cited in Sahabdeen M. M (1995) they reported that the measurements of the stiffness in the conventional test are generally unreliable at the strains less than 1% in unconsolidated samples and slightly smaller strains in isotopically consolidated samples. Consequently, the shear modulus from the triaxial test and the unconfined compression test is recommended to determine the modulus at large strain levels.

2.4.2 Elastic shear modulus method at small strain levels and very small strain levels

The method for determining the elastic shear modulus at small strain levels can be by using the wave propagation techniques and considering the resonant frequency, the amplitudes, the calibration constants, the specimen dimension, and the soil mass. The experiment in laboratory i.e. Hardin Resonant Column test, Drnevich Resonant Column test, and Ultra Sonic Shear-wave Velocity Measurement test were conducted to evaluate elastic shear modulus at the small strain level. During the late 1980 and early 1990, dynamic soil stiffness was being measured in the laboratory using a small strain resonant column apparatus. The result from the investigators of dynamic soil stiffness of strain level ($0.001 \% < \gamma < 0.1\%$) can be back-analyzed from dynamic modulus to static modulus. They realized that the differences in modulus measured in the past between static tests (conventional triaxial) and dynamic tests (resonant column) were related to the strain level. The wave propagation method has widely determined the elastic shear modulus. Both Body Wave (*P-Wave*) and Shear Wave (*S-Wave*) were perpendicular.

2.5 Factors affecting elastic shear modulus

Several researchers carried out on clayed soils through resonant column tests or improved triaxial tests in an early study to evaluate elastic shear modulus. The factors affecting elastic shear moduli such as mean effective principal stress (p') and void ratio(e) of the soil, and over consolidation ratio, OCR, for cohesive soil were related. Consequently, the elastic shear modulus can be expressed by using a function, G ;

$$G = f(\sigma'_0, e, H, S, C, t, \tau_0, f, \theta, T) \quad (2.4)$$

Where σ'_0 = Effective octahedral normal stress
 H = Stress history and Vibration history
 e = Void ratio
 S = Degree situation of soil
 C = Characteristics of soil, Grain Size, Mineralogy
 t = Secondary time effective
 τ_0 = Octahedral shear stress
 f = Frequency of vibration
 θ = Soil structure
 T = Temperature

Many previous researchers studied factors affecting elastic shear modulus on clayey soils through resonant column test or triaxial test ((Hardin & Richart Jr, 1963), (Hardin & Black, 1968), (T. T. Iwasaki, F. and Takagi, Y, 1978). were referred from the paper by (Chuan Gu 2012). They reported that the small strain shear modulus G_{\max} ($\gamma < 10^{-5}$) of soil was implicated with the mean effective confining pressure (σ'_m) and void ratio (e) of the soil, and even over consolidation ratio, and OCR, for cohesive soil. The small strain shear modulus G_{\max} ($\gamma < 10^{-5}$) its usually determined by Hardin and Richart equation which is shown in Equation 2.5. The previous experimental data also showed that the stiffness of clay at very small strain static conditions and dynamic tests is independent on of the rate of loading direction.

$$G_{\max} = AF(e)\sigma'_m{}^n OCR^k \quad (2.5)$$

Where, A = the empirical constant reflecting soil fabric formed through various stress or strain histories.

n = the empirical exponent related to the mean effective principle stress σ'_m

σ'_m = the mean effective confining pressure $\sigma'_m = (\sigma'_v + 2\sigma'_h) / 3$ where σ'_v is vertical effective consolidation stress, and σ'_h is horizontal effective consolidation stress.

$F(e)$ = the void ratio function

k = the empirical exponent related to OCR

In the case of non-cohesive, soils, (Ishihara, 1996). the studied factors on affecting elastic shear modulus by using the sand with resonant column test. It results show that the factors affecting elastic shear modulus related i.e. mean effective principal stress (p') and void ratio (e) of the void ratio, confining effective stress can be affected elastic shear modulus. The equation is as follow;

$$G_0 = AF(e) \left(\frac{\sigma'_m}{p'_a} \right)^n \quad (2.6)$$

Where,

σ'_m = the mean effective confining pressure.

p_a = reference stress, usually taken as the atmospheric pressure.

$F(e)$ = the void ratio function

A = the empirical constant reflecting soil fabric formed through various stress or strain histories.

n = the empirical exponent related to the mean effective principle stress

Moreover, (Roesler, 1979) and (Escribano & Nash, 2015) reposted that the stress in wave and particle direction is dependent on the void ratio function, bulk modulus vertical stress, and effective confining stress. Equation of elastic shear modulus taking can be determined by;

$$G = K \cdot f(e) \cdot \sigma_1^{,2m} \cdot \sigma_3^{,2n} \quad (2.7)$$

Where,

K = Bulk modulus

$f(e)$ = the void ratio function

σ_1 = vertical stress

σ_3 = horizontal stress

m, n = material constant

Techaworasinsakul and Pongvithayapanu (2016) studied the shear wave velocity in sand using the triaxial test with piezoelectric transducers. This experimental study about the shear wave velocity along the path of the triaxial compression test. Three types of sand i.e. Low to medium sphericity with angular shape (D16), Low to medium sphericity with angular shape (D40), and High sphericity with well-rounded shape (Silica) were used to study. This experimental study shows that the shear wave velocity during this stage was almost constant with respect to the mean effective stress and vertical stress was found to be more favorable at this

stage. Since confining stress was kept constant as shown in Figure 2.4. Therefore wave velocity, V_s , is governed by the states of effective stresses, which could be the mean effective stress (Teachavorasinskun & Amornwithayalax, 2002). and (Flores-Guzmán, Ovando-Shelley, & Valle-Molina, 2014) or those stress components in the wave motion plane (Roesler, 1979), (Yu & Richart Jr, 1984) and (Ku & Mayne, 2015).

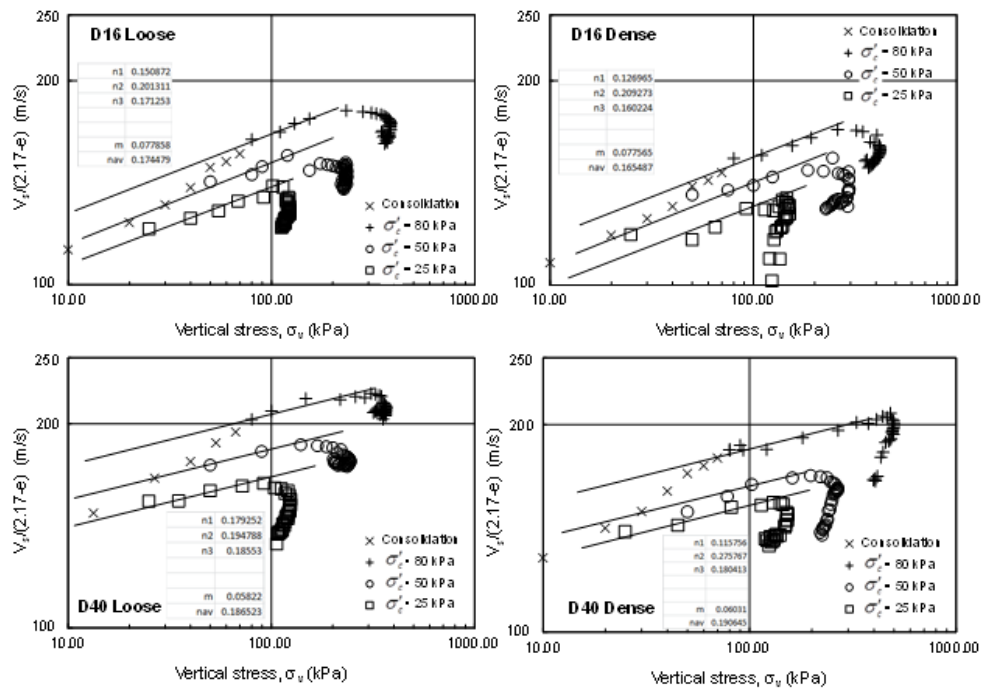


Figure 2.4 Relationship between the vertical stress and shear wave velocity of angular shape (D16), Low to medium sphericity with angular shape (D40) (Techaworasinsakul, 2014)

When $G = \rho v^2$ (2.8)

$$V_s = K \cdot \frac{(2.17 - e)}{\sqrt{G_s \rho_w}} \cdot \sigma_1^m \cdot \sigma_3^n \quad (2.9)$$

$$f(e) = \frac{(2.17 - e)^2}{(1 + e)} \quad (2.10)$$

$$\rho = \rho_d = \frac{G_s \rho_w}{(1 + e)} \quad (2.11)$$

$$\log\left(\frac{V_s}{2.17 - e}\right) = \log\left(\frac{K}{\sqrt{G_s \rho_w}}\right) + n \log(\sigma'_3) + m \log(\sigma'_1) \quad (2.12)$$

2.5.1 Void ratio function

The void ratio function, $F(e)$ is one important determiner to interpret soil stiffness at the small as well as large strain. Many years ago, the Researcher developed the empirical void ratio function, $F(e)$. (Bui, Clayton, & Priest, 2010) recommended the void ratio function to interpret of shear wave velocity and shear modulus as shown in table 2.2

Table 2.2 The void ratio function using to interpret of shear modulus proposed by (Mitchell & Soga, 2005)

References	Soils	Void ratio	F(e)	n
Hardin & Richart (1963)	Ottawa sand	0.37-0.78	$(2.174 - e)(1 + e)^{-2}$	0.5
Hardin & Black (1966)	Crushed quartz	0.63-1.26	$(2.973 - e)(1 + e)^{-2}$	0.5
Hardin & Black (1968)	NC Kaolinite	0.76-0.9	$(2.973 - e)(1 + e)^{-2}$	0.5
Hardin & Black (1969)	A few soils	0.59-1.98	$(2.973 - e)(1 + e)^{-2}$	0.5
Hardin & Drnevich (1972)	A few soils	0.57-0.98	$(2.973 - e)(1 + e)^{-2}$	0.5
Marcuson & Wahls (1972)	Kaolinite	1.1-1.31	$(2.973 - e)(1 + e)^{-2}$	0.5
	Bentonite	1.61-2.48	$(4.4 - e)*(1 + e)^{-2}$	0.5
Kokusho et al. (1982)	NC clay	1.73-3.86	$(7.32 - e)*(1 + e)^{-2}$	0.6
Athanasopoulos & Richart (1983)	Powdered Kaolinite clay	0.9-1.2	$(0.3 + 0.7e^2)^{-1.361}$	0.49
Lo Presti et al. (1993)	Ticino sand	0.61-0.80	$(2.27 - e)(1 + e)^{-2}$	0.43
Jamiolkowski et al. (1995)	Panigaglia Clay	1.4-1.8	$e^{-1.3}$	0.5
	Pisa Clay	0.8-1.8	$e^{-1.43}$	0.44
	Garigliano clay	0.9-1.2	$e^{-1.11}$	0.58
	Fucino clay	1.6-3.0	$e^{-1.52}$	0.4
	Montalvo di Castro clay	0.6-0.8	$e^{-1.33}$	0.4
	Avezzano clay	1.0-1.8	$e^{-1.27}$	0.46
Shibuya & Tanaka (1996)	Insitu slight OC clay	1.3-4.5	$e^{-1.5}$	0.5
Shibuya et al. (1997)	Natural sediment	1.0-6.0	$(1 + e)^{-2.4}$	0.5
Lo Presti et al. (1997)	Toyoura sand	0.81-0.98	$e^{-1.3}$	0.45
	Quiou sand	0.84-1.18	$e^{-1.3}$	0.62
Wichtmann & Triantafyllidis (2004)	Fine, medium sands	0.57-0.76	$(1.46 - e)(1 + e)^{-2}$	0.42

2.6. Bender Elements

2.6.1 Bender Elements

The bender element method was developed by Shirley & Hampton (1978) in a soil laboratory. Then, (Dyvik & Madshus, 1985) successfully developed bender elements for testing saturated soils. The bender element is a thin shim which has two sheets of a piezoelectric ceramic material such as barium titanate, or lead titanate sandwiching as center shim of brass, stainless steel, or other ferrous nickel alloys to increase strain to bender element (Leong, Yeo, & Rahardjo, 2005). Therefore, the bender element now is well known as a transducer to measure shear wave velocity for estimating the shear modulus. The two piezoelectric sheets which are made of ceramic material must be installed into two types of connection which are excited voltage series and parallel. The parallel type was recommended to acts as source and series type as receiver. The transmitter bender element is now acted as the function generator. It can generate the shear wave (*S*-wave) and primary wave (*P*-wave) as show in Figure 2.5.

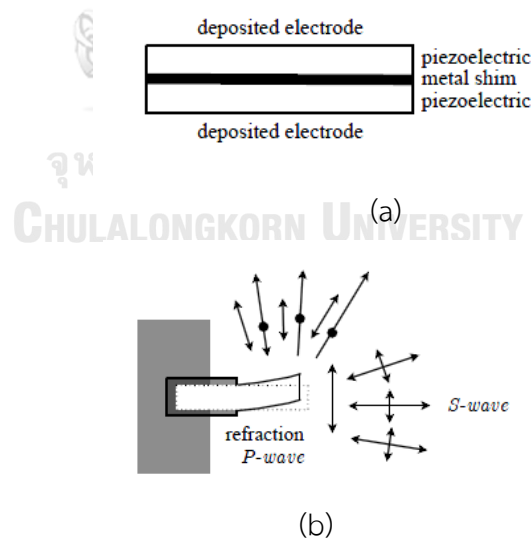


Figure 2.5 (a) schematic representation of a bender element, (b) directivity: both *P*- and *S*-waves are generated (Lee & Santamarina, 2005)

After applying voltage, (Dyvik & Madshus, 1985), (Brignoli, Gotti, & Stokoe, 1996), (Viggiani & Atkinson, 1995), (Jovicic, 1996) have computed the shear wave velocity of the specimen from bender element which act as a transmitter and receiver measuring the travel time of the wave, the wave velocity V_s is determined as follows;

$$V_s = \frac{L_{tt}}{t} \quad (2.13)$$

where, L_{tt} = the tip to tip distance between transmitter and receiver bender elements.

t = the travel time of the wave from the transmitter and the receiver.

According to the above shear wave velocity, the shear stiffness G_{\max} can be calculated from the elastic wave propagation theory as this equation $G_{\max} = \rho V_s^2$ where, ρ = the total density of the soil specimen. The density of the cylindrical soil specimen can be determined correctly by direct measurement, but it is not easy to determined L and t .

2.6.2. Types of Bender Elements

Figure 2.6 as show as the polarization of the bender elements: X-poled and Y-poled. There are two types of bender elements that were developed by Piezo System, Inc From the energy point of view, there is no difference between X-poled and Y-poled bender elements. Both X-poled and Y-poled bender elements act similarly when connected in a series connection and a parallel connection, respectively. The important parameters of a transmitter bender element are the free deflection x_f and the maximum force generated F_{\max} . For the receiver bender element, the important parameter is the voltage generated V_0 . The Y-poled bender element in parallel connection is more suited as a transmitter as it needs lower voltage to generate motion compared to the X-poled bender element in series

connection. Whereas, the X-poled bender element in series connection is more suitable as a receiver as it generates higher output voltage per unit force applied to the tip of the bender element (Leong et al., 2005).

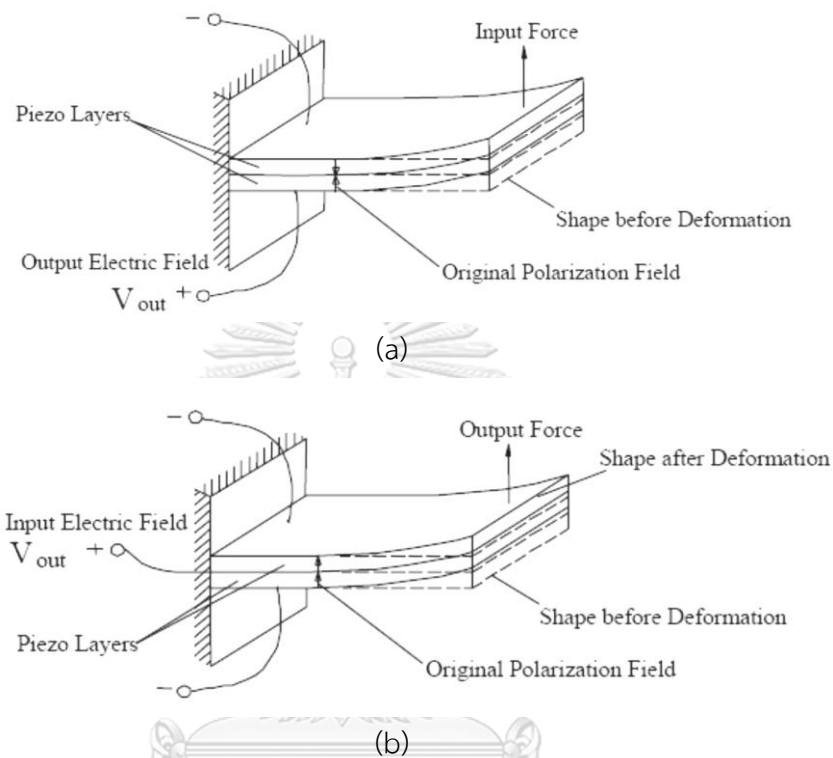


Figure 2.6 (a) X-poled bender Element Poled for Series Operation (2 wires)
 (b) Y-poled bender Element Poled for Parallel Operation (3 wires)
 (Source: Piezo System, Inc)

2.6.3. Determining of effective length

The relationship between travel time and lengths tips of bender elements in Figure 2.7 shows that the different lengths of the bender elements in the kaolin sample have effective in travel time. Since different stress states are different the test data drop on straight lines. It can see that each with an intercept of about 6 mm on the vertical axis, which conforms that length of bender element should be taken as the distance between the tips of bender elements rather than the whole length of the specimen report by (Viggiani & Atkinson, 1995)

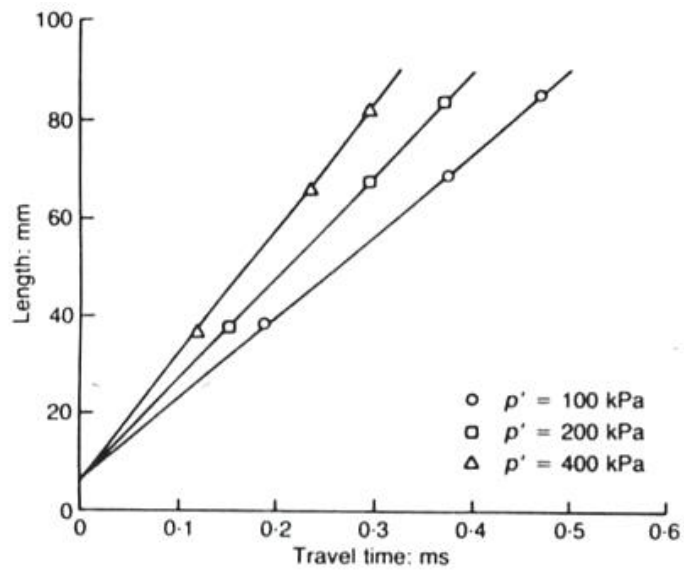


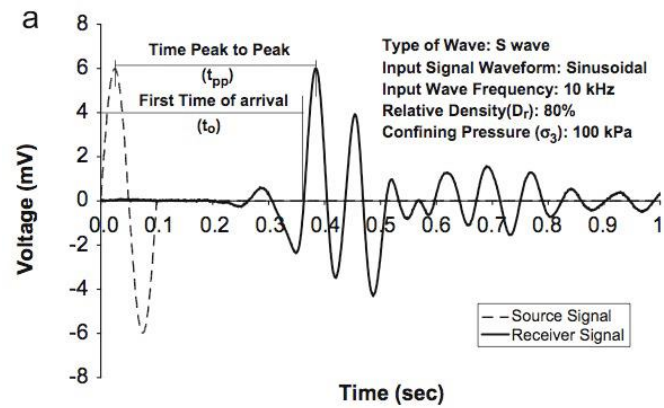
Figure 2.7 Relationship between travel time and specimen length
(Viggiani & Atkinson, 1995)

2.6.4. Determination of Travel Time

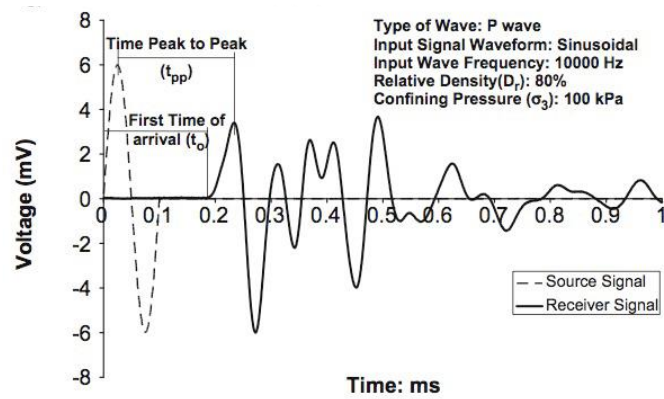
When considering travel time, many researchers have claimed that it is difficult to identify the travel time of the arrived signal exactly. There are three different methods used to find or interpret the time of travel from transmitter to receiver. The description of this method is given below.

2.6.4.1 First time of arrival

The first time arrived is one popular of the first time of arrival method used to find the time of travel. The first time according to (Kumar & Madhusudhan, 2010) of the first time of arrival is the difference time between the source signal and to receiver single. There also started the s-wave and p-wave measurement as shown in Figure 2.8



(a) S-wave



(b) P-wave

Figure 2.8 The travel time of arrived signal (t_0) and the time between first peak to peak (t_{pp}) with Of S-wave and (a) with P-wave (b) (Kumar and Madhusudhan, 2010)

They also point out the difference between s-wave and p-wave measurement. The difference between these two waves is the presence of the initial week single for the receiver. In the case of s-wave measurement, the initial week single for the receiver was presented while there was no percent of any initial week single in case of s-wave measurement.

2.6.4.2 First major peak to peak

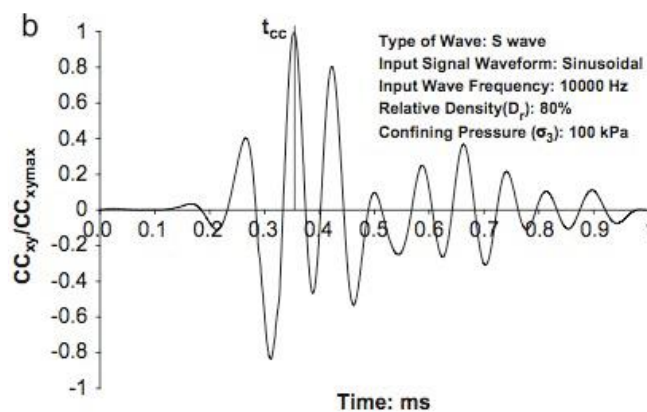
Viggiani and Atkinson 1995, Chan 2007 started that base on the assumption that the received signal bears a high resemblance to the transmitted. The first major peak-to-peak method is used to find the travel time between the peak of the transmitted signal and the first major peak of the received signal as shown in Figure Figure 2.9. The shear wave velocity can be taken as the time between two peak points. One is the peak of the transmitted signal and another is the first major peak of the received signal.

2.6.4.3 Cross-correlation

Shear wave travel time can be taken as the time shift (t_{cc}) that process the peak correlation between the transmitted signal and received signal. This method is considered to be the most accurate method to find shear wave velocity. Both *S-* and *P-waves* of the cross-correlation method are shown in Figure 2.9. The cross-correlation coefficient between transmitted, $T(t)$ and received, $R(t)$, as expressed by the cross-correlation coefficient, $CC_{TR}(t_s)$:

$$CC_{TR}(t_s) = \lim_{T_r \rightarrow \infty} \frac{1}{T_r} \int T(t+t_s)R(t)dt \quad (2.14)$$

where T_r is the time record and (t_s) is the time shift between the two signals.



(a) S-wave

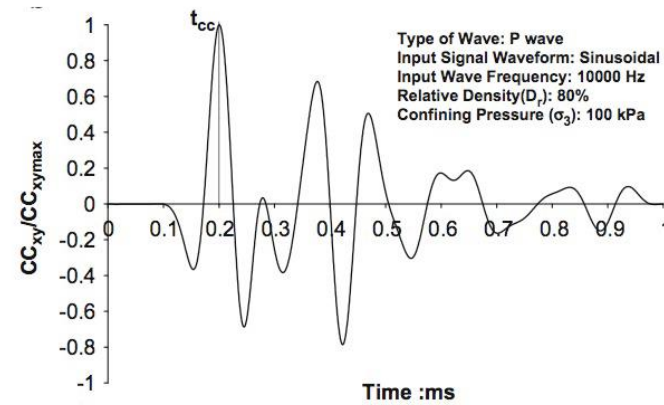
(b) *P*-wave

Figure 2.9 The time of arrival using cross-correlation method (t_{cc}) with of S-wave and (a) with P-wave (b) (Kumar and Madhusudhan, 2010)

2.6.5. Driving waveform

Many previous researchers suggested driving waveform the waveform, magnitude, and frequency to apply to the transmitter bender element and the soil specimen. These three types of the wave from that are commonly used such as sine wave, square wave, and continuous sine wave as shown in Figure 2.10. These waveforms were driven by a function generator which is an exciting voltage for the waveform. In this study, a square wave was used to the transmitter the bender element. Since, the soil specimen is clayed soil suggested by (Dyvik & Madshus, 1985). Moreover, the waveform, magnitude, frequency of applied voltage and soil types were summarized in Table 2.2

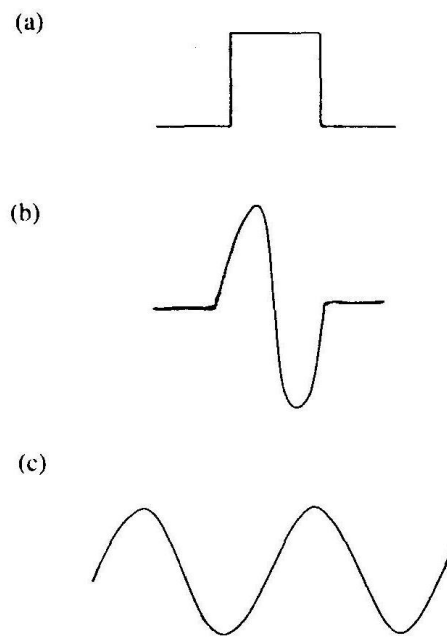


Figure 2.10 (a) square pulse, (b) sine pulse, and (c) continuous sine wave
(Blewett et al, 2000)



Table 2.3 Summary of waveform, magnitude, and frequency of applied voltage and soil type used by previous researchers (After Leong et al., 2005)

Reference	Voltage Applied			Soil Type	Method of Interpretation
	Waveform	Magnitude (V _{pp})	Frequency (Hz)		
Dyvik and Madshus (1985)	Square	20	5–100	Clay	First arrival (first reversal)
Bates (1989)	Square	10	2	Sand	First arrival (?*)
Argawal and Ishibashi (1991)	Sine	100–600	13 560	Glass spheres	First arrival (?)
Viggiani and Atkinson (1995)	Square Sine	20	50 ;000–10 000	Clay	First arrival (first deflection, first reversal) Characteristics points Cross correlation Cross power
Brignoli et al. (1996)	Sine	20	3000–10 000	Clay Sand	First arrival (first reversal)
Gajo et al. (1997)	Square Sine	150	10 000	Sand	First arrival (first deflection)
Arulnathan et al. (1998)	Sine	20	900–4,500	Organic soil	First arrival (?) Characteristics points Cross correlation Cross power
Lohani et al. (1999)	Square	20	50	Clay	First arrival (first reversal)
Blewett et al. (2000)	Sine	—	200–10 000	Sand	—
Diaz-Rodriguez et al. (2001)	Square	20	7	Silty clay	First peak
Kawaguchi et al. (2001)	Square Sine	20	100 1,2,4,8	Clay	First arrival (average of first rise and first peak)
Pennington et al. (2001)	Sine	20	8000–25 000	Clay	First arrival (first deflection)
Callisto and Rampello (2002)	Square Sine	20	50 10 000	Clay	Average of first deflection and reversal point Characteristics peaks

* Not specified.

2.7 Some of the previous work

(Teachavorasinskun, Thongchim, & Lukkunaprasit, 2002) have studied stress rate effect on the stiffness of Bangkok soft clay using triaxial cyclic compression tests under undrained triaxial and drained triaxial conditions. Bangkok soft clay 6-9 m depth specimens were used to study with mean effective 50 kPa and 100 kPa conducted. Those specimens were sheared by continuous cyclic loading and staged cyclic loading which was a sine wave cyclic test. Results of this study showed that the stress rate effect on the stiffness of soft clay using triaxial cyclic compression tests and the shearing method was very small as shown in Figure 2.11

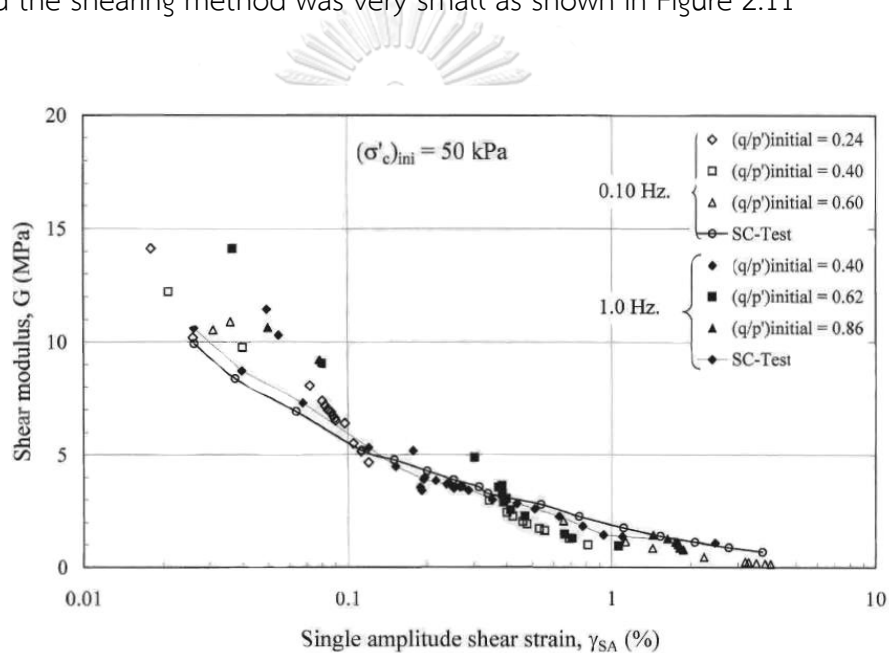


Figure 2.11 stress rate effect on stiffness of bangkok soft clay using triaxial cyclic compression tests as mean effective 50 kPa
(Teachavorasinsakun and Thongchimp (2002))

(Teachavorasinskun & Amornwithayalax, 2002) studied the elastic shear modulus of Bangkok clay during undrained triaxial compression tests with bender element. An undisturbed sample of Bangkok soft clay specimens was used to study. Results of this study report that the effect of the deviator stress was very small. However, there was a sudden drop in elastic shear modulus when the peak deviator stress was attained. This was believed to be the result of some permanent changes induced inside the sample as shown in Figure 2.12.

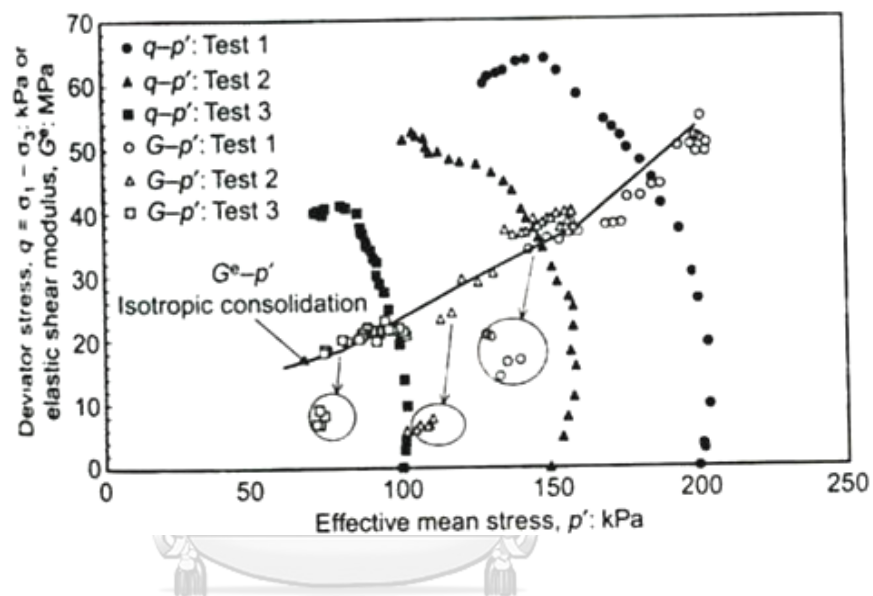


Figure 2.12 Variation of elastic shear modulus during undrained shearing

Moreover, the result shows the elastic shear modulus paths of Bangkok clays under loading and unloading were also studied. The relationships between the shear modulus and the mean effective stress under loading and unloading as show that path of the shear modulus, G^e reduced after unloading as shown in Figure 2.13.

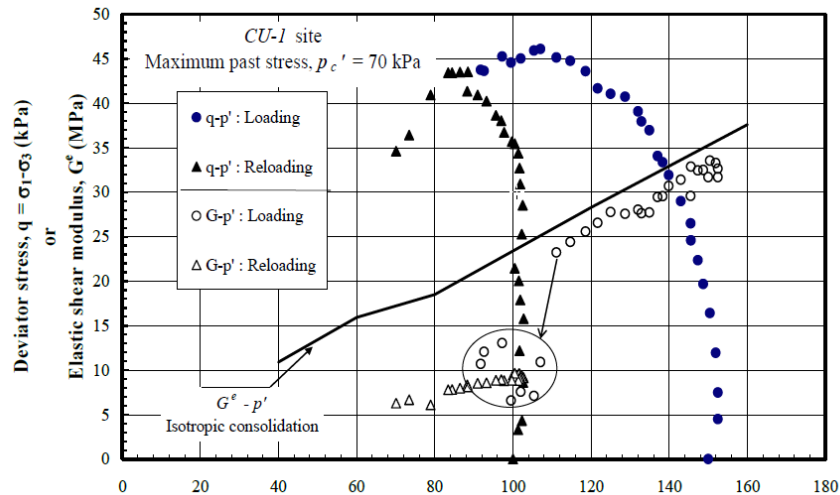


Figure 2.13 Variation of elastic shear modulus during loading and reloading cycle (Teachavorasinskun, S and Amornwithayalax, T, 2002).

(Dano & Hicher, 2002) studied the elastic shear modulus in granular materials along isotropic and deviatoric stress paths as shown in Figure 2.14 by using triaxial tests which were carried out on three unbound granular materials and the shear modulus was continuously measured using piezoelectric transducers. This experimental study shows that the power laws, usually considered to describe the effect of the mean effective stress on the shear modulus, are suitable only along isotropic stress paths and along deviatoric stress paths as long as the volumetric behavior is contracting. Indeed, when dilation appears, the shear modulus G_{\max} gradually decreases during shearing. The empirical relations of G_{\max} that they suggested were similar to those presented in previous researches (Hardin & Richart Jr, 1963), (T. Iwasaki & Tatsuoka, 1977) as shown in the general form:

$$G_{v\max} = \frac{K}{F(e)} \times P'^n \quad (2.15)$$

Where, K and n are material constants, P'^n is the mean effective stress, and $F(e)$ is a function of void ratio. Figure 2.15 represents a non-exhaustive compilation of experimental data relative to sands and gravels found in the literature.

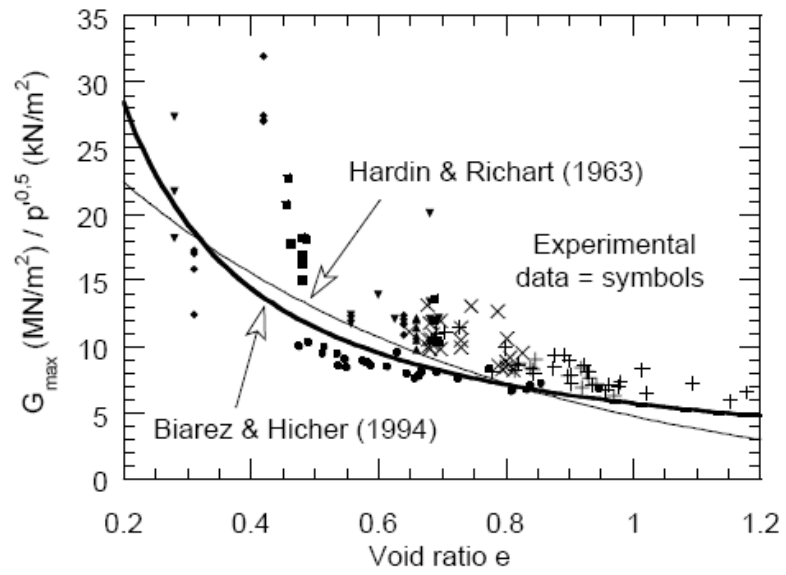
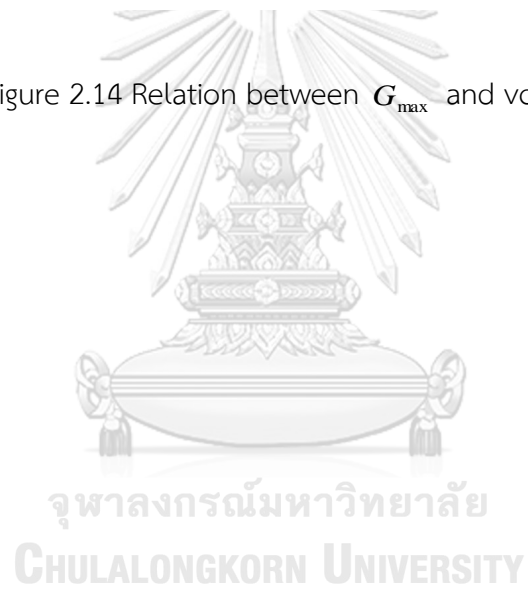


Figure 2.14 Relation between G_{\max} and void ratio e



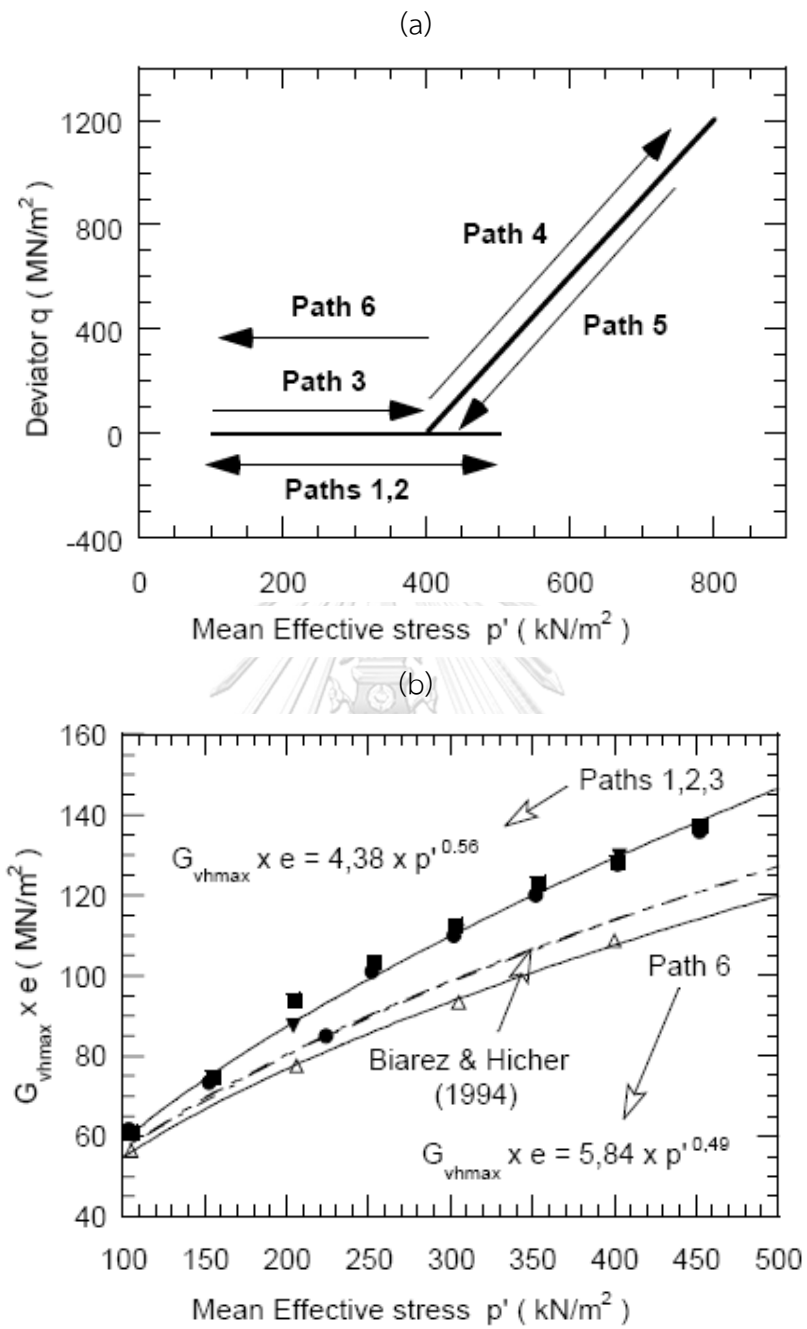
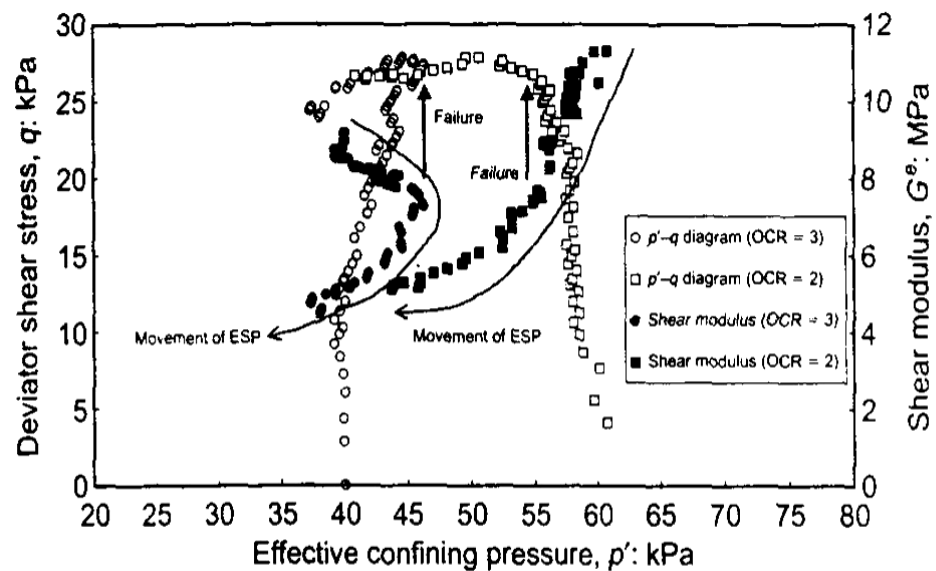


Figure 2.15 (a) and (b) evaluation of $G_{vh\max}$ along isotropic stress paths (Dano & Hicher, 2002)

(Teachavorasinskun & Akkarakun, 2004) have studied elastic shear modulus paths of Bangkok clays. Both OC clay and NC clay were collected to study. The results showed that the deviator stress applied during shearing significantly influenced the elastic shear modulus of OC clay, whereas it plays a minor role in the elastic shear modulus of NC clay. It is believed that the stiffer structures during isotropic unloading of OC samples might be destroyed during shearing.



CHULALONGKORN UNIVERSITY

Figure 2.16 Effect of stress path and ESP of Bangkok clay

CHAPTER III

RESEARCH METHODOLOGY

3.1. Clayey soil Materials

Undisturbed clay soil specimens of Bangkok clay were collected from Taling-chan located in Bangkok in the central area of Thailand. Each specimen was taken from a depth of 9.5 to 12.5 m. The basic physical properties of clay soil i.e. Liquid limit, Plasticity index, Initial void ratio as well as specific gravity are summarized in Table 3.1.

Table 3.1 Properties of soft Bangkok clay

Properties	Standard Test	Value
Water content, W_c , %	ASTM D 4959-00	55-65
Total Unit Weight, γ_t , t/m ³	ASTM D 4253-00	1.55
Liquid limit, LL , (%)	ASTM D 4318	85
Plastic limit, PL , %	ASTM D 4318	29
Plasticity index, PI , (%)	ASTM D 4318	56
Specific gravity, G_s	ASTM D 854 – 00	2.69
Initial void ratio, e	*	1.83-1.90

*The Initial void ratio, e can be calculated by equation;

$$e = \frac{G_s}{\rho_d} - 1 \quad (3.1)$$

Where e is an actual void ratio, G_s is the specific gravity of clayey soil, and ρ_d is the dry density of clayey soil

3.2 Testing equipment

In this study, the test programs were conducted on the clayed soil at the Laboratory, Faculty of Civil Engineering, Chulalongkorn University. The multiple testing programs subjected to triaxial loading were carried out under the triaxial strain control test and stress control test with the bender element measurement system. These schematic detail for both the strain control test and stress control test are shown in Figure 3.1 and Figure 3.2. The components of the equipment are as follows:

- (a) Loading frame device, triaxial cell (chamber), rubber membrane
- (b) De-aired system, vacuum pump
- (c) Air pressure system
- (d) Internal axial force transducer, axial displacement transducer, and pressure transducers
- (e) Computer and acquire data
- (f) Digital Oscilloscope
- (g) Function generator
- (h) Computer and acquire data
- (i) Pneumatic air cylinder

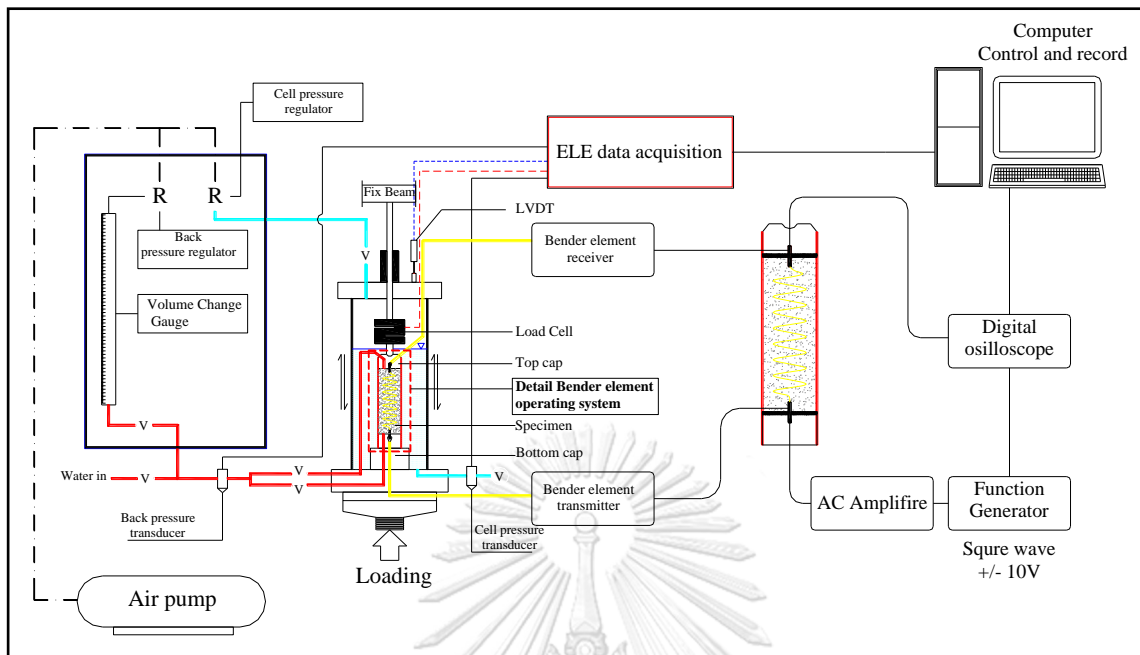


Figure 3.1 The schematic detail of the triaxial strain control test with bender element measurement system

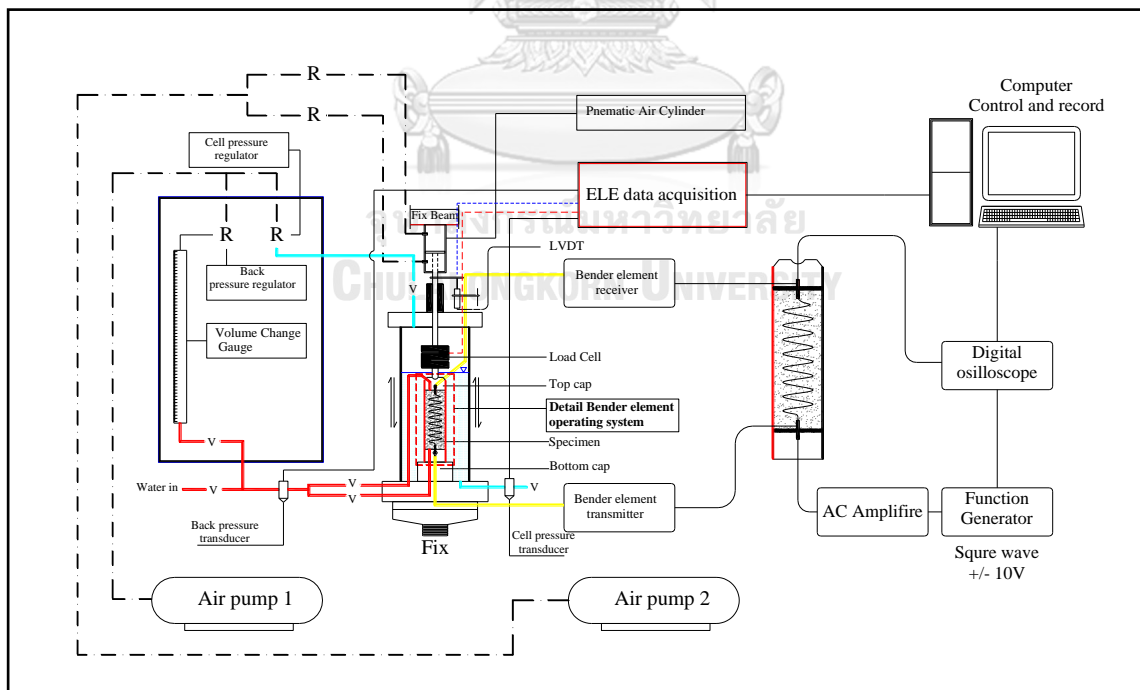


Figure 3.2 The schematic detail of the triaxial stress control test with the bender element measurement system

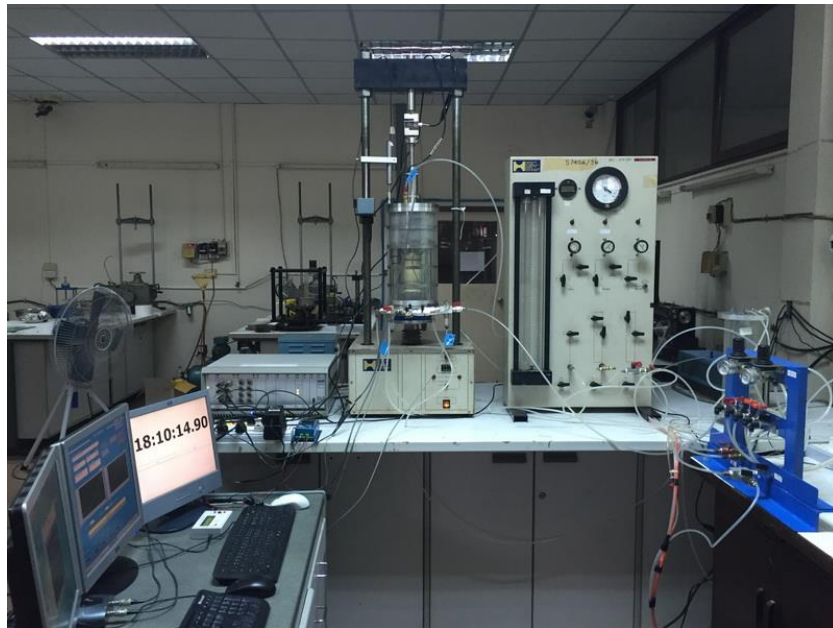


Figure 3.0.3 The triaxial strain control test with bender element measurement system

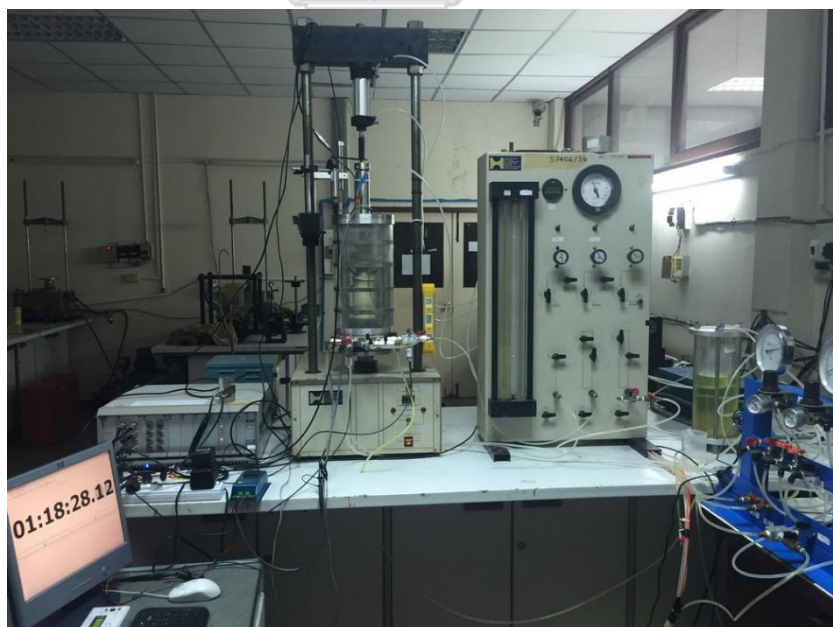


Figure 3.4 The triaxial stress control test with bender element measurement system

3.3. Bender Element Test

3.3.1 Bender Element setup

A couple of bender element types T 226- A4-303Y (Transmitter) and T 226- A4 -303X (Receiver) with dimensions of $31.7 \times 12.7 \times 0.66$ mm (length \times width \times thickness) were employed in this research study. The bender elements were developed by PIEZO SYSTEMS, INC. to measure the stiffness of soil at a small strain level. Both the piezoceramic bender element transmitter and receiver were an electromechanical transducer which was usually efficient in converting mechanical energy from the function generator. These bender elements were installed in the top cap and pedestal in the triaxial device. The transmitter element is mounted with epoxy in the top cap and the receiver element in the pedestal as shown in Figure 3.5. The three-wire parallel connection and same-sense polarization needed for a typical transmitter element. The receiver element has a two-wire series connection and opposite-sense polarization. A pair of bender element was coated with an approximately 1 mm epoxy on the bender element surface to prevent short-circuiting when in contact with water as shown in Figure 3.6.

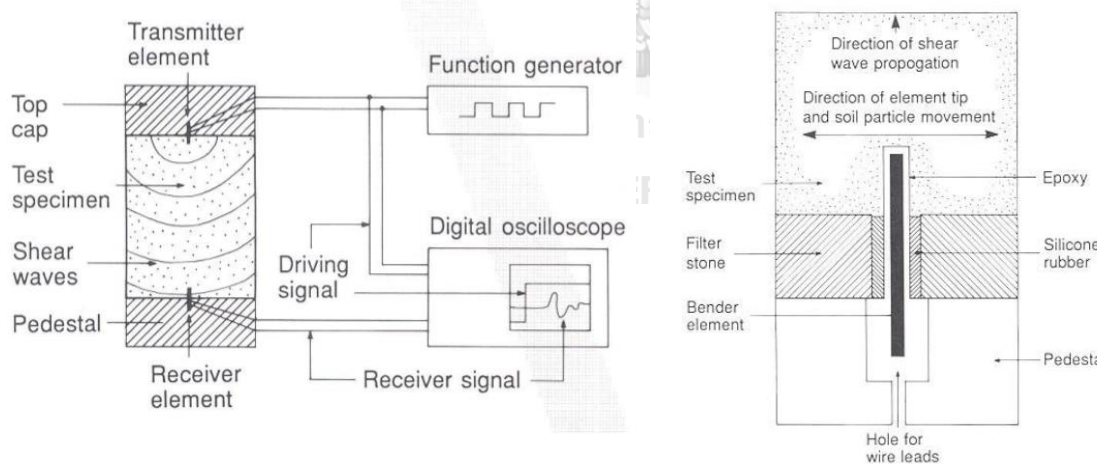
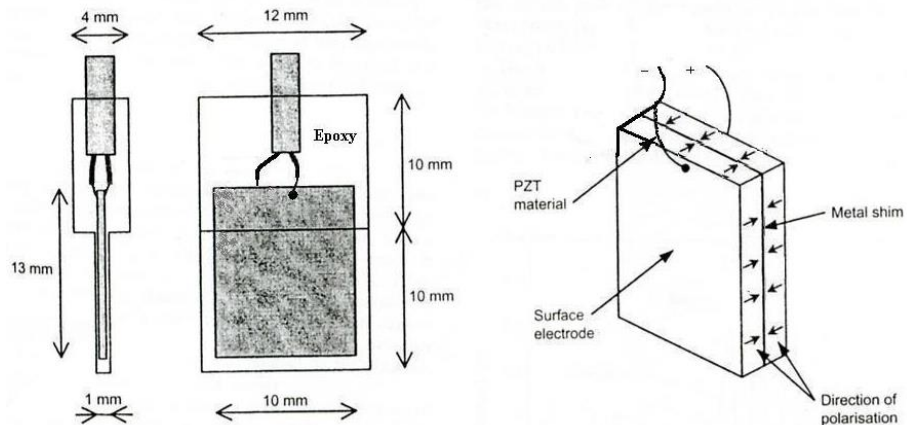
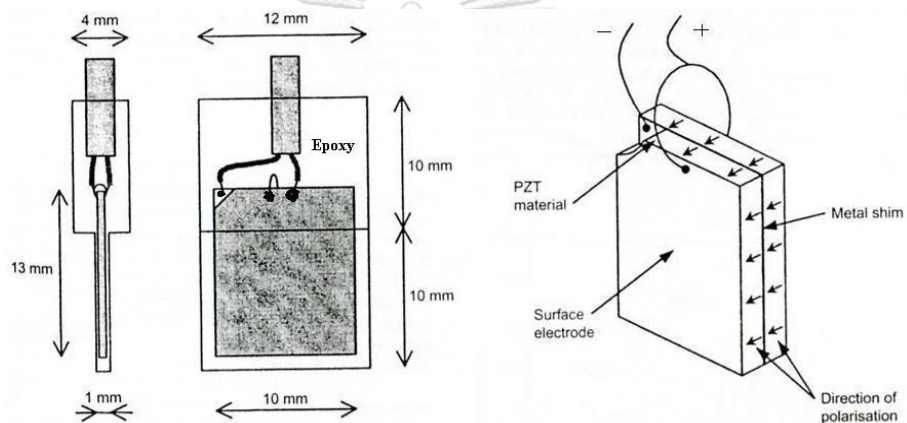


Figure 3.5 The bender element detail installed in the top cap and in the pedestal of the triaxial apparatus



(a) T 226- A4 -303X (Receiver)



(b) T 226- A4-303Y (Transmitter)

Figure 3.6 Wiring and coating of bender elements (a) Receiver (b) Transmitter

(Lings & Greening, 2001)

A pair of bender element types x-poled and y-poled were fixed in 10 mm depth 12 mm diameter slot top and pedestals of the conventional triaxial apparatus by using epoxy. A pair of porous stone was to make a small rectangular hole to install on the top cap and the pedestal before to install filter paper for the conventional triaxial apparatus as shown in Figure 3.7

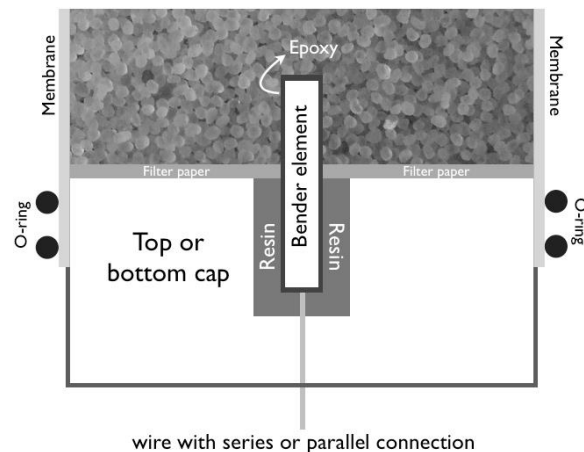


Figure 3.7 The installation detail of parallel- or series-type for bender element in the top cap and the pedestal of the triaxial apparatus (Pongvitthayapranu,2010)

3.3.2 Bender measurement system

The Bender measurement system is important for measuring the travel time to compute the shear modulus. The main components of the bender measurement system comprised of a digital oscilloscope, function generator, amplified voltage, and data logger. The 50 Hz with an amplitude of +10 V and - 10 V (20 V peak to peak) square wave used in this study is recommended by (Viggiani & Atkinson, 1995). The FDS 100 function generator was used to provide excitation voltage to the amplifier voltage which is applied to the transmitter bender element in the bottom pedestal of the triaxial apparatus. Consequently, when applied excitation voltage from the function generator is sent to the transmitter bender element, this can cause vibration in the transmitter bender element in order to generate the shear wave which propagated through the soil specimen. The wave traveling through the soil specimen was received by the receiver bender element in the top cap. Both the applied voltage and the receiver signal were recorded in the digital oscilloscope. Both the square wave and receiver signal from the receiver bender element were recorded by the digital oscilloscope were transferred to the computer. The schematic diagram was shown in Figure 3.8

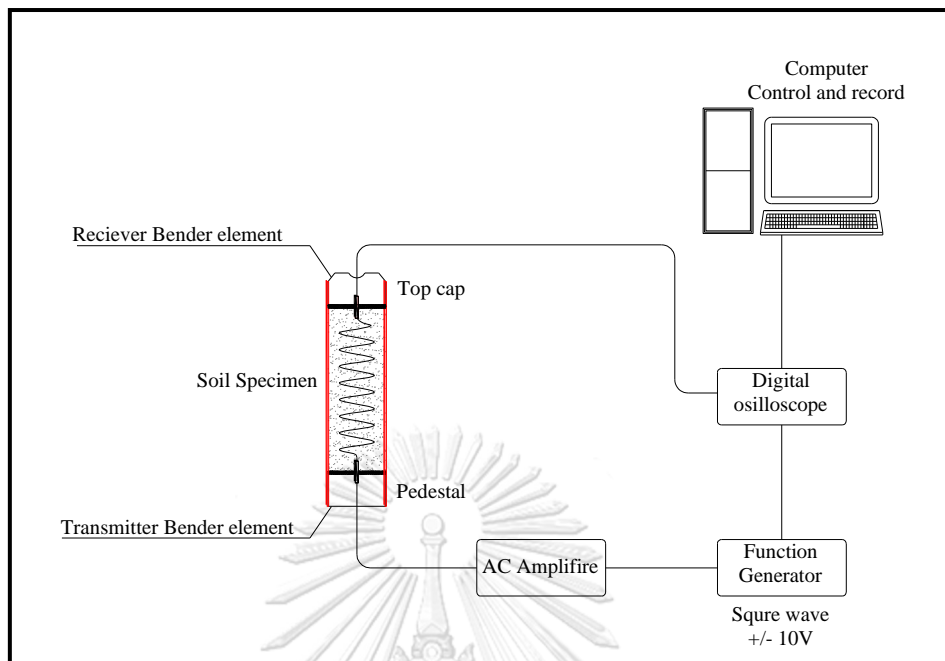


Figure 3.8 Bender element tests set-up

3.4 Testing Procedure

3.4.1. Preparation of Specimens

All series experimental programs of Bangkok clay specimens were performed under isotropic conditions ($K=0$). The entire specimens were prepared to cylinder shape with approximately 10 cm high and approximately 5 cm outer diameter after wax and cling-film removed. The filter paper and porous stone (the filter place on top porous stone) were placed on the top cap and the pedestal of the conventional triaxial apparatus in order to reduced consolidation time and increase the permeability of soil samples. Moreover, the filter can reduce the excess water pressure during drain shearing specimens in a triaxial test proposed by (V. SIVAKUMAR 2010). The vertical filter papers were mounted around vertical alignment of soil specimens. The schematic diagram was shown in Figure 3.9. After completion, the specimen was mounted in the conventional triaxial apparatus.

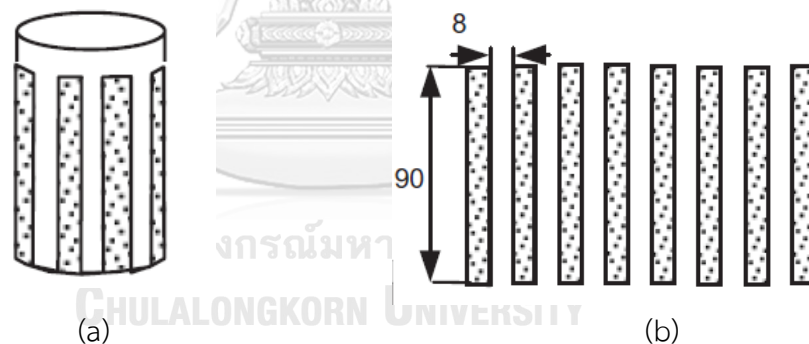


Figure 3.9 Vertical filter paper (a) Vertical filter paper attached to the specimen (b) size of vertical filter paper proposed by Sivakumar, V. et al. (2010)

3.4.2 Triaxial preparation setup on triaxial apparatus

1. Make sure the all devices can be operated for the test, all instrument shall be calibrated.
2. Place porous stones and filter paper on the bottom pedestal.
3. Attach the vertical filter paper around the specimen.
4. Place a soil sample on the bottom pedestal on the triaxial apparatus.
5. Place a porous stone and filter paper on the top of the specimen.
6. Wear a rubber membrane in the specimen.
7. Fasten "O" rings on the top and bottom pedestal in order to prevent water in the cell from absorbing into the specimen.
8. Install chamber acrylic cell in the triaxial apparatus, the place a top plate on top and lock together with bolt
9. Fill water in cell triaxial test, the level of water shell be lower than the load cell.
10. Setup the Linear Variable Differential Transformer (LVDT) on the triaxial apparatus

3.4.3 Triaxial de-air and suction Technique

De-air system of conventional triaxial machine to de-air in soil specimen was developed by the researcher. This simple de-air system comprised of suction value in cell, the suction value in back pressure, water tank, vacuum gauge valve, and two vacuum pumps as shown in Figure 3.10.

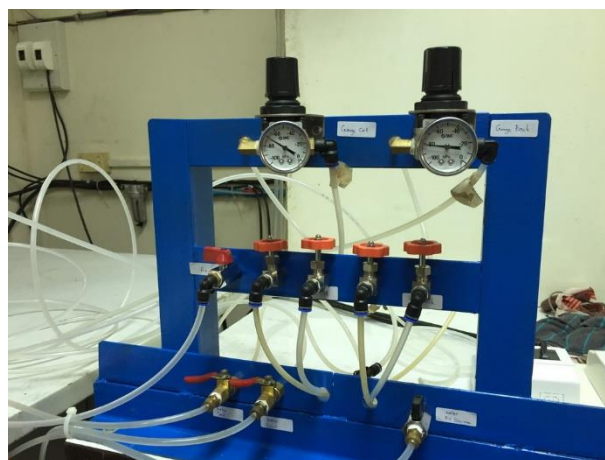


Figure 3.10 Value control in triaxial apparatus

The route of de-air system in triaxial apparatus was divided into two ways, one is suction in cell pressure and the other one is in backpressure line. Both de-air systems in cell line and de-air system in the backpressure line were connected with the vacuum pump. This de-airing process was commonly required in order to ensure that air void was removed in soil specimens. The suction procedure was proposed in table 3.2. After air void removed that ensure avoid removed from soil specimen, the ball valve of the water tank will be open in order to fill water in soil specimen until the air in the backpressure line cannot be seen. To release the suction step, the specimen was continued into a saturation procedure.

Table 3.2 Suction step in triaxial apparatus

Suction step			Release suction step	
Duration time (min)	Back Pressure (kPa)	Cell Pressure (kPa)	Back Pressure (kPa)	Cell Pressure (kPa)
15	-20	0	-90	-70
15	-20	0	-90	-70
15	-40	-20	-80	-60
30	-60	-40	-60	-40
30	-80	-60	-40	-20
60	-90	-70	-20	Stop Vacuum
Continued to release suction step			Stop Vacuum	-

3.4.4 Saturation of specimens

After de-air process in specimens was carried out. Four series of CIU-UL, mono-CID, CID-UL, and CIDS triaxial tests were fully saturated by using back pressure of 100 *kPa* with mean effective stress of 300 *kPa*. This stage can be confirmed by *B* value before being isotropically consolidated and sheared specimen. The *B* value can be expressed as;

$$B = \frac{\Delta u}{\Delta \sigma_3} = 1 \text{ or } B \geq 99.5\% \quad (3.1)$$

Where B is degree saturation of specimen, $\Delta\sigma_3$ is a small increase $\Delta\sigma_3$ in confining pressure after closing the drainage system and Δu is the change in pore pressure in backpressure. Normally, $B \geq 99.5\%$ is required to generate meaningful pore pressure. Otherwise, partial saturation would result in erroneous pore pressure and undrained shear strength. The degree of saturation can be increased by increasing the back pressure and confining pressure continuously. For all experimental study, backpressure and confining pressure were then increased. The effective backpressure and 20 kPa confining pressure were used to maintain until the specimen saturated. Both back pressure at 280 kPa and confining pressure at 300 kPa were used to saturate for CID-LU and CIU-LU test and control stress CIDS condition.

3.4.5 Consolidation of Specimens

After the stage of saturation is completed. This consolidation of specimens was carried out using isotropic consolidations. Both effective horizontal and vertical principal stresses ($K = \sigma'_h / \sigma'_v$) are equal to 1. Keep the back-pressure constant, and increase the cell pressure until effective confining pressure was required, the axial displacement of the displacement transducer and the value of volume change transducer were recorded in each step of consolidation stage. The travel time of the shear wave was measured by a pair of bender elements when the dissipation of the excess pore water pressure was ensured at the end of each consolidation step of specimens

3.4.6 Shearing mode of specimens

3.4.6.1 Undrained triaxial test with small loading-unloading (CIU-LU)

After the consolidation step was carried out. The drainage valve was immediately closed, after that the soil specimen was then sheared until the shear strain is approximately 10% strain deformation. Strain rate machine control was followed by the ASTM Standard ASTM D4767 – 11 Standard Test Method for Consolidated Undrained Triaxial Compression Test for Cohesive Soils (Strain rate = 0.02 mm/min). Multiple stages of triaxial compression and extension were controlled in this study. About $\approx 0.2\%$ of strain unloading was carried out after strain loading increase by about $\approx 1\%$ until the strain is at $\approx n\%$. State of small loading and reloading control period and travel time measurement from a pair of the bender element on undrained Triaxial test were sketched in Figure 3.11. The pore pressure readings, the cell pressure readings, and the axial force transducer readings, axial displacement readings were automatically is recorded by ELE data Logger which is a log-time data record. Travel time readings were recorded the strain is at 10% strain.

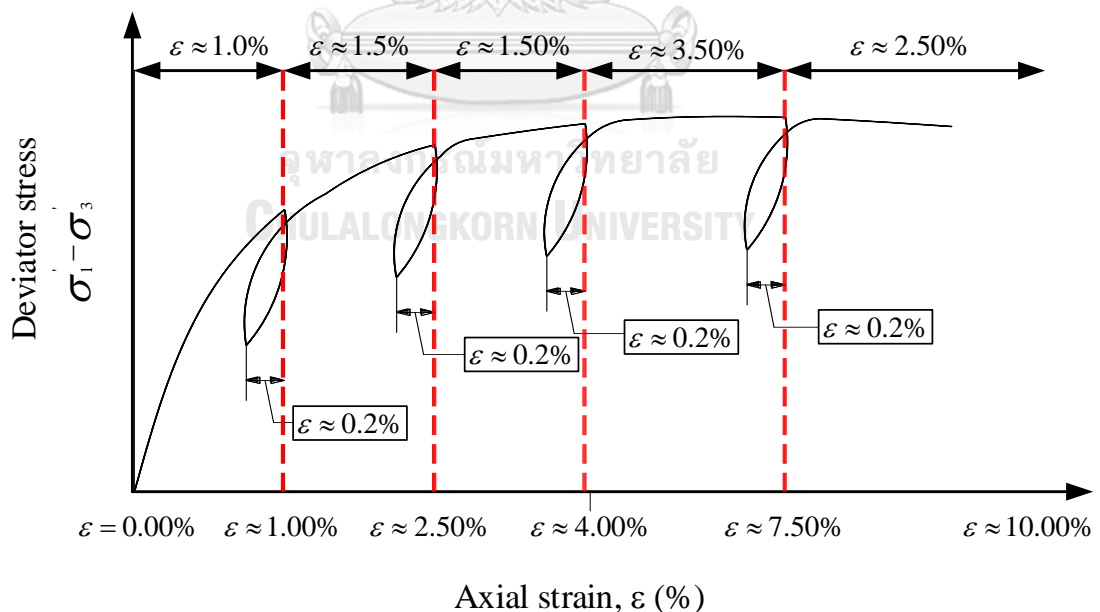


Figure 3.11 Control diagram of undrain triaxial small loading-unloading test

3.4.6.2 Monotonic drained triaxial compression test (CID-mono)

Monotonic drain triaxial compression test is one important method to investigate the shear wave velocity and the shear modulus in terms of effective stress. As for drained triaxial test, at the end of a consolidation period and final mean effective stress, the water drainage valves were immediately opened and then the specimen was sheared to failed with the strain rate (between 0.004 mm/min). The strain rate machine control was followed by the Standard ASTM D7181 – 11 Method for Consolidated Drained Triaxial Compression Test for Soils. The slow rate of strain was used so that the travel time of the shear wave could be accurately measured and recorded. The pore pressure readings, the cell pressure readings, the axial force transducer readings, axial displacement, and volume-change reading were automatically recorded by ELE data Logger which is a log-time data record. Travel time readings were recorded until the shear strain is approximately at 10% strain

3.4.6.3 Triaxial with a small loading-unloading drained test (CID-LU)

A series of experiments were carried out by small loading-unloading drained triaxial tests in order to investigate the behavior of shear wave velocity. After the stage of saturation was attained. These specimens were isotopically consolidated in triaxial apparatus with difference confining stress pressure 150, 225, and 300 *kPa*, respectively. After that drainage valve was immediately open. The sample was sheared by strain control with a strain rate an approximately 0.004 mm/min. To evaluate the variation shear wave velocity, six cycles of small loading and unloading strain-controlled were implemented for this experiment. The flowchart control diagram for the drained triaxial loading-unloading test was shown in Figure 3.12. During the test, the pore pressure readings, the cell pressure readings, and the axial force transducer readings, axial displacement readings, and travel time measured from the bender element were recorded.

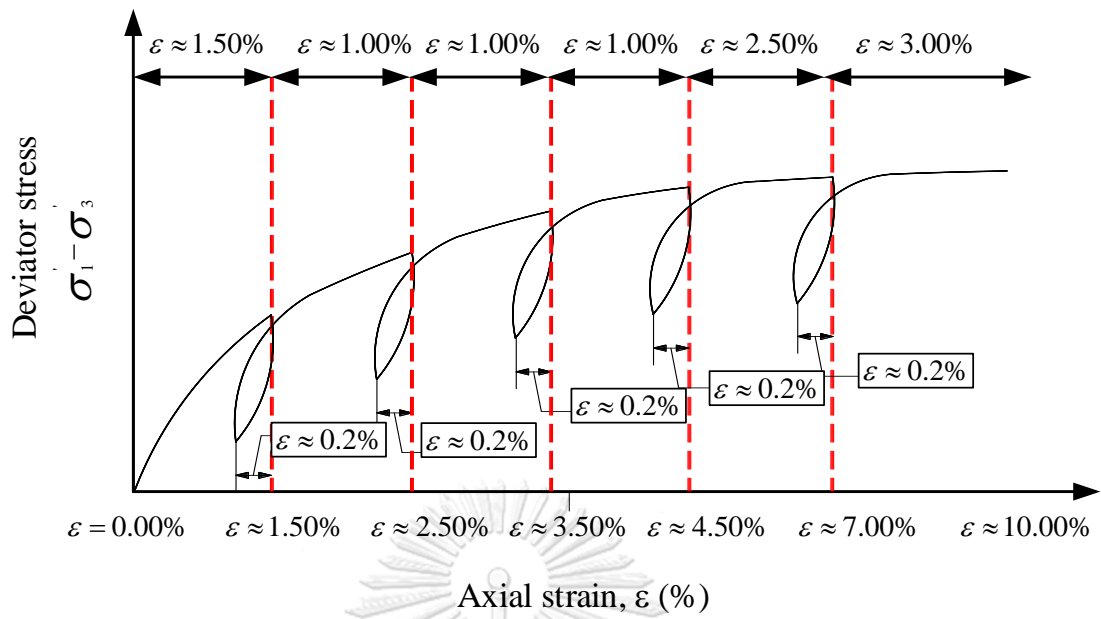


Figure 3.12 Control diagram of drained triaxial small loading-unloading test

3.4.6.4 Drain triaxial stress control (CIDS)

In this study, the triaxial p' constant test was performed under isotropic consolidation test in order to evaluate the shear wave velocity (V_s) and shear modulus (G) compared for undrained triaxial test and drained triaxial. The flowchart diagram of the method control path loop was shown in Figure 3.13. The pneumatic air cylinder (double action) was mounted at top beam in triaxial apparatus so that any required stress path on the triaxial test can be maintained axial load until the dissipation of the excess pore water pressure was ceased. The process of the manual controller was defined by mean effective stress (p') which can be determined the following:

$$p' = \frac{1}{3}(\sigma'_1 + 2\sigma'_3) \quad (3.2)$$

$$\frac{P}{A} = 3p' - 2(CP - BP) \quad (3.3)$$

$$q = \frac{P}{A} = \sigma'_1 - \sigma'_3 \quad (3.4)$$

Where

- p' = mean effective stress (kPa)
- q = deviator stress (kPa)
- P = Axial load (N)
- CP = Cell pressure (kPa)
- BP = Back pressure (kPa)
- σ'_1 = Vertical effective stress (kPa)
- σ'_3 = Confining effective stress (kPa)

After end of consolidation period was end, the process of manual controller is followed;

1. The pneumatic air cylinder applied load into shearing specimen stage (Stage $\sigma_{1-1}, \sigma_{3-0}$) together with the measurement of the travel time.
2. Maintain axial load until the dissipation of the excess pore water pressure appeared together with the measurement of the travel time.
3. Keep backpressure and release the Cell pressure (Point $\sigma_{1-1}, \sigma_{3-1}$), then consolidate the specimen until the dissipation of the excess pore water pressure was stop with the measurement of the travel time.
4. Repeat steps 1-3 until axial strain more than 10% strain.

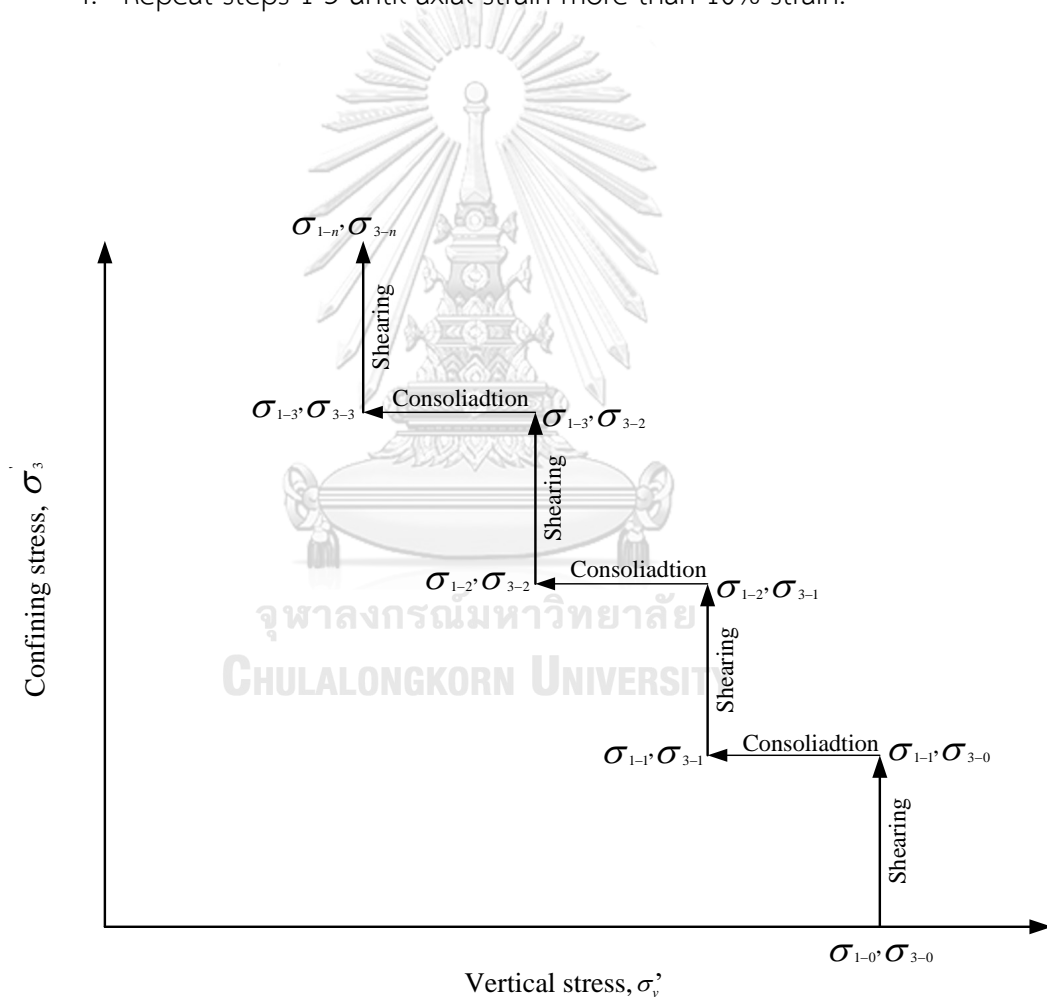


Figure 3.13 An idea diagram for confining stress control

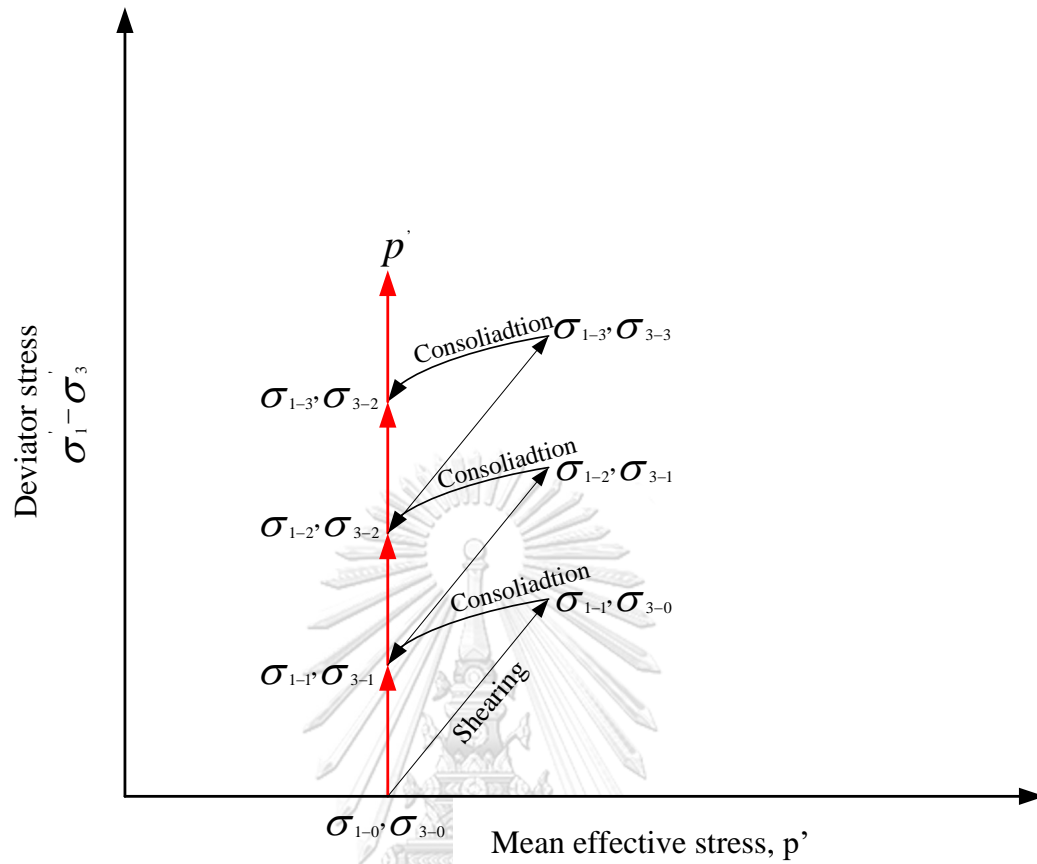


Figure 3.14 The diagram of stress control test

3.4.6.5 Drained triaxial extension (CIDE) and undrained triaxial extension (CIUE)

In this study, the drained triaxial extension (CIDE) and undrained triaxial extension (CIUE) which were manually controlled by using a pneumatic air cylinder (double action) to shear the clayey soil specimens. The confining pressure of 50, 150, and 225 kPa was demonstrated for both drained triaxial extension (CIDE) and undrained triaxial extension. In these conditions, the soil specimen was installed in both of the top cap and pedestal in the triaxial apparatus while the top cap and piston for extension specimens were fixed by epoxy. When the consolidation step was carried out. The specimen was sheared by increasing extension load from pneumatic air cylinder while drained value was closed. For drained triaxial extension (CIDE), the soil specimen was also sheared by increasing extension load from pneumatic air cylinder while drained value was opened in order to measure the value of shear wave velocity under the effective term. In the case of the drained triaxial extension and undrained triaxial extension, the strain for shearing clayey soil specimen about approximately 3-4% strain was applied. Because the gap between top caps may occur at a very large strain level. The entire pore pressure, the cell pressure, the axial force transducer, and axial displacement were automatically recorded by ELE data Logger whereas the travel time readings were recorded by oscilloscope then the data was recorded by the computer.

3.5 Travel time and shear wave velocities determination

In this study, travel time measurement (t) was suggested by Viggiana & Atkinson (1995). The first major peak to peak of wave propagation from both the bender element transmitter and the receiver was used to calculate the shear wave velocity as shown in Figure 3.15. Several researchers are using equation 3.5 to calculate the shear wave velocity, V_s as:

$$V_s = \frac{L_{tt}}{t} \quad (3.5)$$

Where V_s is shear wave velocity, L_{tt} is the distance between bender element transmitter and receiver, and t is travel time measurement from the first major peak to peak method. Shear modulus of soil sample (G) can be determined by shear wave velocity V_s with the following equation;

$$G = \rho V_s^2 \quad (3.6)$$

Where G is Shear modulus of the soil sample, ρ is the mass density of soil and V_s is the shear wave velocity

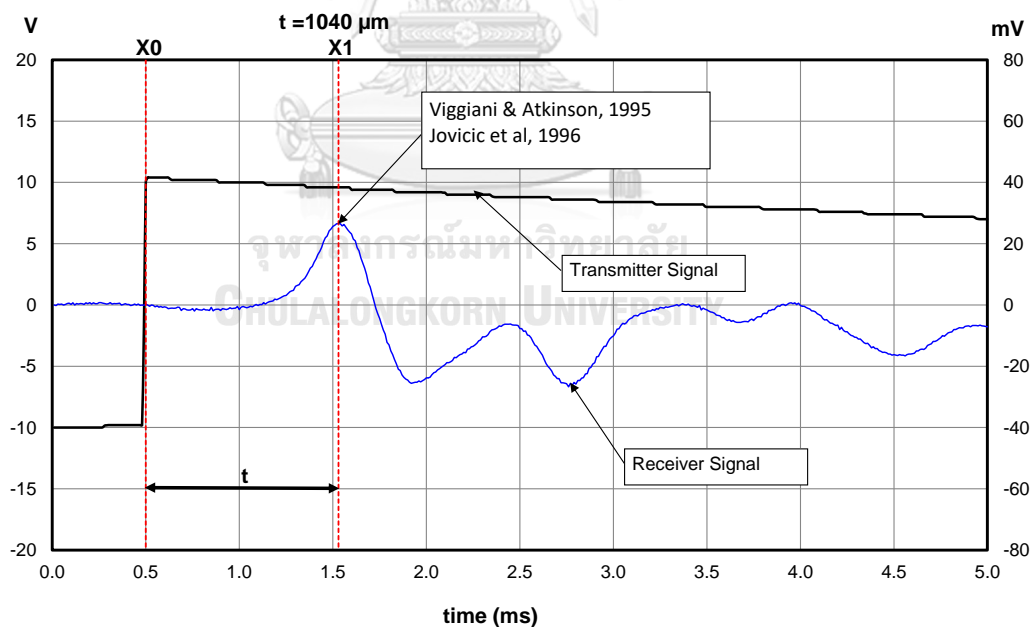


Figure 3.15 Oscilloscope signals from the transmitter and receiver bender elements

In order to confirm travel time measurement, t , the travel time was measured from the first peak of the wave propagation from transmitter and receiver bender element. The direction of the trigger from function generator should be polarity. Figure 3.16 show the two times trigger to input difference the excitation voltage from function generator where line A is the starting time of trigger from function generator. The travel time distance between line A and line B is travel time, t to determine the shear wave velocity

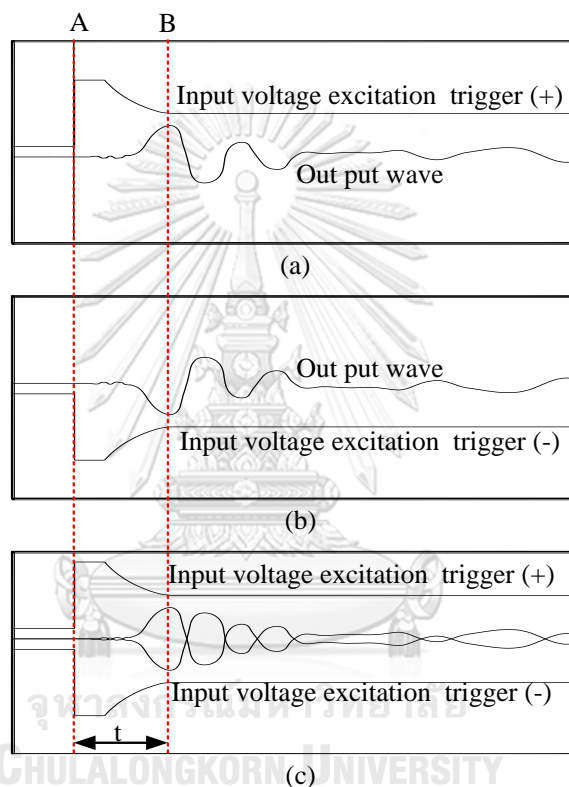


Figure 3.16 (a) Bender elements signals from square pulse +10 voltage excitation, (b) bender elements signals from square pulse -10 voltage excitation, and (c) Cross check signal from the bender elements

3.6 Summary of Testing Program

In this research is to identify the shear wave velocity with elastic shear modulus under triaxial undrained small loading-unloading test (CIU-UL), monotonic triaxial drained compression test (CID), triaxial drained small loading-unloading test (CID-UL), triaxial stress control test (CIDS), undrained triaxial extension (CIUE) and drained triaxial extension (CIDE) measured using the bender elements was proposed. The flowchart outlined was presented in Figure 3.17.

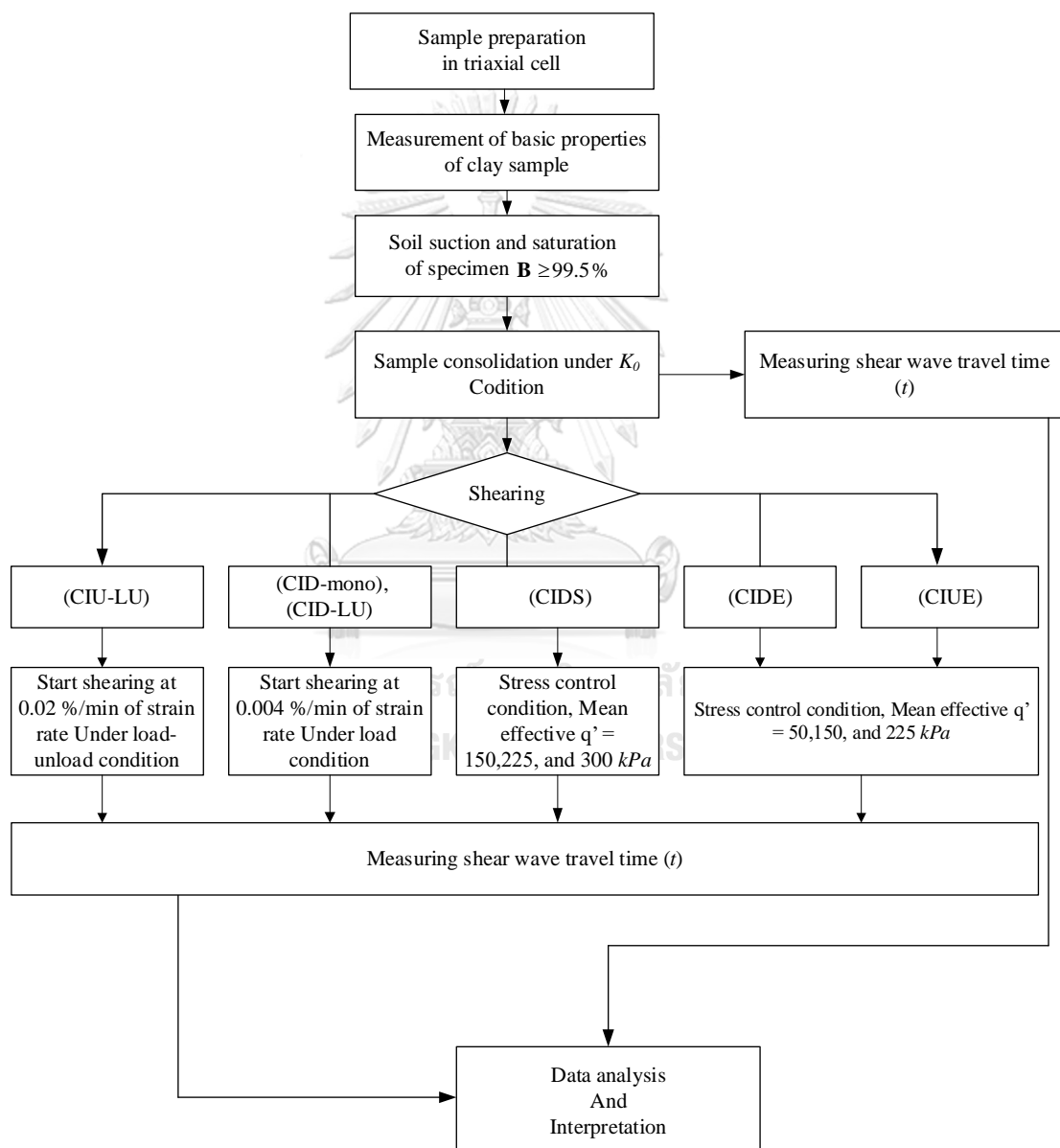


Figure 3.17 Schematic diagram of testing procedure

CHAPTER IV

RESULTS AND ANALYSIS

4.1 Dependency of stress-strain responses from triaxial tests

Dissimilarity of stress-strain responses from triaxial tests is dependent on the mode of shearing. The test results from the entire series of triaxial tests in this study are indicated that the void ratio and mean effective stress are influenced by stress-strain during consolidation state and shearing state. In comparison, the stress-strain response between undrained small loading-unloading (CIU-LU) condition tests and drained monotonic loading (CID-mono) condition with various confining pressure of 150, 225, and 300 *kPa* isotropic confining pressure is shown in Figure 4.1 and Figure 4.12. For undrained small loading-unloading (CIU-LU) condition tests in Figure 4.1, the results show that higher the isotropic confining pressure was observed the maximum stress while the stress-strain and mean effective stress as unloading step were also decreased. This occurs because the vertical stress was decreased. The friction angle is equal to 8.6 while cohesion is equal to 29.

On the other hand, in case of drained monotonic loading (CID-mono) condition test, it is seen from Figure 4.2 that the maximum path of stress from higher confining pressure was observed. These results as various isotropic confining pressure were obtained no dominated peak stress at strain about 0-10%. As for the results of drained triaxial drained small loading-unloading (CID-LU) condition tests show that the dependency of deviator stress increased when the effective stress also increased while effective stress as unloading stage was decreased by reduction of vertical stress as confining stress pressure constant. This behavior of every circle load-unloading shearing specimens was almost the same for three specimens with 150, 225, and 300 *kPa* confining stress pressure. These results in this condition study were obtained no dominated peak stress at strain about 0-10%. For drained-monotonic compression test and drained with small loading-unloading cycles, the average value of angle of internal friction and cohesion is equal to 9.8 and 15.1 respectively. The test results of the stress-strain relationship were illustrated in Figure 4.2.

The stress-strain responses from drain triaxial stress control test (CIDS) shown in Figure 4.4 were performed on three clay soil specimens various p' constant of 150, 225, and 300 kPa . Since the process of the manual controller was defined by mean effective stress. The stress-strain relationship from three values of mean effective stress was increased step by step. The higher stress was observed at higher mean effective stress value controlled. For the undrained triaxial extension, the deviator stress decreases when mean effective decreases in both drained and undrained extension test. This behavior is almost the same. This is due to the same direction of mean effective stress. The stress-strain relationship from three values was plotted in Figure 4.5-4.6.

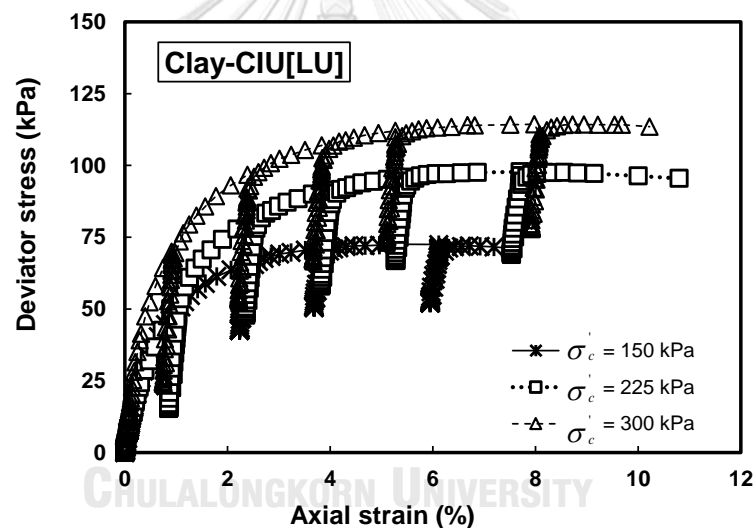


Figure 4.1 The stress-strain relation of undrain loading-unloading condition tests with 150, 225, and 300 kPa isotropic confining pressure

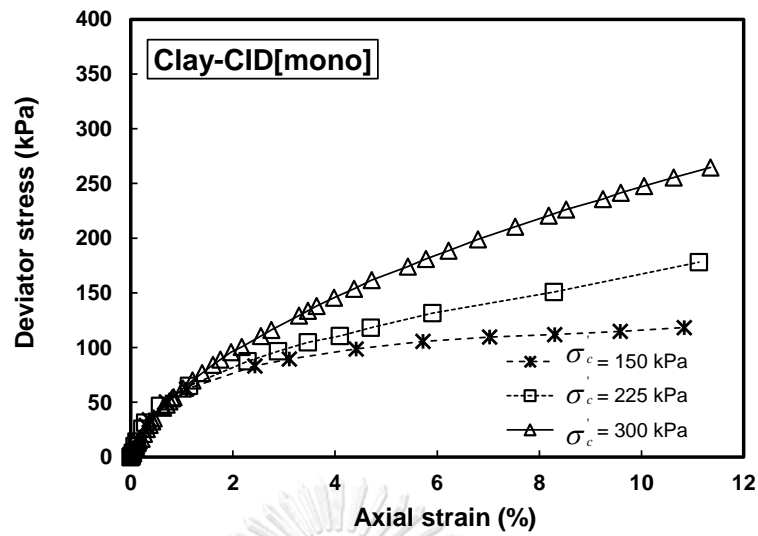


Figure 4.2 The stress-strain relation of drain loading condition tests with 150, 225, and 300 kPa isotropic confining pressure

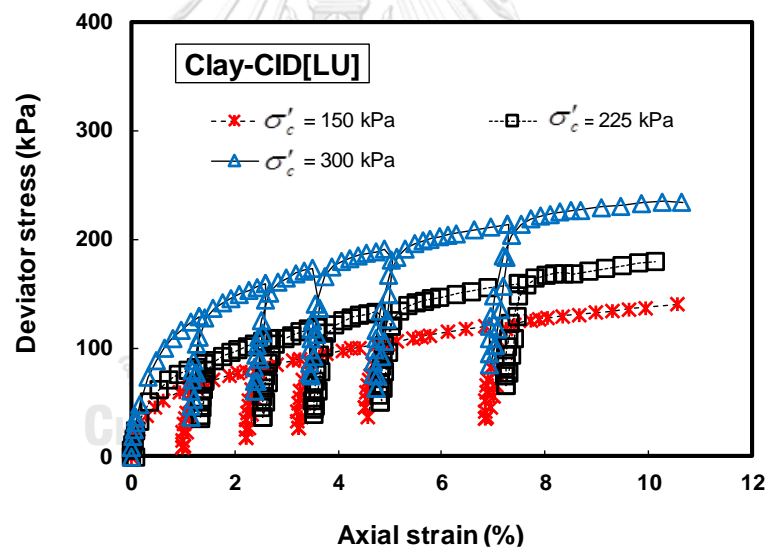


Figure 4.3 The stress-strain relation of drain load-unloading condition tests with 150, 225, and 300 kPa stress-controlled

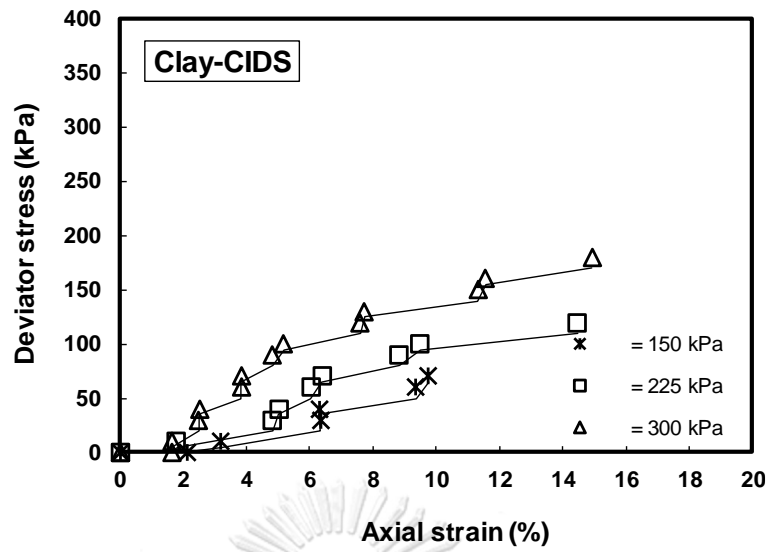


Figure 4.4 The stress-strain relation of drain loading condition tests with 150, 225, and 300 kPa stress-controlled

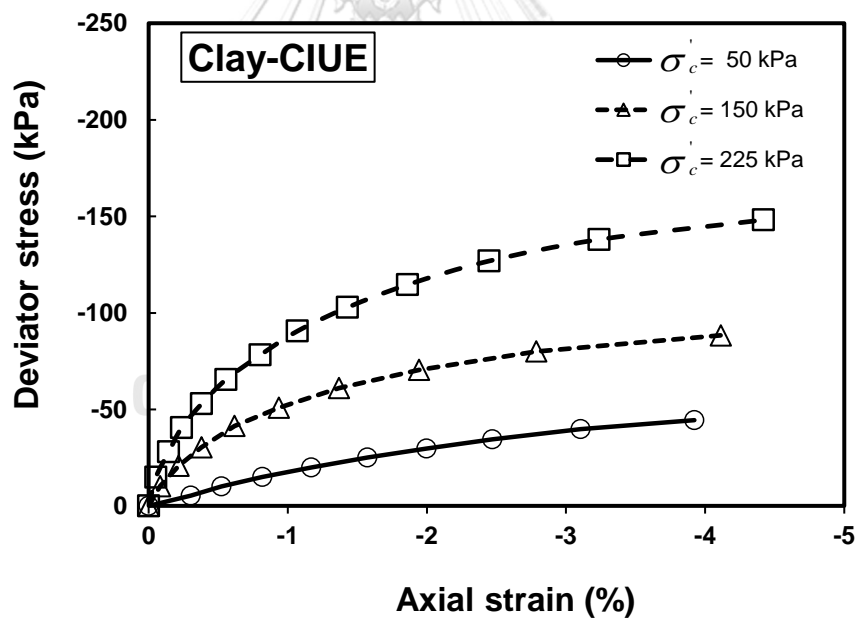


Figure 4.5 The stress-strain relation of undrain triaxial extension tests with 50, 150, and 225 kPa

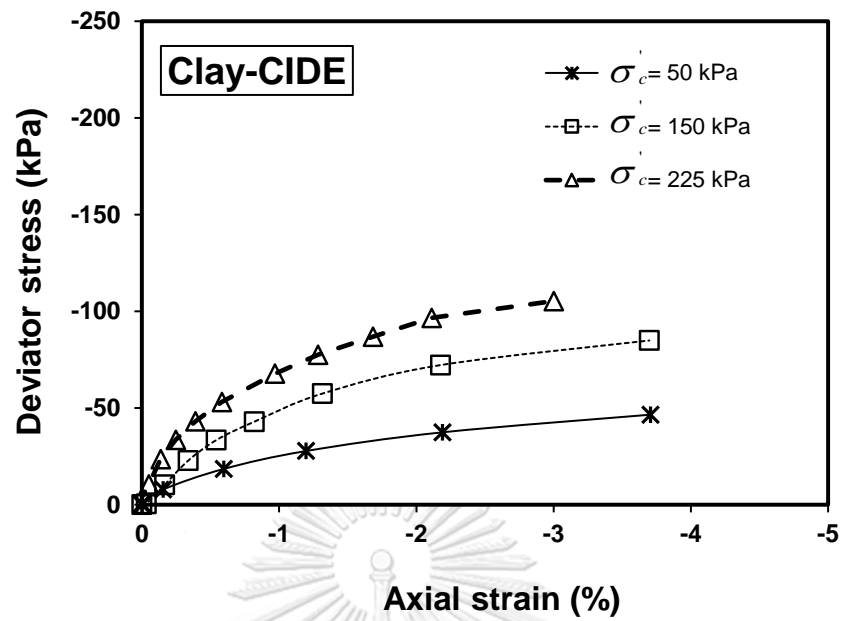


Figure 4.6 The stress-strain relation of drain triaxial extension tests with 50, 150, and 225 kPa

4.2 Shear wave velocity of Bangkok clay from triaxial tests

In general, the shear wave velocity of soil is classified into two categories: induced undrained and induced drained, following the concepts adopted by many researchers, e.g. (Bartake et al., 2008), (Oh et al., 2017). The estimation of undrained shear strength is determined by using shear wave velocity. The undrained shear strength, void ratio, and shear wave velocity are entirely related. As presented in previous literature, researchers developed an empirical expression model under a variation of mean effective stress, p' , and void ratio, which was proposed by (Hardin & Richart Jr, 1963), and (T. Iwasaki & Tatsuoka, 1977). The empirical equation of elastic shear modulus, G_{max} , is as follows:

$$G_{max} = AF(e) \left(\frac{P'}{P_o} \right)^n \quad (4.1)$$

Where A is the coefficient of uniformity of a specimen, $F(e)$ is the function of void ratio, and P_o is the reference pressure for normalization

Very recently, Escribano and Nash (2015) proposed that both stresses in the particle motion directions and wave propagation are the primary components affecting the shear wave velocity, as the elastic shear modulus function as stress acts orthogonally to the wave motion plane. Equation (4.2) has been extended for elastic shear modulus as:

$$G = K \cdot f(e) \cdot \sigma_1^{2m} \cdot \sigma_3^{2n} \quad (4.2)$$

Where K is σ_h / σ_v ($K=1$ for isotropic condition), $F(e)$ is the function of void ratio, and m and n are the coefficients corresponding to the direction of vertical effective stress, σ_1' , and horizontal effective stress, σ_3' . Based on equation (4.2), a new G_{max} model is directly related to developing a new empirical equation for determining shear wave velocity of soil.

According to past research, (Santamarina, Klein, & Fam, 2001) state that the shear wave velocity is governed by mean effective stress. The correlation function under isotropic loading conditions is proposed as below:

$$V_s = K \left(\frac{\sigma_1' + 2\sigma_3'}{2} \right)^R \quad (4.3)$$

Where K is a parameter containing the influence of the void ratio, σ_1' and σ_3' are the vertical and confining stresses, and R is a constant. That behavior can be found in various literature i.e. (Bartake et al., 2008), (Patel & Singh, 2009). However, the correlation function can be used to determine the path for shear wave velocity. Escribano and Nash (2015) proposed that the elastic shear modulus, Equation (4.2), on stress has been well recognized to be dependent on the particle motion directions, both σ_1' and σ_3' , as vertical and horizontal planes respectively. On the other hand, the shear wave velocity on stress acting on the wave motion included in the direction plane can be expressed in terms of elastic shear modulus. Since the clayey soil in this study was normally consolidate soil. The function of void ratio $F(e) = (7.32-e)^2/(1+e)$ was proposed by (Kokusho et al., 1982)

Consequently, in terms of $G_{max} = \rho V_s^2$, where ρ is the total density of the soil specimen and V_s is shear wave velocity of the soil mass, the V_s function $\rho = \rho_d = G_s/(1+e)$ can be used. Subsequently, the Equation (4.4) can be re-written in terms of V_s as;

$$V_s = K \cdot \left(\frac{7.32 - e}{\sqrt{G_s \rho_w}} \right) \cdot \sigma_1'^m \cdot \sigma_3'^n \quad (4.4)$$

Or

$$\log \left(\frac{V_s}{7.32 - e} \right) = \log \left(\frac{K}{\sqrt{G_s \rho_w}} \right) + m \log \sigma_1' + n \log \sigma_3' \quad (4.5)$$

Where K is ($K=1$ for isotropic condition), m and n are the constant coefficient of the vertical and horizontal effective stress respectively, ρ_d = dry density of the soil specimen, ρ_w = density of water, and G_s = specific gravity of clayed soil.

4.2.1 Shear wave velocity under monotonic drain triaxial tests (CID-mono)

In case of drain triaxial tests (CID-mono), three specimens of Bangkok clay with monotonic drain triaxial tests were carried out. The monotonic axial strain loading to the shear specimen is approximately 10% an axial strain deformation. During state to shear specimens, the peak of the shear wave velocity from relationships between the mean effective stress, q' , and shear wave velocity, V_s , during drained compression tests in Figure 4.7 has appeared. It is noted that the shear wave velocity, V_s' about 0-8% an axial strain deformation is increased. After an axial strain deformation 8 %, the shear wave velocity paths are decreased. While the relationships between shear wave velocity normalized, $V_s/F(e)$ and vertical stress, σ_1' , during drained shearing is plotted Figure 4.8 in which can be seen that shear wave velocity, V_s of CID-mono can, therefore, give the one of best presentation for the shear wave velocity normalized paths in drained triaxial compression tests. Since, the curve between shear wave velocity normalized and vertical stress, σ_1' on the logarithmic plot should be linear as very confining effective stress 150, 225, and 300 kPa . Based on equation (4.5), the values of n_1 , n_2 , and n_3 from the vertical gap between liner lines at difference confining stress are computed whereas m coefficient is to determine from the slope of the best-fitted line. The constant n determined from the gap at confining pressure stresses 150 kPa , 225 kPa , and 300 kPa are 0.6861, 0.6536, and 0.6386 respectively. The constant m is determined by the slope of the best-fitted line to be 0.0129. Consequently, it is clearly seen that those stress parameters as well as m and n coefficient direction could reasonably be presented for the drained triaxial monotonic compression test of clay. When considering the relationships between shear wave velocity and the mean effective stress, q' in Figure 4.10 under logarithmic scale the result shown that the parts of shear wave velocity as various confining of 150, 225, and 300 kPa was almost linear. The best function for determining the shear wave velocity under mean effective stress was proposed in Equation (4.6).

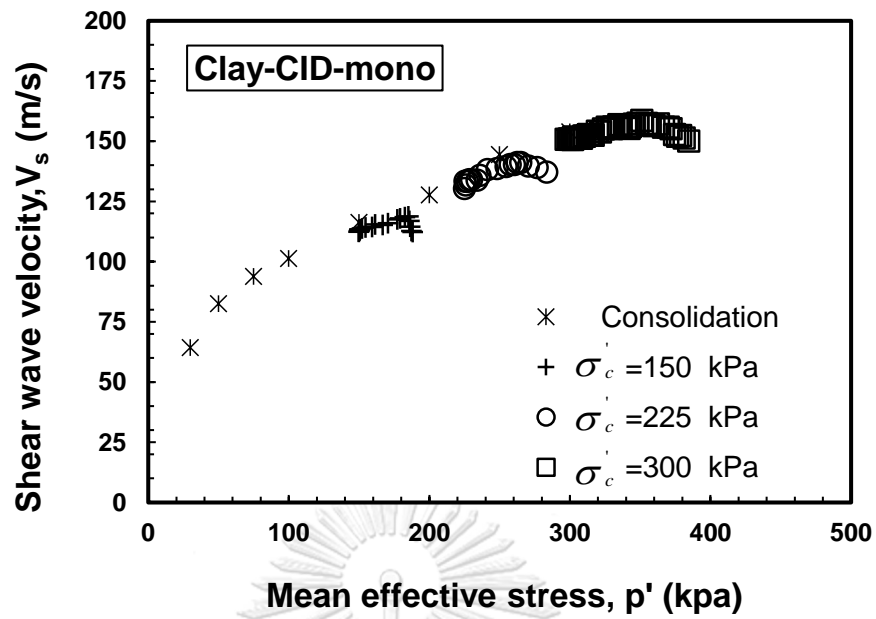


Figure 4.7 The relationship between mean effective stress and shear wave velocity of CID-mono

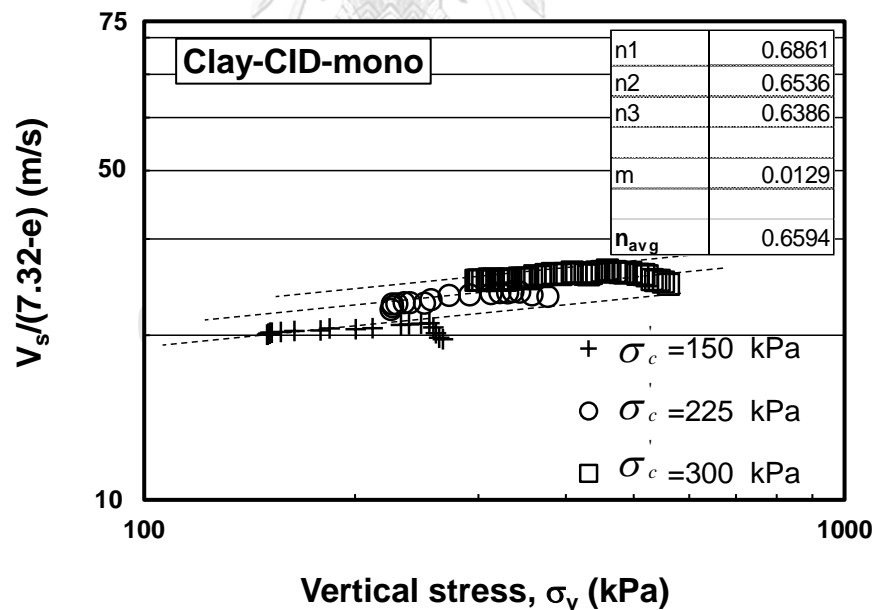


Figure 4.8 The relationship between vertical stress and $V_s/F(e)$ of clay for CID-mono

4.2.2 Shear wave velocity under load-unloading drained triaxial tests (CID-UL)

In these experimental studies, three specimens of clayey with the small loading-unloading triaxial test were carried out. This specimen was consolidated at different confining stresses (150; 225 and 300 kPa). These specimens were sheared at strain an increased about 10% strain deformation under loading-unloading triaxial tests with measured shear wave velocity using bender element during the shearing process. The paths of shear wave velocity normalized with vertical stress, σ_1' on the logarithmic curve were presented in Figure 4.10. When vertical stress, σ_1' increased. The shear wave velocity normalized at different confining pressure stresses (150; 225 and 300 kPa) is also increased. The constant n determined from gap at confining pressure stresses 150 kPa, 225 kPa, and 300 kPa are 0.6790, 0.6348, and 0.6447 respectively. The constant m is determined by the slope of the best-fitted line to be 0.0093. When comparison the influence of vertical stress, σ_1' and horizontal stress, σ_3' under the small loading-unloading drained condition with monotonic drained triaxial compression tests the results are shown that the paths of shear wave velocity are also similar. It is implied that the effect of vertical stress, σ_1' on shear wave velocity is very small or can be neglected. Therefore, it can be concluded the shear wave velocity normalized is controlled by vertical stress, σ_1' whereas the horizontal stress, σ_3' constant. This is clear that the shear wave velocity normalized is not influenced by a small loading-unloading condition.

While the paths of shear wave velocity and mean effective stress were considered under the drained triaxial loading-unloading test is shown in Figure 4.9. The result is shown that the shear wave velocity paths of each cycle as loading-unload at each confining pressure 150, 225, and 300 kPa are similarly a bit variation even though the specimens were applied by the small loading-unloading condition. This similar may be due to the state of the specimens along the path of testing is an elastic state.

By referring the relationship between shear wave velocity and mean effective stress under both conditions of CID-mono and CID-UL in Figure 4.11. This curve plots a significant were not different. There is one the best-fitted line in this curve. The best function for estimating the shear wave velocity is proposed as below:

$$V_{s\text{-drained}} = 27.38p'^{0.28} \quad (4.6)$$

The equation (4.6) can be applied to give $V_{s\text{-drained}}$ under the drained conditions in both monotonic loading and loading-unloading conditions.



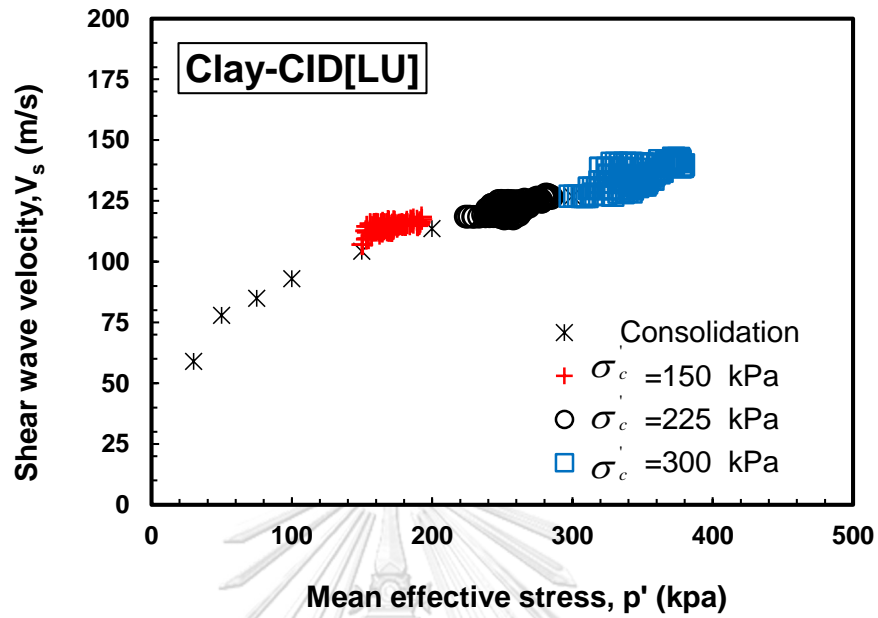


Figure 4.9 The relationship between mean effective stress and shear wave velocity of CID-LU

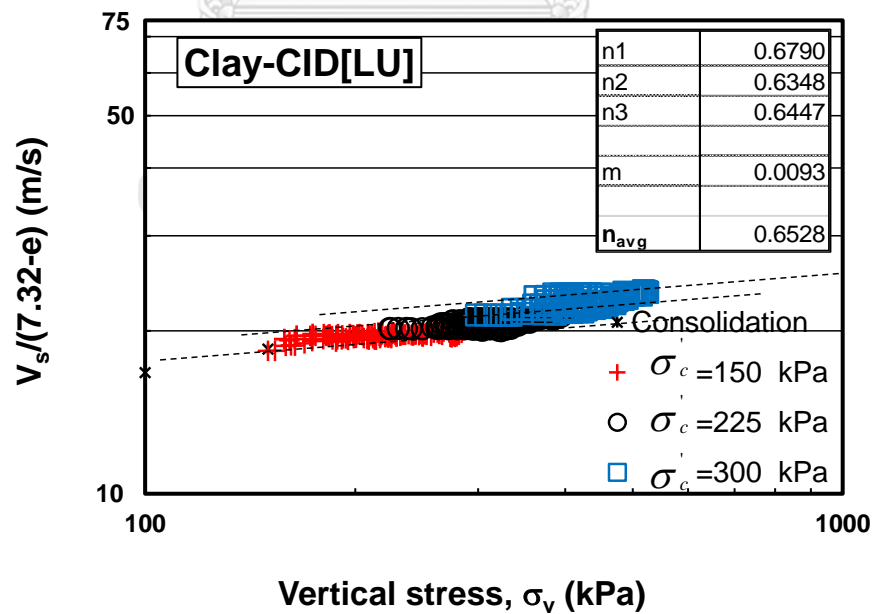


Figure 4.10 The relationship between vertical stress and $V_s/F(e)$ of clay for CID-UL

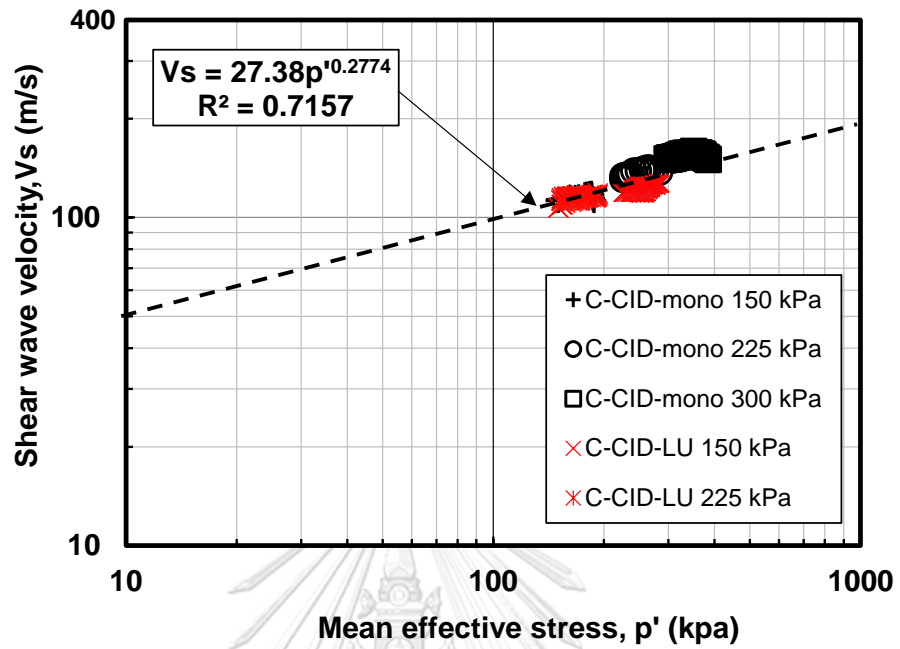


Figure 4.11 The relationship between mean effective stresses and shear wave velocity of CID-mono and CID-LU

4.2.2 Shear wave velocity under load-unloading undrained triaxial tests (CID-UL) and triaxial stress control tests (CIDS)

The entire axial strain load-unloading to the shear specimen is approximately 10% an axial strain deformation. The loading and unloading stage are presented at axial strain deformation about 10 % with strain rate to sheared specimen 0.02 min/min. In the illustrated, the peak of the deviator stress at confining stress 150 *kPa*, 225*kPa*, and 300 *kPa* that occur at strain is reached at 5.2 %, 4.7%, and 5.4% respectively. When considering the influence of the vertical effective stress σ_1' , horizontal stress σ_3' and void ratio, the results from the CIU-LU experiments in Figure 4.12. are present that the vertical effective stress σ_1' and horizontal stress σ_3' are affected by the magnitude of shear wave velocity. Note that in case of undrained triaxial compression tests, the void ratio during shearing is constant. On the other hand, The paths of shear wave velocity with mean effective stress, p' are presented in Figure 4.14. The result indicated that the shear wave velocity of undrained shearing is governed by the mean effective stress. The variation of shear wave velocity during load-unload tests to shear specimens is very small. The scatter data obtained from three confining pressure was a liner.

When considering the paths of shear wave velocity normalized $V_s/F(e)$ for undrained triaxial tests (CIU-LU) and triaxial stress control tests (CIDS), both CIU-LU and CIDS have similar developments of vertical effective stress, σ_1' , whereas the horizontal effective stress, σ_3' , along paths of the tested have changed. The dependency paths between shear wave velocity normalized $V_s/F(e)$ and vertical effective stress, σ_1' , of CIU-LU is plotted in Figure 4.12a whereas the paths between shear wave velocity normalized $V_s/F(e)$ and vertical effective stress, σ_3' , is plotted in Figure 4.12b. Base on equation (4.5), this equation to correlation shear wave velocity path cannot be used to apply for CIU-LU case.

Consequently, based on the experiments the results of the tests, the proposed an appropriate function for determining the shear wave velocity under undrained triaxial isotropic consolidation tests was presented as bellow:

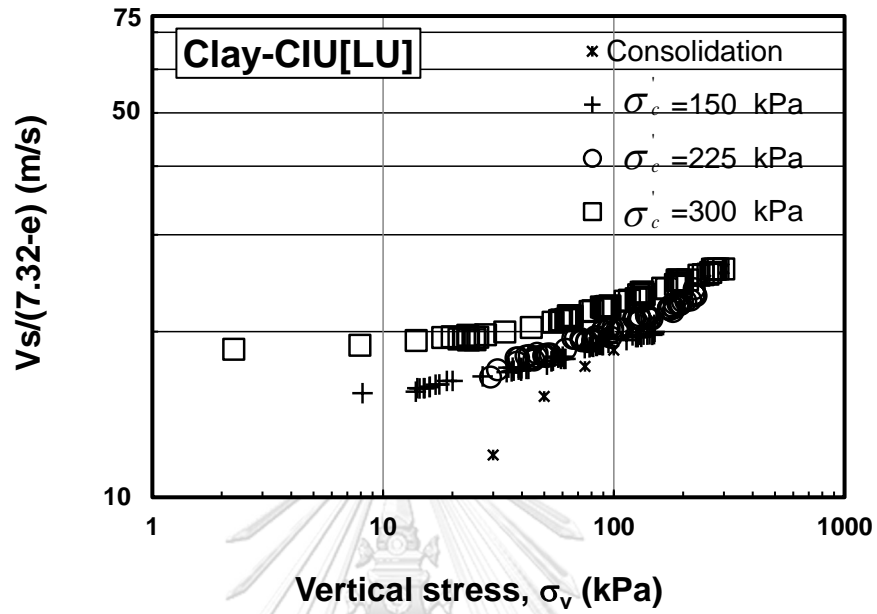
$$V_{s\text{-undrained}} = 17.572p^{0.3784} \quad (4.7)$$

It is good accuracy for under undrained triaxial isotropic consolidation tests due to R^2 more than 0.9676.

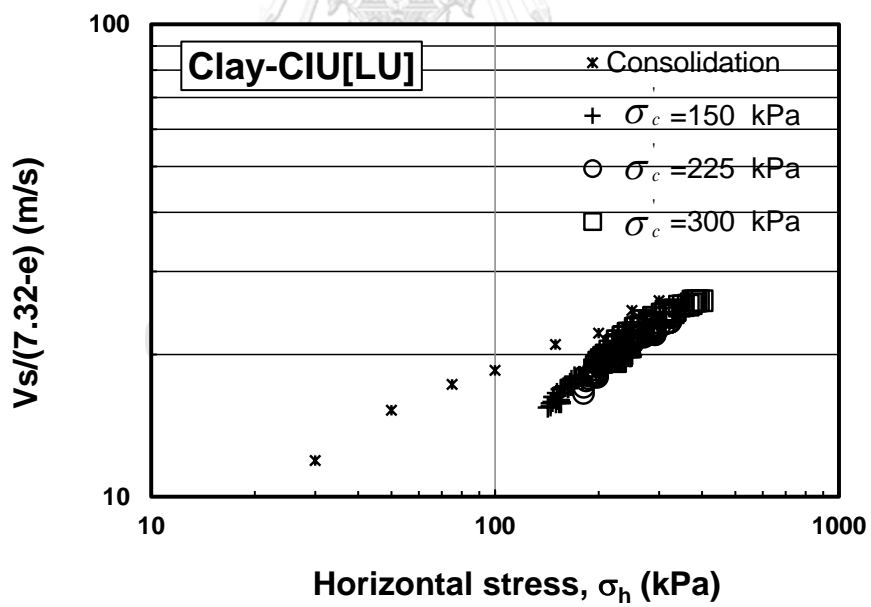
As regarding for CIDS experiments, the stress with mean effective constant, p' 150, 225, and 300 *kPa* were performed. The strain loading of each specimen was approach to axial strain approximately 8% to 14%. The results of vertical effective stress with shear wave velocity are illustrated in Figure 4.13a. The results demonstrate that the path of shear wave velocity of each sample during increasing the vertical stress, σ_1' , while decreasing the horizontal stress, σ_3' , are almost constant. Moreover, when considering the effects of void ratio from the path of shear wave velocity normalized $V_s/F(e)$ with vertical stress, σ_1' , and the horizontal stress, σ_3' , in the logarithmic curve are illustrated in 4.13a and 4.13b. The results indicated that the shear wave velocity normalized, $V_s/F(e)$ significantly increase when increasing vertical stress, σ_1' , whereas the horizontal stress, σ_3' , decreased is observed. The best-fitted lines from logarithmic at each effective confining pressure on the results were significantly linear. The $V_{s\text{-CIDS}}$ function equation (4.8) is proposed as bellow:

$$V_{s\text{-CIDS}} = 70.631 p'^{0.1308} \quad (4.8)$$

It is clear that in case of vertical effective stress σ_1' and horizontal stress σ_3' changes during shearing, the V_s can be estimated by equation (4.8).

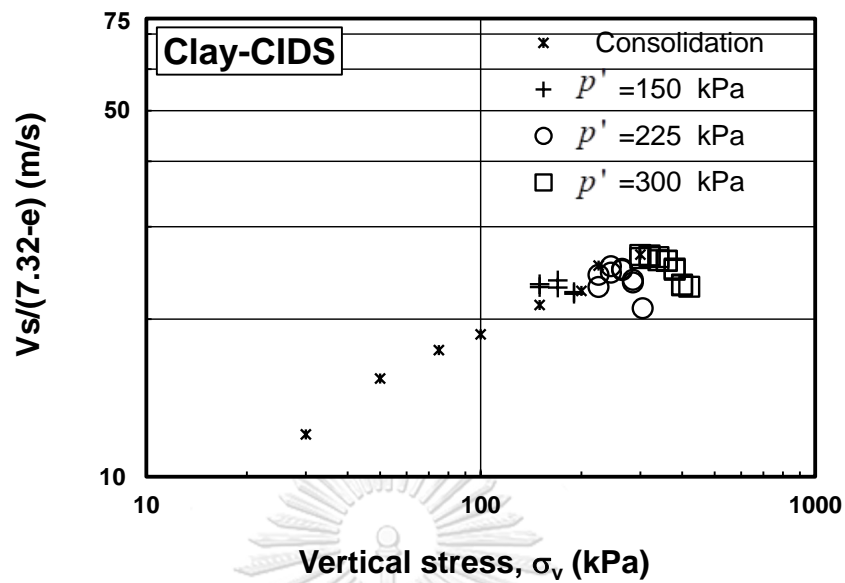


(a)

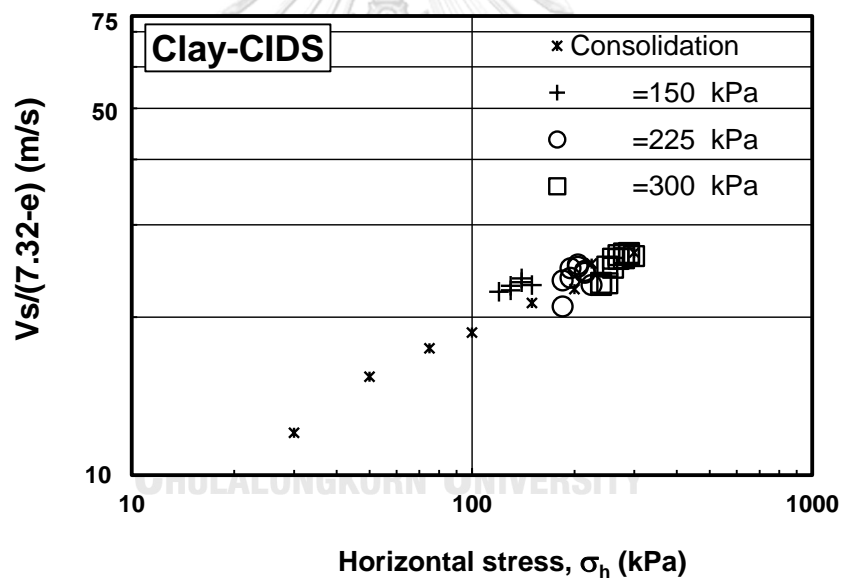


(b)

Figure 4.12 (a) shows the relationship between vertical stress, σ_v , and V_s normalized of CIU-LU and (b) shows the relationship between horizontal stress, σ_h , and V_s normalized



(a)



(b)

Figure 4.13 (a) shows the relationship between vertical stress, σ_v' , and V_s normalized of CIU-LU and (b) shows the relationship between horizontal stress, σ_h' , and V_s normalized

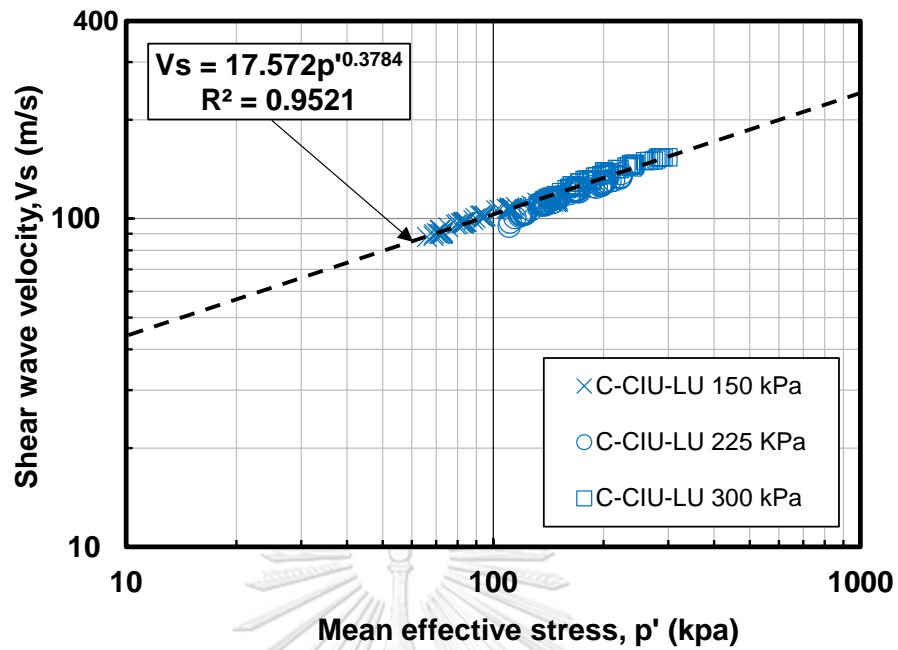


Figure 4.14 The relationship between mean effective stress and shear wave velocity of CIU-LU

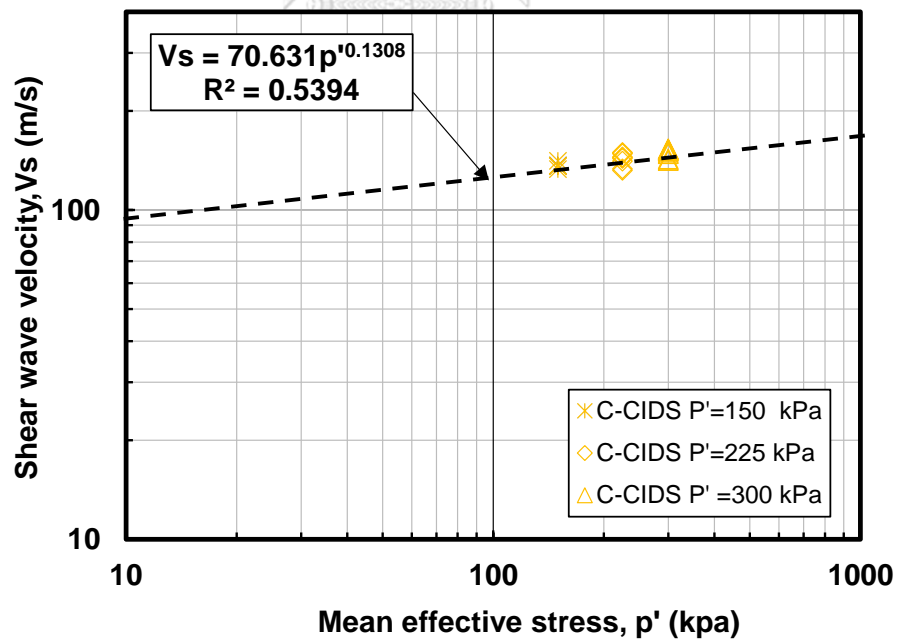


Figure 4.15 The relationship between mean effective stress and shear wave velocity of CIDS

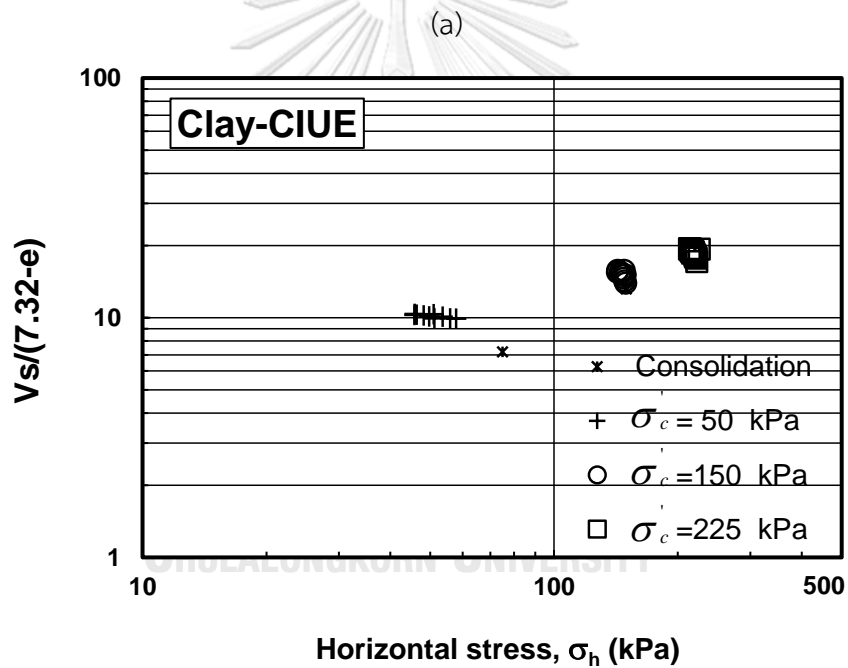
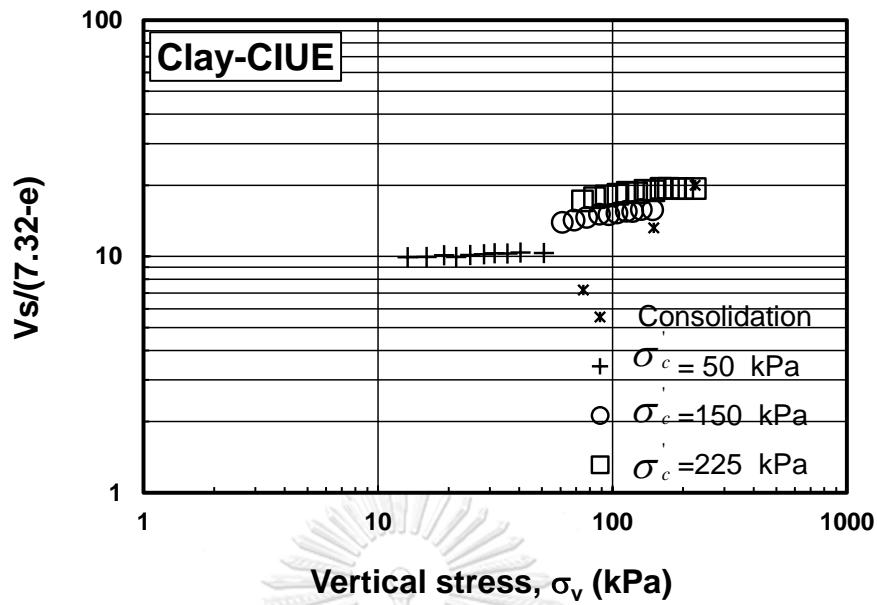
4.2.3 Shear wave velocity under drained triaxial extension (CIDE) and undrained triaxial extension (CIDE)

In this experimental study, the drained triaxial extension and undrained triaxial extension various confining of 50, 225, and 300 were experimental by a stress control test. These specimens were sheared at strain an increased about 3-4% strain deformation. Based on finding in Figure 4.17. The data have shown that the paths of the shear wave velocity various confining pressure under drained triaxial extension and undrained triaxial extension on the logarithmic curve were linear. The paths of shear wave velocity in both conditions are the same. Since the same magnitude of confining pressure was employed.

The best-fitted lines from the logarithmic curve at each effective confining pressure on the results were significantly linear. The V_{s-CIUE} and V_{s-CIDE} function equation (4.9) is proposed as bellow:

$$V_{s-CIUE}, V_{s-CIDE} = 12.696 p^{0.42} \quad (4.9)$$

Therefore, the results indicated that paths of shear wave velocity of the drained and undrained triaxial extension were not governed by deviator stress. On the other hand, the paths of shear wave velocity under drained and undrained triaxial extension were dependent on mean effective stress.



(b)

Figure 4.16 (a) shows relationship between vertical stress, σ_v' , and V_s normalized of CIUE and (b) shows relationship between horizontal stress, σ_h' , and V_s normalized

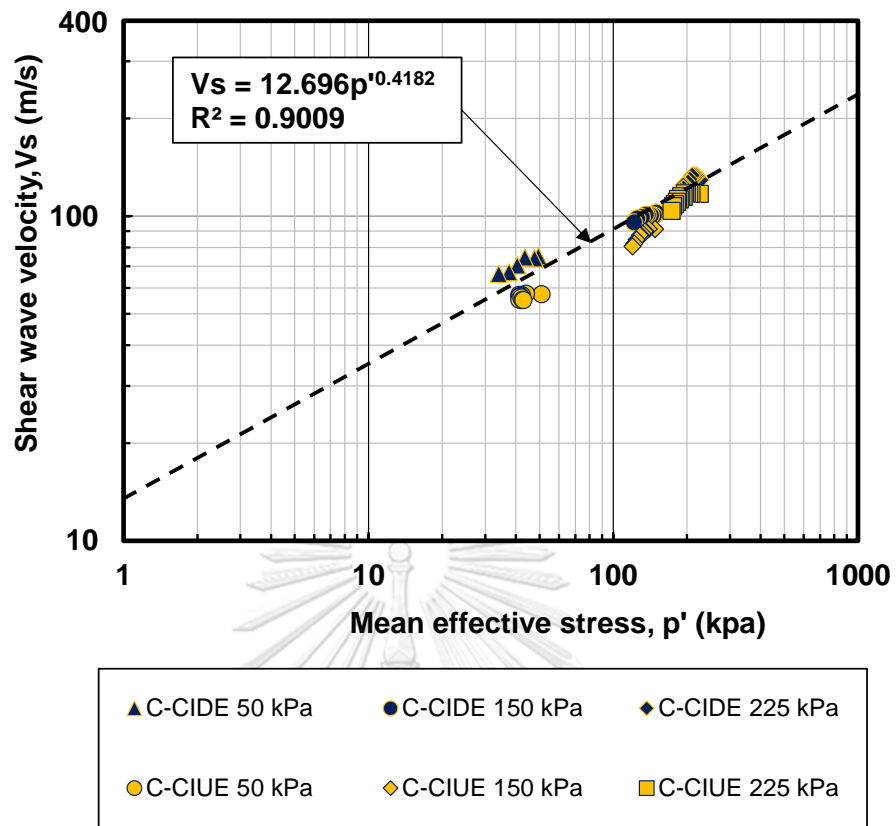


Figure 4.17 The relationship between mean effective stress and shear wave velocity of drained triaxial extension (CIDE) and undrained triaxial extension (CIUE)

3.3 An identification stress parameter for clay-based on shear wave velocity

In this study, the characteristics of shear wave velocity were categorized into two groups. Herein, both drained and undrained conditions were explored to optimize the correlation function in order to estimate the shear wave velocity under various stress paths of clay. As the results show, the main empirical equation (4.5) is adopted to find out the stress parameter as acting on vertical effective stress, σ_1' and horizontal effective stress, σ_3' whereas the void ratio function proposed by (Jamiolkowski, Lancellotta, & Lo Presti, 1995) was randomly selected by an initial void ratio value of clayed soil specimen. The equation (4.5) is not sufficient to calculate the path of shear wave velocity for undrained as well as mean effective constant, p' conditions.

According to the test results, the paths of shear wave velocity against mean effective stress of clay soil under CID-mono, CID-LU, CIU-LU, CIUE, CIDE, and CIDS triaxial testing in Figure 4.18. The scatter under the entire conditions tests in this figure given the straight-line equation to V_s value was proposed which gives rise to

$$V_s = 23.248p'^{0.3112} \quad (4.10)$$

These results concluded that a new V_s function is applicable for predicting the path of shear wave velocity. This is done separately for CID-mono, CID-LU, CIU-LU, CIUE, CIDE, and CIDS for clay.

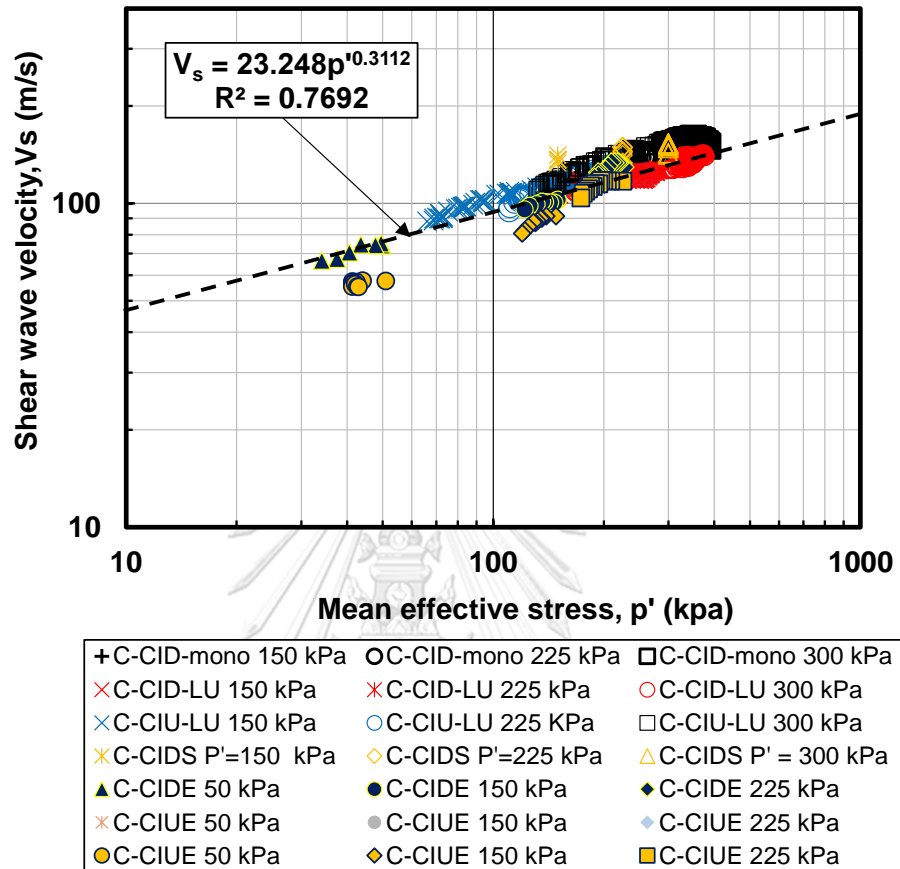


Figure 4.18 Shows the paths of shear wave velocity various mean effective stress of clay soil under CID-mono, CID-LU, CIU-LU, CIUE, CIDE and CIDS triaxial testing

4.3 Dependency of the elastic shear modulus of Bangkok clay from triaxial tests

4.3.1 Dependency of elastic shear modulus subjected to monotonic drained triaxial compression tests (CID-mono)

This is widely recognized that the shear wave velocity, the shear stiffness G_{\max} can be calculated from the elastic wave propagation theory as this equation :

$$G_{\max} = \rho V_s^2 \quad (4.11)$$

where, ρ is the total density of the soil specimen V_s and shear wave velocity of the soil mass. Base on (Roesler, 1979) and (Escribano & Nash, 2015), In case of triaxial drained compression tests, the dependency for the elastic shear stiffness in wave propagation paths and particle motion directions can be explained by σ_1^m and σ_3^n . The dependency of stress to correlate the shear modulus can be expressed as :

$$G = K_1 \cdot F(e) \cdot \sigma_1^{m'} \cdot \sigma_3^{n'} \quad (4.12)$$

In term of normalized elastic shear modulus can be rewritten as:

$$\frac{G}{F(e)} = K \cdot \sigma_1^{m'} \cdot \sigma_3^{n'} \quad (4.13)$$

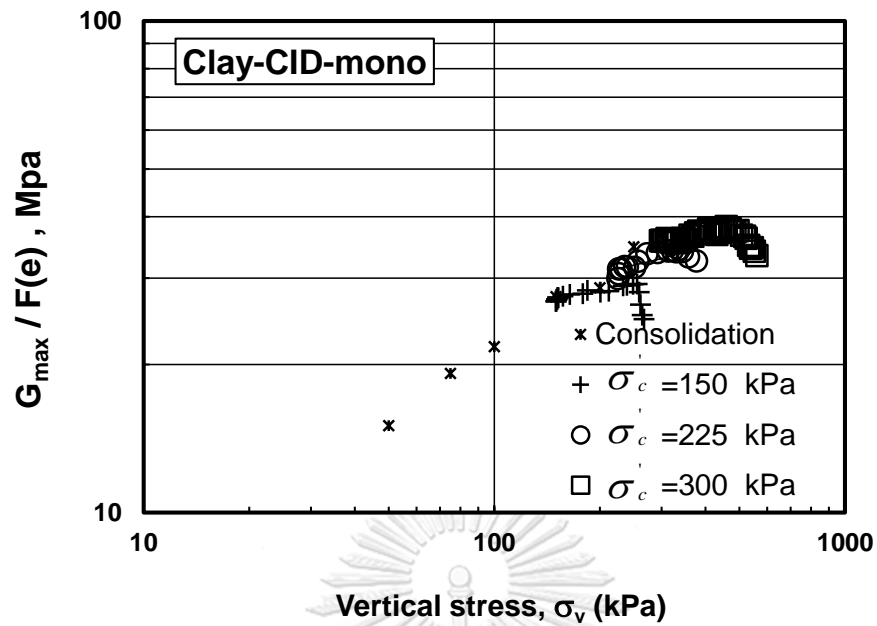
Or

$$\log\left(\frac{G}{F(e)}\right) = \log K + m \log(\sigma_1') + n \log(\sigma_3') \quad (4.14)$$

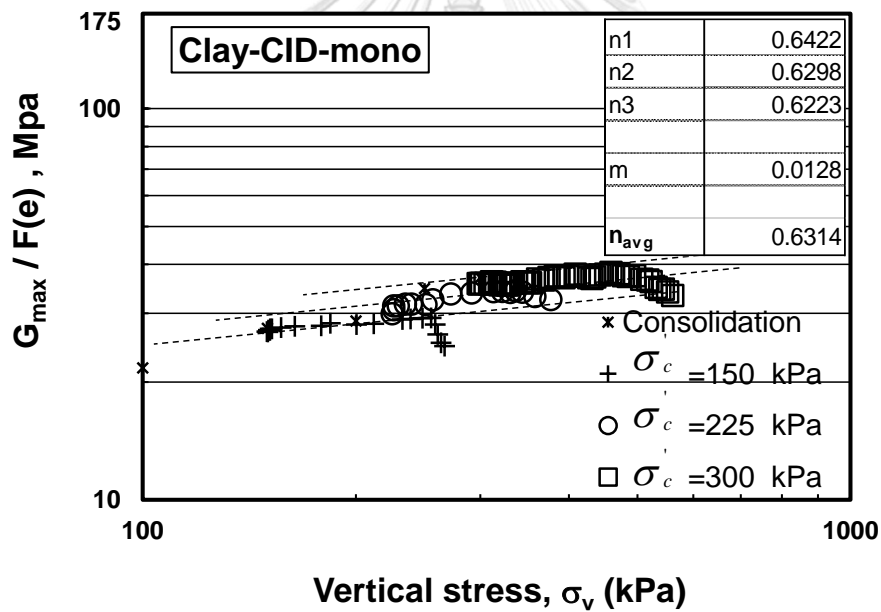
Where G is elastic shear modulus, $F(e) = (7.32-e)^2/(1+e)$ (e.g Kokusho et al., 1982), is adopted for clay, K isare the n and m ($K=1$ for isotropic condition), σ_h'/σ_v constant coefficient of the effective vertical stress σ_1' and effective horizontal stress respectively. The relationships between elastic shear modulus normalized, $G/F(e)$ and vertical stress, σ_1' , during drained shearing is plotted Figure 4.19a and 4.19b in which can be seen that the elastic shear modulus normalized, $G/F(e)$ of CID-mono can therefore give the one of best presentation for the elastic shear modulus normalized paths in drained triaxial compression test. Since, the curve between

elastic shear modulus normalized and vertical stress on the logarithmic plot should be linear as very confining effective stress 150, 225 and 300 kPa. The n_1 , n_2 , and n_3 from the vertical gap between liner lines at difference confining stress are computed by Equation (4.14) whereas m coefficient is to determine from the slope of the best-fitted line. For monotonic drained triaxial compression tests (CID-mono), the constant n determined from a gap at confining pressure stresses 150 kPa, 225 kPa, and 300 kPa are 0.6422, 0.6298, and 0.6223 respectively. The average is 0.6314 while constant m is determined by the slope of the best-fitted line to be 0.0128. Consequently, it is seen that those stress parameters, as well as m and n coefficient direction, could reasonably be presented for the drained triaxial compression test of clay.

As regards the drained triaxial compression tests, the corresponding elastic shear modulus and elastic shear modulus normalized which indicated that the mean effective stress, $(\sigma'_1 + 2\sigma'_3)/3$, are influenced in Figure 4.21 and Figure 4.22. the results indicated that the value of elastic shear modulus at various effective confining pressure of 150, 225, and 300 kPa are dependent on the value of effective confining pressure and void ratio during shearing specimen.



(a)

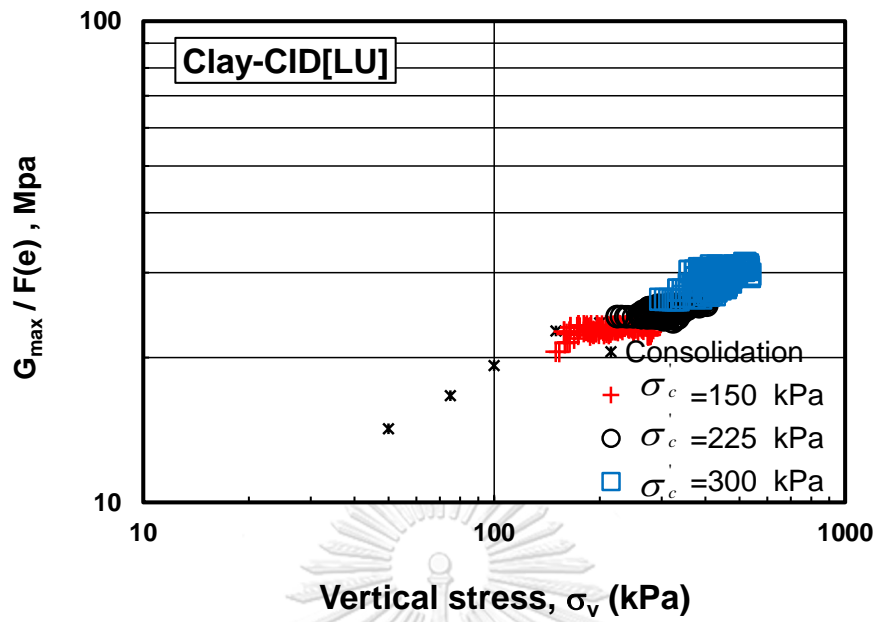


(b)

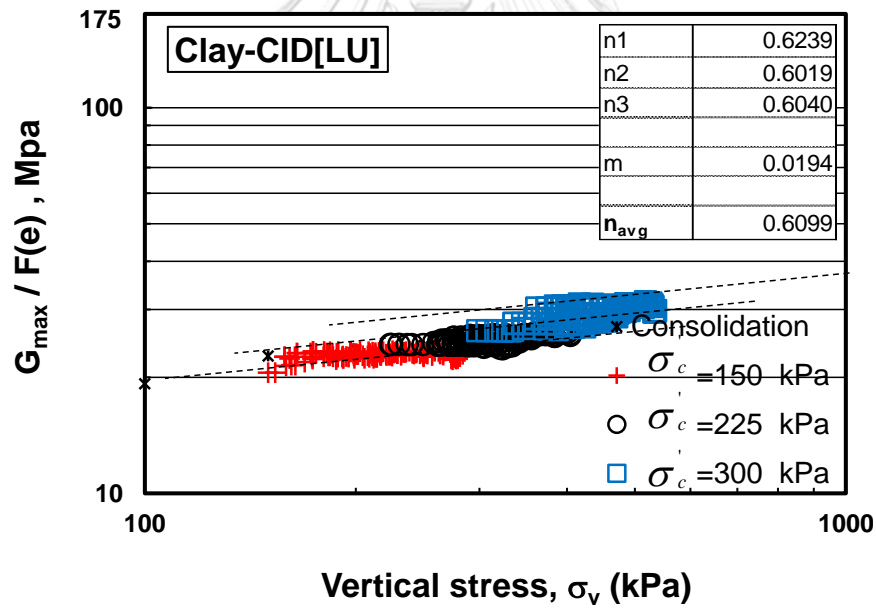
Figure 4.19 The results of CID-mono test on clay soil specimens: (a) and (b) vertical effective stress and elastic shear modulus normalized

4.3.2 Dependency of elastic shear modulus subjected to drained triaxial loading-unloading tests (CID-LU)

A series of clayed soil specimens subjected to drained triaxial small loading-unloading tests were performed. The small loading and unloading stage is approached at axial strain deformation about 10 %. Each cycle load-unloading shearing specimens, 0.2 % axial strain deformation was applied. For the results of the tests, the paths of elastic shear modulus various vertical stress effective stress were considered under the drained triaxial small loading-unloading test is shown in Figure 4.20a. The result is indicated that the elastic shear modulus paths of each cycle as loading-unloading at each confining pressure 150, 225, and 300 kPa are almost similar when compared with monotonic drained triaxial compression tests. Since the entire specimens during testing is an elastic state. Consequently, the method to determine m and n coefficient from the vertical gap between liner lines and the slope of the best-fitted line at different confining stresses was perfectly related with the monotonic drained triaxial compression tests (CID-mono). In the case of CID-LU test, the constant n determined from the gap at confining pressure stresses 150 kPa, 225 kPa, and 300 kPa are 0.6239, 0.6019, and 0.6040 respectively. The average is 0.6099 while constant m is determined by the slope of the best-fitted line to be 0.0194. When comparison m and n coefficient from monotonic drained triaxial compression tests (CID-mono) and drained triaxial small loading-unloading tests (CID-LU), it was found that m and n coefficient under both cases of CID are almost similar.



(a)



(b)

Figure 4.20 The results of CID-LU test on clay soil specimens: (a) and (b) vertical effective stress and elastic shear modulus normalized

When considering the relationship between mean effective stress with elastic shear modulus and elastic shear modulus normalized under drained triaxial monotonic tests and drained triaxial small loading-unloading tests in Figure 4.21 and Figure 4.22. The paths observed of elastic shear modulus under both applied conditions as the various effective confining pressure of 150 kPa 225kPa and 300 kPa were small variation. On the other hand, by referring to the relationship between mean effective and elastic shear modulus normalized under drained triaxial monotonic tests and drained triaxial small loading-unloading tests in Figure 4.22, the paths of both conditions were little deviate. As the same various effective confining pressure of 150 kPa 225kPa and 300 kPa the small variation of elastic shear modulus normalized due to loading-unloading was observed. The scatter of the results is the curve can be obtained to give the elastic shear modulus and the elastic shear modulus normalized function under the isotropic drained condition and the isotropic drained loading-unloading condition as follows:

The elastic shear modulus is

$$G_{\max} = 1.038p^{0.59} \quad (4.15)$$

The elastic shear modulus normalized is

$$G/F(e) = 3.41p^{0.37} \quad (4.16)$$

Consequently, elastic shear modulus normalized calculated under drained conditions tests was close to calculate from two methods. One is under both of vertical effective stress and horizontal effective stress and another one is mean effective stresses. In this case the researcher proposed that the elastic shear modulus normalized under mean effective stress is sufficient to calculated G in finite element.

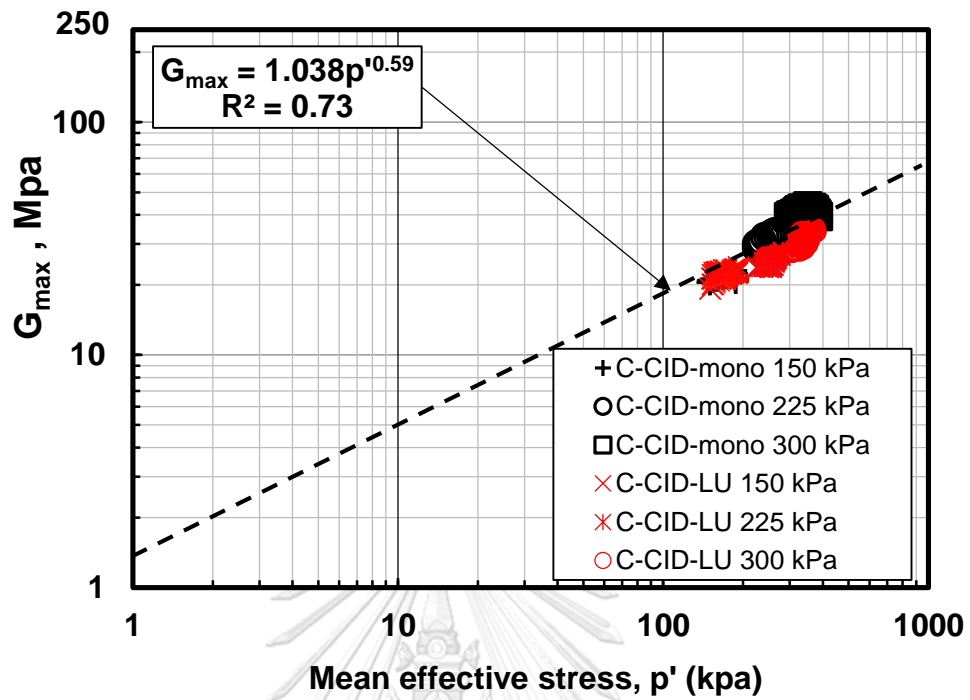


Figure 4.21 The results of CID-mono and CID-LU test on clay soil specimens: mean effective stress and elastic shear modulus

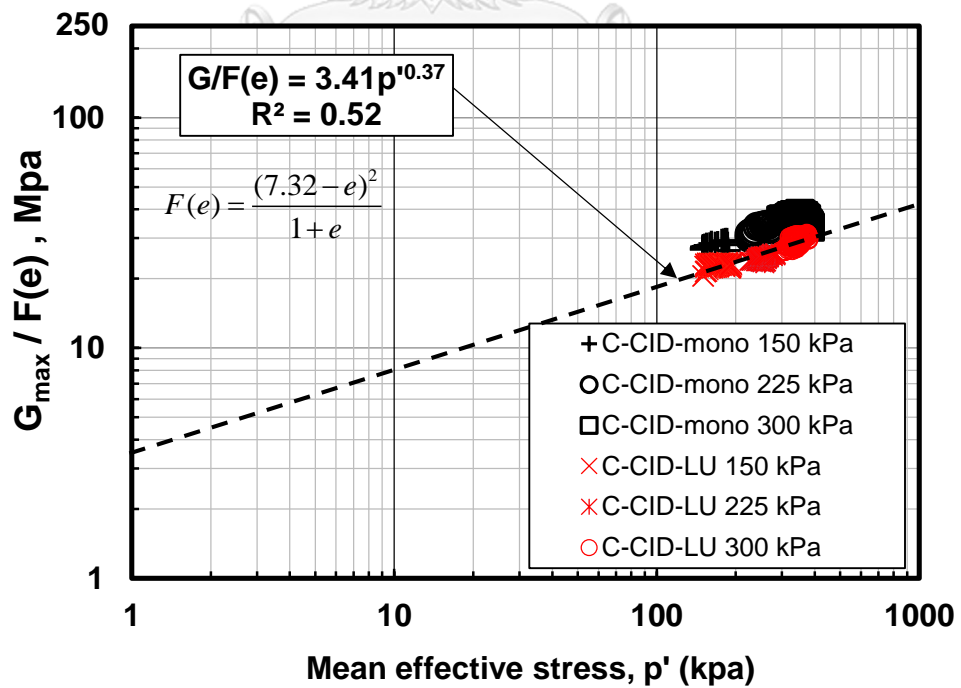


Figure 4.22 The results of CID-mono and CID-LU test on clay soil specimens: mean effective stress and elastic shear modulus normalized

4.3.3 Dependency of elastic shear modulus subjected to undrained triaxial small loading-unloading tests (CIU-LU)

A series of isotopically consolidation triaxial undrained compression tests were tested. For results carried out are plotted in Figure 4.23 to Figure 4.25. The compression and small extension stages are demonstrated at axial strain deformation about 10 % with strain rate to sheared specimen 0.02 min/min. For the relationship between vertical effective stress, σ'_1 and horizontal effective stress, σ'_3 with elastic shear modulus normalized, $G/F(e)$ in Figure 4.23a and 4.23b at strain, ϵ about 0-10%, it was observed that the vertical stress σ'_1 and the elastic shear modulus normalized, $G/F(e)$ and the horizontal stress σ'_3 and the elastic shear modulus normalized cannot, therefore, give the of linear paths in both direction under undrained triaxial compression tests. Consequently, the normalized empirical equation (4.12) and equation (4.13) from previous studies as drained condition tests for clay are not sufficient to determine the m and n constant. On the other hand, when considering the relationship between mean effective stress, p' with elastic shear modulus and elastic shear modulus normalized are shown in Figure 4.24 and 4.25. These results indicated that the path of elastic shear modulus was developed by the mean effective stress, p' or the stress state during shearing (Teachavorasinskun & Amornwithayalax, 2002) and (Teachavorasinskun et al., 2002) or those stress components in the polarization planes) (Roesler, 1979). It can be implied that the trend of elastic shear modulus, variations with the effective confining stress was relatively affected by those specimens . Besides, the paths to examine the value of elastic shear modulus function under the isotropic undrained condition triaxial tests with various confining pressure of 150, 225, and 300 kPa were proposed. The relationship between mean effective stress and elastic shear modulus was illustrated in Figure 4.24. It is seen that the straight paths of elastic shear modulus function with various confining pressure of 150, 225, and 300 kPa were obtained. The scatter of the results is the curve can be obtained to give the best function under the isotropic undrained condition as follows:

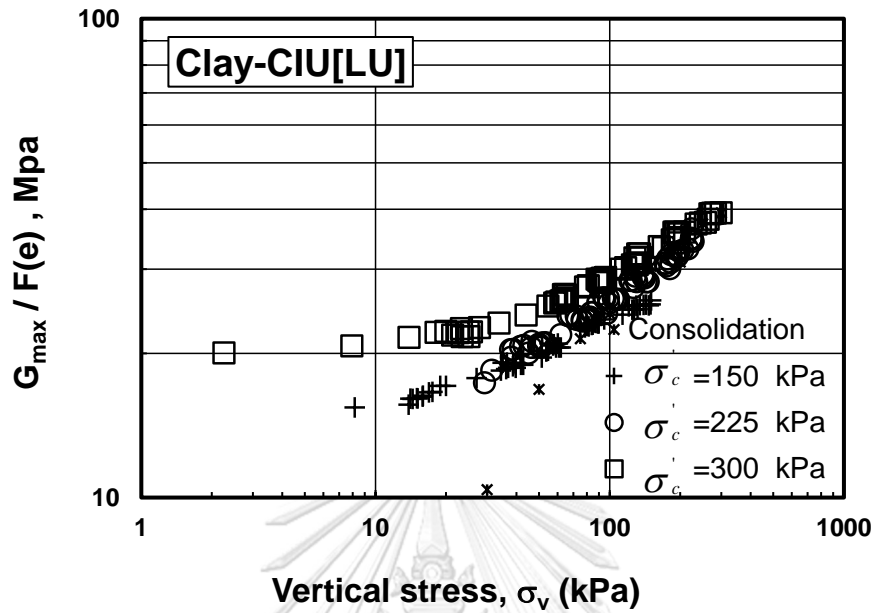
$$G_{\max [\text{undrained}]} = 0.451p'^{0.78} \quad (4.17)$$

The value of elastic shear modulus from this study was lower than the value of G_{\max} which is compared by Likitlersuang & Teachavorasinskun, 2007, and (Ratananikom, Likitlersuang, & Yimsiri, 2013). It may be due to the effect of varying conditions of soil which were included by the stress history of soil, different depth of the soil and the initial state of the clayey soil.

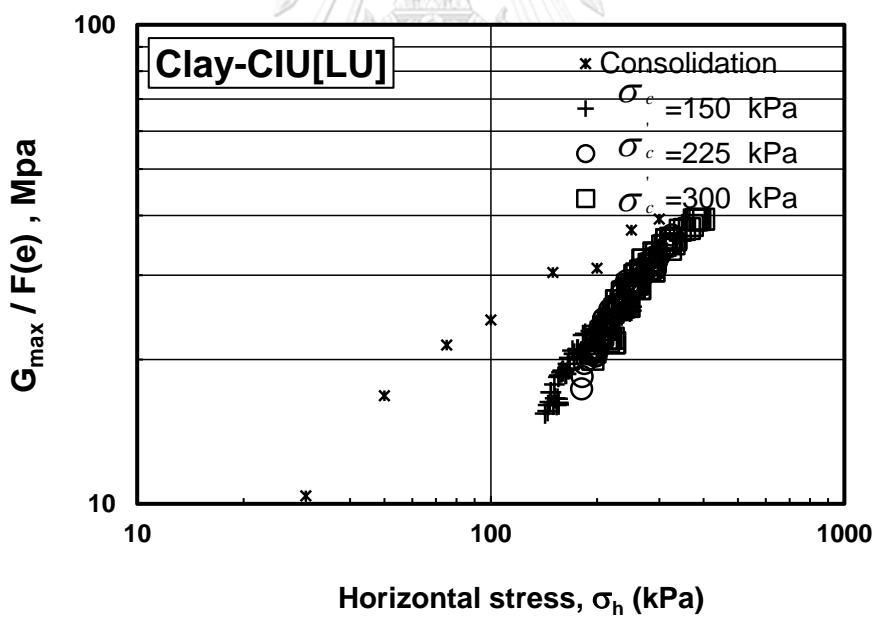
When considering the relationship between mean effective stress and elastic shear modulus normalized in Figure 4.25. The results indicated that the trend of paths elastic shear modulus normalized as various confining pressure of 150, 225, and 300 kPa were practically to linear. The scatter of the results is the curve can be obtained to give the elastic shear modulus function under the isotropic undrained condition as follows:

$$G/F(e)_{[\text{undrained}]} = 1.067p'^{0.64} \quad (4.18)$$

In case of under isotropic undrained condition, the Equation (4.18) can be employed to determine G . When the relationship between mean effective stress and elastic shear modulus normalized proposed by Teachavorasinskun S and Akkarun T, 2004 and Sumaryono, 2004 was compared in Figure 4.25. The result showed that the paths of elastic shear modulus normalized from previous studies were little variation. It may be due to different conditions of soil properties, void ratio function adopted, different depth of the soil, and stress history of the clayey soil.



(a)



(b)

Figure 4.23 The results of CID-LU test on clay soil specimens: (a) vertical effective stress with elastic shear modulus normalized, and (b) horizontal effective stress with elastic shear modulus normalized.

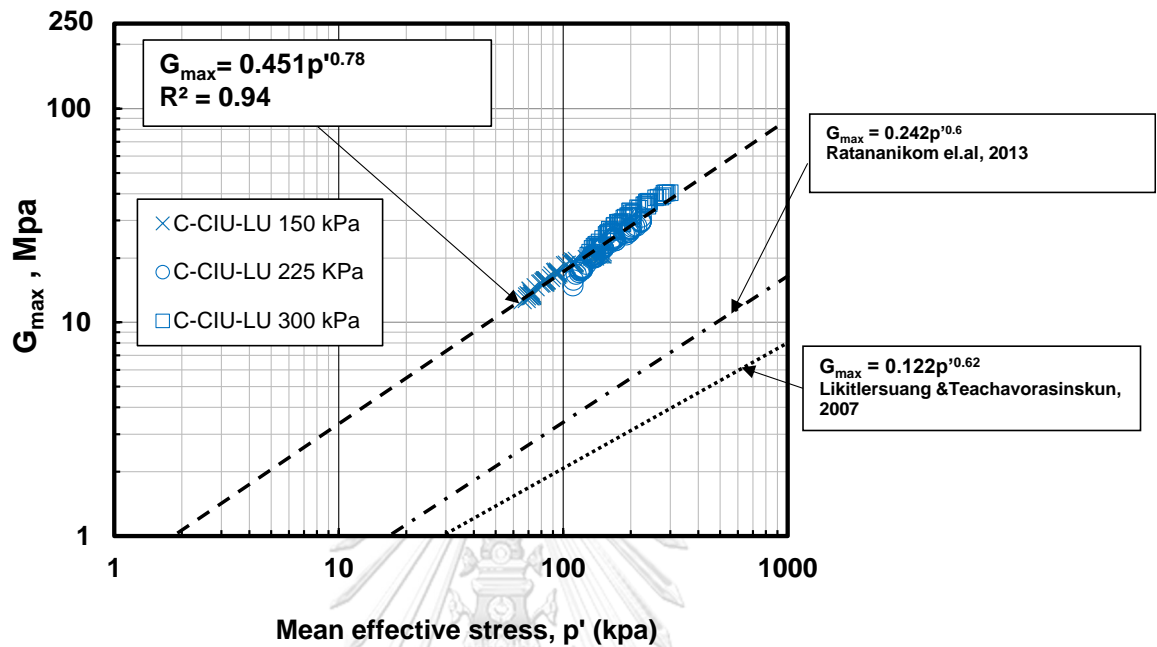


Figure 4.24 The results of CIU-LU test on clay soil specimens: mean effective stress and elastic shear modulus

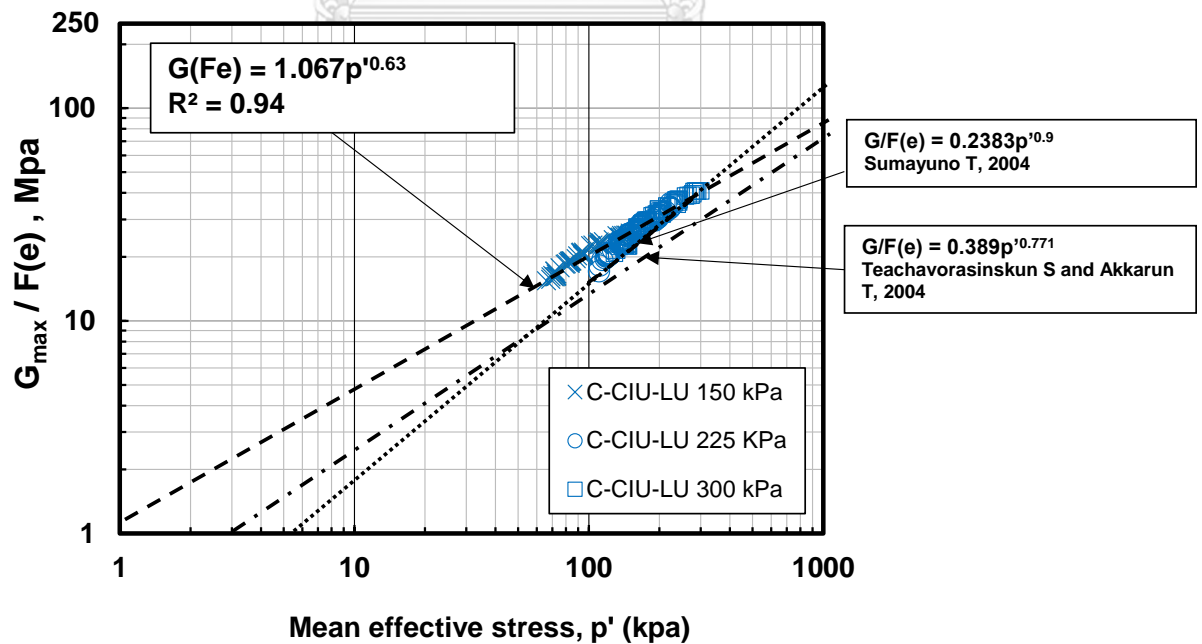


Figure 4.25 The results of CIU-LU test on clay soil specimens: mean effective stress and elastic shear modulus normalized

4.3.4 Dependency of elastic shear modulus under stress control tests (CIDS)

These results of elastic shear modulus attained in stress-controlled tests can also be performed by stress-controlled test results as shown in Figure 4.26-4.28. The vertical stress, σ'_1 and horizontal stress, σ'_3 with elastic shear modulus normalized, $G/F(e)$ during shearing are plotted Figure 4.26a and Figure 4.26b which can be indicated that the development of the elastic shear modulus normalized govern by the vertical stress, σ'_1 and horizontal stress, σ'_3 during shearing. The orientation path of shear modulus normalized, $G/F(e)$ about 0-4 % strain, ϵ was almost stable. Since the path of shear wave velocities motion during shearing was almost stable at 0-4 % strain. At strain more than 4%, the path of shear wave velocities and the path of shear modulus normalized, $G/F(e)$ can also be decreased depending on the magnitude of shear wave velocities motion during shearing. Consequently, in case of p' constant, the paths of elastic shear modulus normalized in the plan of vertical effective stress, σ'_1 and horizontal effective stress, σ'_3 cannot be able to determine the mand n coefficient.

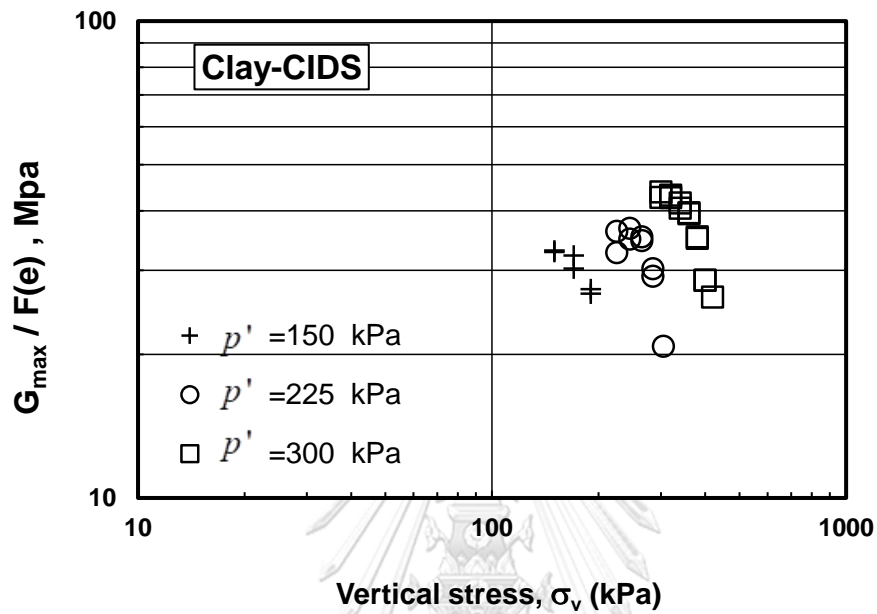
By referring to the relationship between elastic shear modulus and mean effective constant' is presented in Figure 4.27. The value of G_{\max} without normalized with the various mean effective constant of 150 kPa, 225 kPa, and 300 kPa are small variables. The elastic shear modulus function obtained from triaxial mean effective constant is

$$G_{\max [p' \text{ constant}]} = 8.904p'^{0.25} \quad (4.19)$$

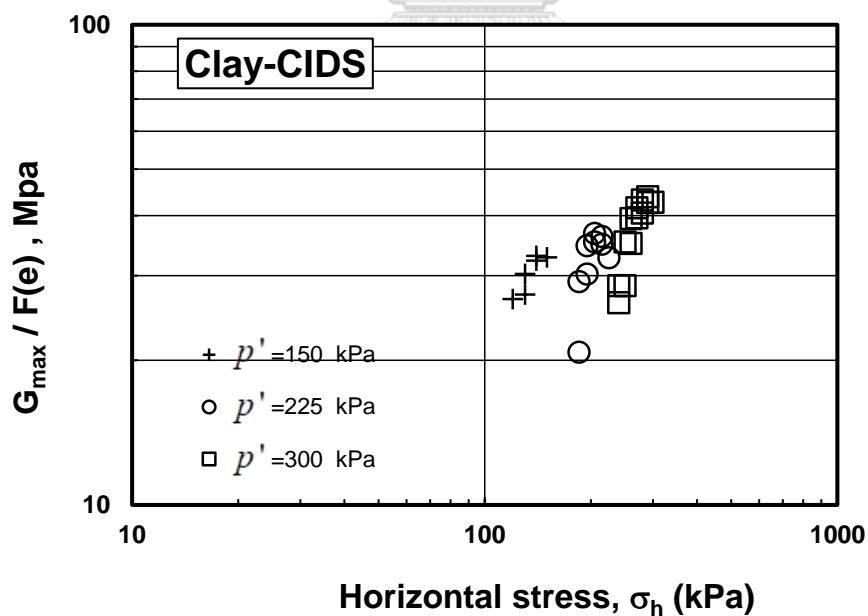
For the elastic shear modulus normalized and mean effective constant' is illustrated in Figure 4.28. The paths of elastic shear modulus normalized as the various mean effective constant of 150 kPa, 225 kPa, and 300 kPa are almost stable. The elastic shear modulus normalized function is governed by fitting the results. The equation for the mean effective constant test is obtained as follows:

$$G/F(e)_{[p' \text{ constant}]} = 8.152p'^{0.26} \quad (4.20)$$

Therefore, the equation (4.19) and equation (4.20) can be adopted to determine the elastic shear modulus and elastic shear modulus normalized at every the mean effective stress.



(a)



(b)

Figure 4.26 The results of CIDS test on clay soil specimens: (a) relationship vertical stress with elastic shear modulus normalized and (b) horizontal stress with elastic shear modulus normalized



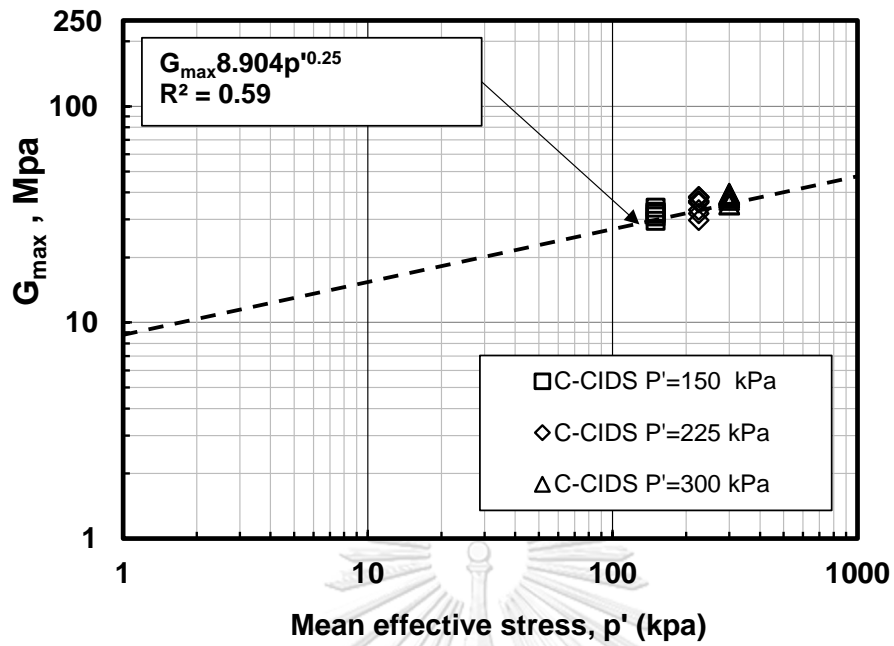


Figure 4.27 The results of CIDS test on clay soil specimens: mean effective stress and elastic shear modulus

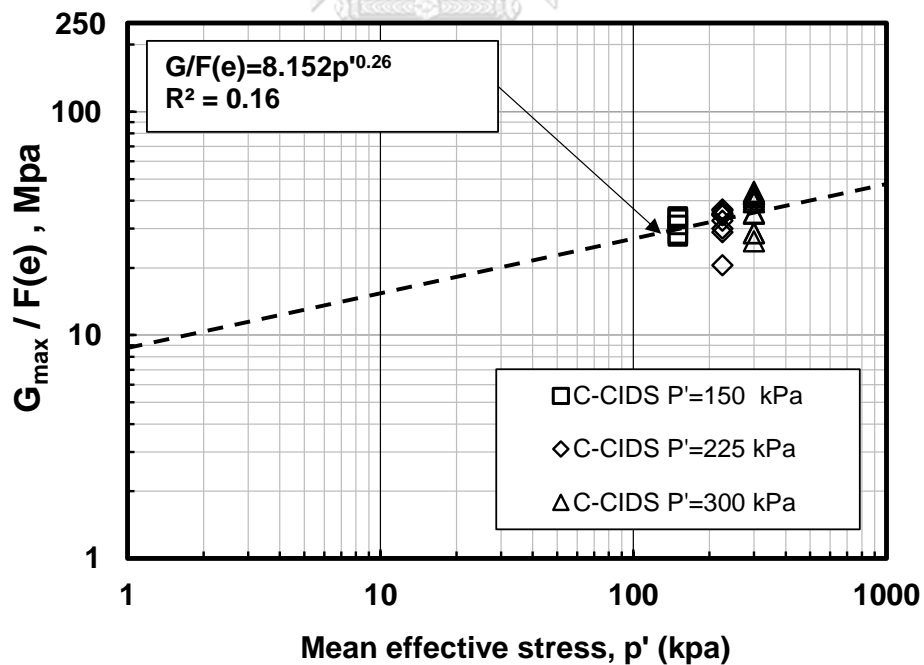


Figure 4.28 The results of CIDS test on clay soil specimens: mean effective stress and elastic shear modulus normalized

4.3.5 Dependency of elastic shear modulus under drained triaxial extension (CIDE) and undrained triaxial extension (CIUE)

This section is to investigate the dependency of elastic shear modulus under drained triaxial extension and undrained triaxial extension which were applied extension load by air pneumatic air cylinder. These series of triaxial extension tests were tested with various confining pressure of 50, 150, and 225 kPa respectively. The results of triaxial extension test were presented in Figure 4.29 to Figure 4.32. For undrained triaxial extension, the vertical effective stress σ_1' , horizontal stress σ_3' with elastic shear modulus normalized) was plotted in Figure 4.29a and Figure 4.29b. The results showed that the path of elastic shear modulus normalized with the vertical effective stress σ_1' as various confining pressure 50, 150, and 225 kPa was almost linear whereas the path elastic shear modulus normalized with horizontal effective stress σ_3' was very deviated. This difference due to the change of horizontal stress σ_3' along path of the tests. Thus, in case of undrained triaxial extension the paths of elastic shear modulus normalized were governed by vertical effective stress σ_1' , horizontal stress σ_3' . The normalized empirical equation (4.13) and equation (4.14) from previous studies as drained condition tests for clay are not sufficient to determine elastic shear modulus in terms of stresses direction. On the other hand, Figure 4.30a to Figure 4.30c presented the relationship between elastic shear modulus normalized against the vertical effective stress σ_1' . The results indicated that the direction paths of elastic shear modulus normalized with vertical effective stress σ_1' on a logarithmic scale with various confining pressure of 50, 150, and 225 kPa were linearly observed. Therefore from the experimental, the equation function (4.14) was sufficient for determining and predicting the path of elastic shear modulus normalized under drained triaxial extension test. The value of coefficient m and coefficient n of Bangkok clay under drained extension condition can be determined by using empirical equation (4.14). From the test results, the coefficient m from the slope line was to be 0.0690 beside n_1 , n_2 , and n_3 were calculated as various confining pressure of 50, 150, and 225 kPa were to be 0.5389, 0.5292, and 0.5553 respectively. Consequently, the empirical equation function (4.14) with

coefficient m and coefficient n calculated was an alternative method for determining the elastic shear modulus normalized under drained triaxial extension test which can be applied for finite element analysis.

In addition, when considering the relationship between elastic shear modulus against mean effective stress and the relationship between elastic shear modulus normalized by void function various mean effective stress in Figure 4.31 and Figure 4.32 was presented. The orientations paths of elastic shear modulus normalized under undrained triaxial extension and drained triaxial extension. These paths were taken from three confining pressure of 50, 150, and 225 kPa using shearing strain about 3% extension. The results indicated that the trend of paths elastic shear modulus normalized as various confining pressure of 50, 150, and 225 kPa were practically to linear. The scatter of the results under undrained triaxial extension and drained triaxial extension from logarithmic plotted can be obtained to give the elastic shear modulus function as follows:

Undrained elastic shear modulus;

$$G_{\max} [\text{undrained extension}] = 0.138p^{0.59} \quad (4.21)$$

$$G/F(e)_{[\text{undrained extension}]} = 0.594p^{0.65} \quad (4.22)$$

Drained elastic shear modulus;

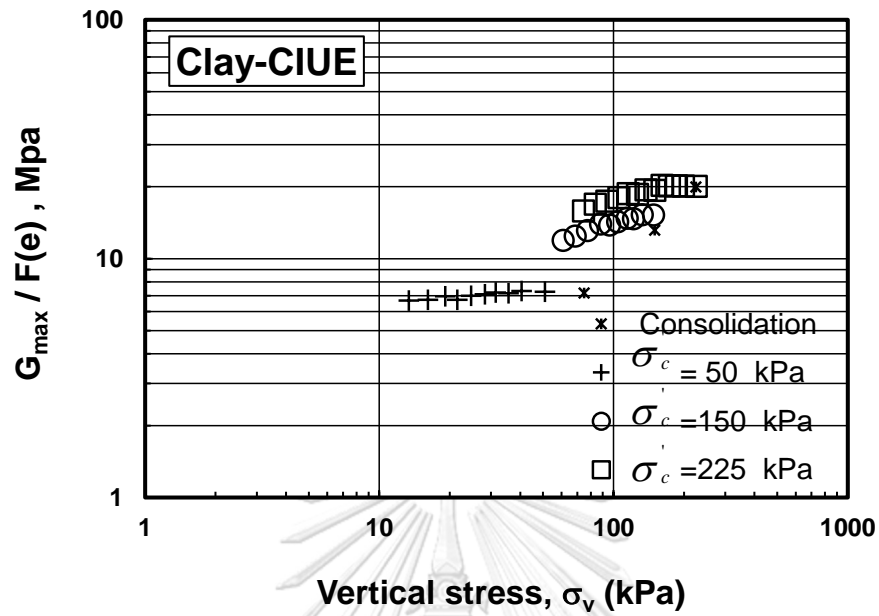
$$G_{\max} [\text{drained extension}] = 0.138p^{0.54} \quad (4.23)$$

$$G/F(e)_{[\text{drained extension}]} = 0.594p^{0.65} \quad (4.24)$$

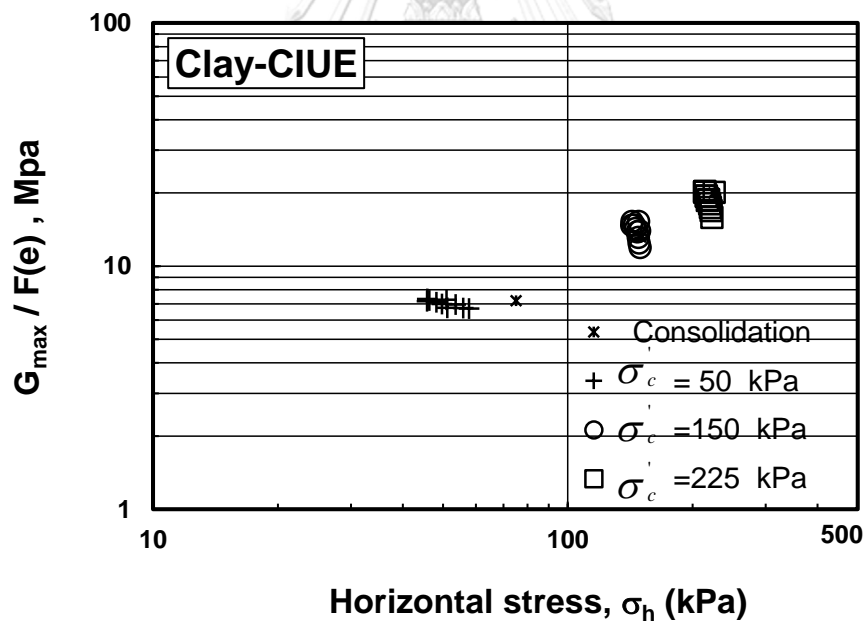
When comparing the paths of elastic shear modulus normalized under undrained triaxial extension and drained triaxial extension, the result indicated that the path of the drained triaxial extension was higher than the path of undrained triaxial extension. The obtained value of elastic shear modulus normalized under undrained triaxial extension was lower than drained triaxial extension. It may be due to the effect of terms of effective stress and void ratio which were effect on the value of elastic shear modulus.

For both condition tests, the failed point was no observed. It is important to note that at the deviator stress measured from the large strain extension may not give true value. It is due to the gape during shearing between top cape and pedestal and clayey soil specimens may be one sores error.



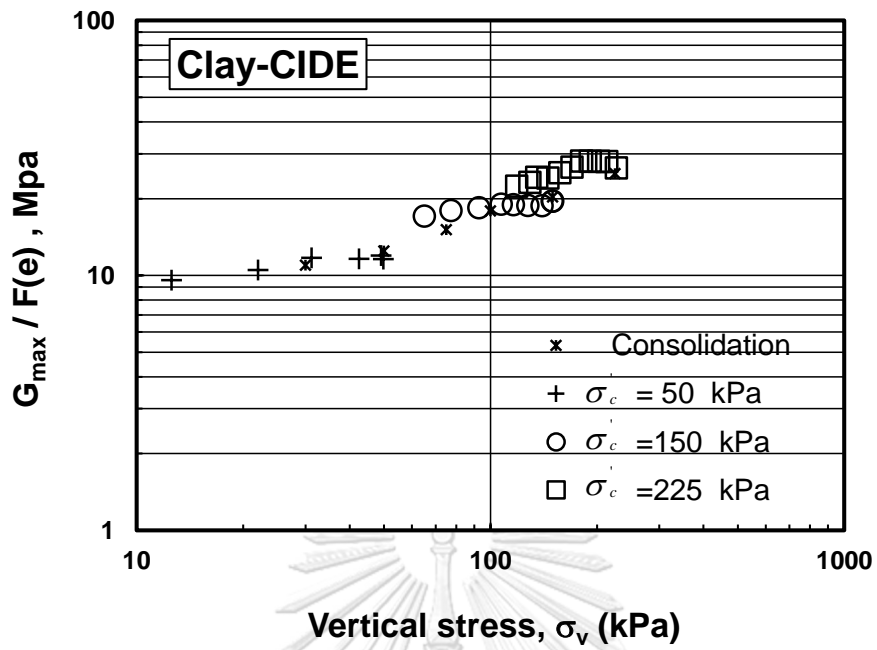


(a)

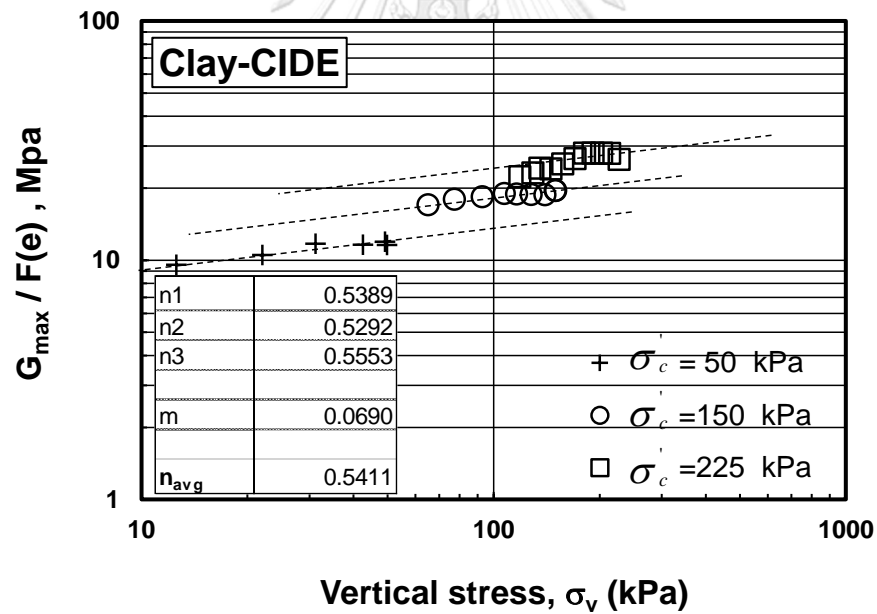


(b)

Figure 4.29 The results of CIUE test on clay soil specimens: (a) relationship vertical stress with elastic shear modulus normalized and (b) horizontal stress with elastic shear modulus normalized



(a)



(b)

Figure 4.30 The results of CIDE test on clay soil specimens: (a) relationship vertical stress with elastic shear modulus normalized and (b) horizontal stress with elastic shear modulus normalized

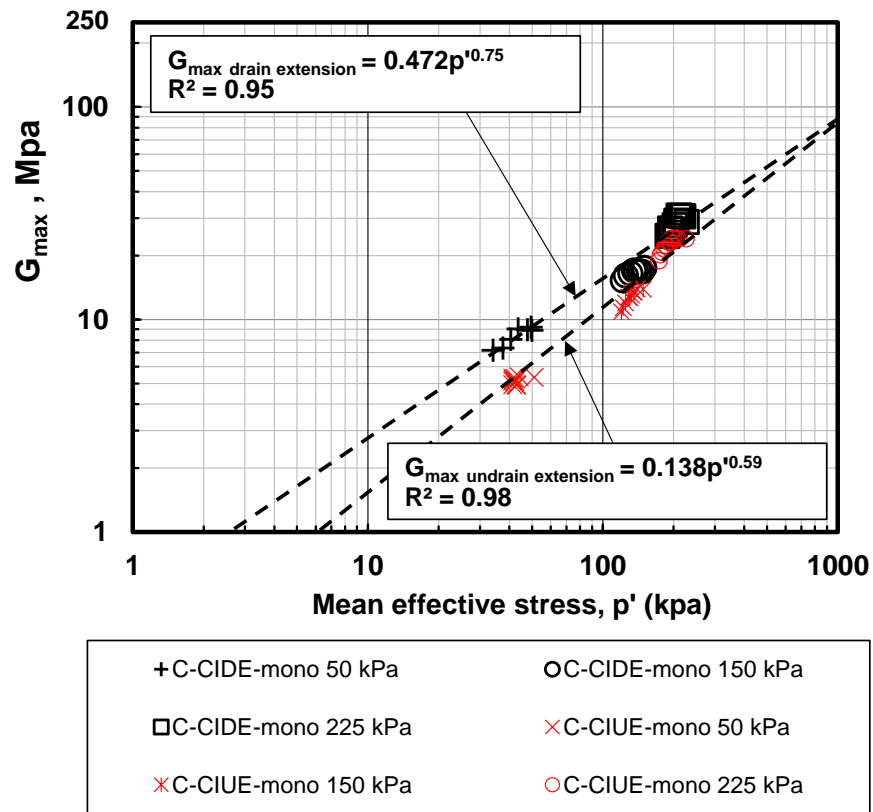


Figure 4.31 The results of CIUE and CIDE on clay soil specimens: mean effective stress and elastic shear modulus

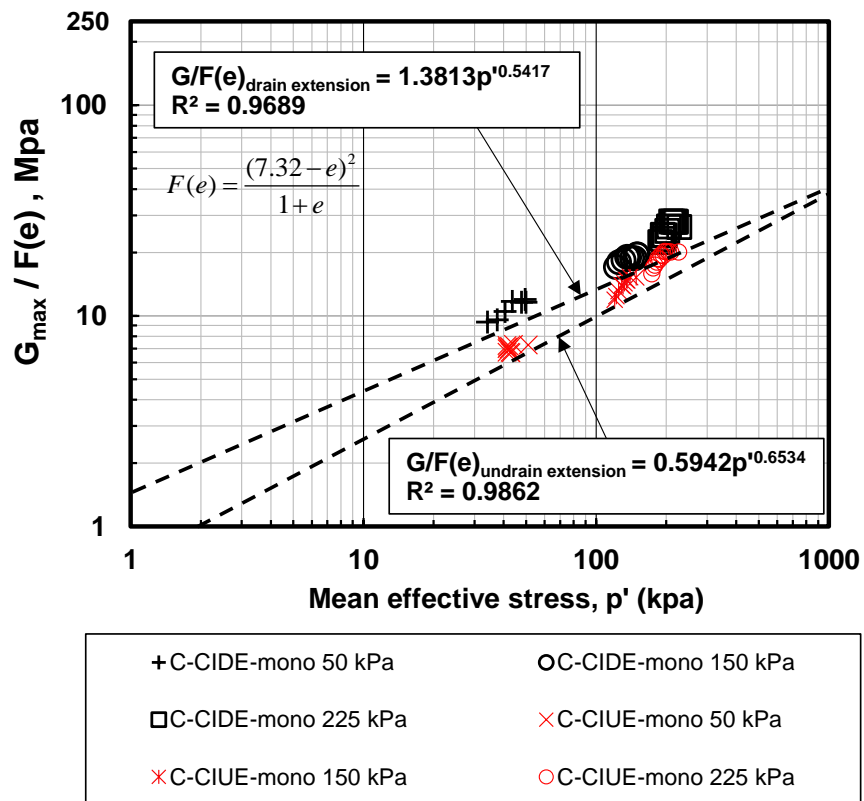


Figure 4.32 The results of CIUE and CIDE on clay soil specimens: mean effective stress and elastic shear modulus normalized

4.3.6 An identification elastic shear modulus for Bangkok clay

As regarding for small strain to large strain loading, the curve fitting technique of normalized elastic shear modulus and vertical stress path from the logarithmic curve was employed to determine the $G/F(e)$ function with n exponent. However, in case of drained condition test coefficient m was computed by slope between vertical stress, σ'_1 and normalized elastic shear modulus $G/F(e)$ while horizontal stress, σ'_3 was constant. It is only practical to adopt the coefficient m and n value for effective confining stress and its constant. Thus, a good agreement between the coefficient m and n was not only performed for undrained and p' constant conditions. Moreover, in the case of CIU-LU, CIUE, and CIDS, the vertical stress and the horizontal stress change during state shearing, the equation of drained condition was not applicable for the entire case.

The paths of elastic shear modulus under triaxial compression and extension against mean effective stress were shown in Figure 4.33. The variation of elastic shear modulus during shearing under triaxial compression and extension are similar. The results indicated that the paths of elastic shear modulus under drained and undrained conditions are dependent on two-component stresses which were the vertical stress and the horizontal stress. Based on the experimental test results, The scatter data from entire result can be given the empirical equation between the mean effective stress and shear modulus for Bangkok clays as follows:

$$G_{\max} = 0.775p'^{0.65} \quad (4.25)$$

By referring $G/F(e)$ with mean effective stress of entire results in Figure 4.34 was presented. The path obtained from entire data of CID-LU, CID-mono, CIU-LU, CIUE, CIDE, and CIDS in logarithmic scale is that the $G/F(e)$ function can be established and is close to $G/F(e)$ calculated under various condition for triaxial isotropic consolidation test. The $G/F(e)$ of the entire is obtained as follows

$$G/F(e) = 2.269p'^{0.46} \quad (4.26)$$

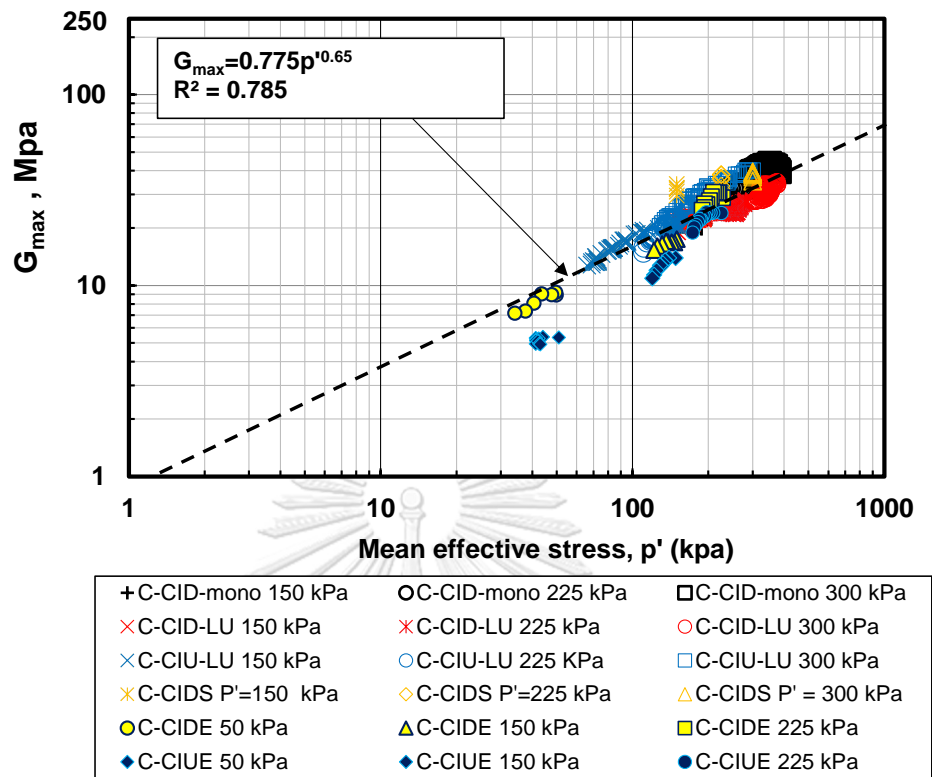


Figure 4.33 Relationship between mean effective stress and elastic shear modulus of entire experiments

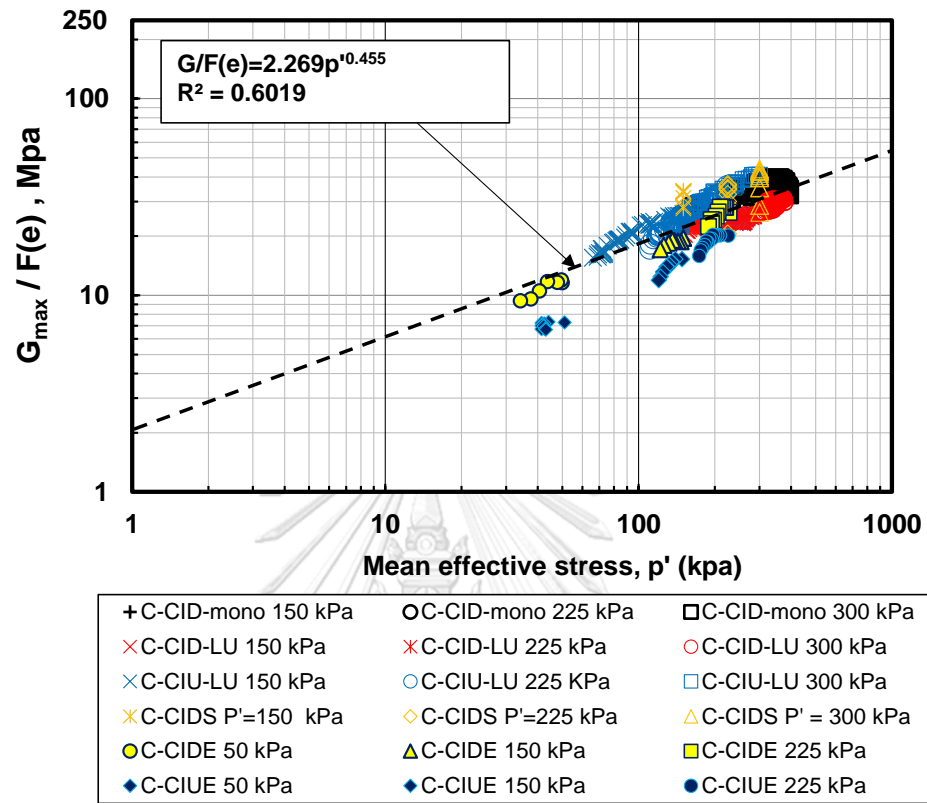


Figure 4.34 Relationship between mean effective stress and elastic shear modulus normalized of entire experiments

4.4 G-bender element and G-secant of Bangkok clay

4.4.1 Undrained G-bender element with G-secant

The degradation curve of both G_{BE} and G_{sec} is proposed in Figure 4.35. These magnitudes of G_{BE} and G_{sec} in an undrained degradation curve along with paths shearing specimens with various confining stress as 150 kPa, 225 kPa, and 300 kPa were usually the difference. A small strain level, G_{BE} is higher than G_{sec} due to the difference method for measuring G . The G-bender during the shearing process can be computed through the relationship between G-bender and G-secant against shear strain. The G-bender equation was proposed by (Chan, 2007). The gap in degradation curve between G_{BE} and G_{sec} with various shear strain, γ can be determined as follows:

$$G_{BE-undrained} = (1-\eta)G_{int,BE} + \eta G_{sec} \quad (4.27)$$

Where η is strain function which is calculated by equation (4.28).

$$\eta = \frac{G_{BE} - G_{int,BE}}{G_{sec} - G_{int,BE}} \quad (4.28)$$

Where η before shearing is equal to zero. Because the range of $G_{int,BE}$ and G_{BE} as first shear strain, γ is the same point. In case of undrained triaxial test, η function as various confining pressure 150 kPa, 225kPa, and 300 kPa can be determined the equation (4.28) . The η average strain function from the relationship between η and various shear strain, γ are:

$$\eta_{undrained} = 0.1817\gamma^{0.32} \quad (4.29)$$

To establish a function for determination $G_{BE-undrained}$, $\eta_{undrained}$,the equation (4.27) is substituted in equation (4.29). The new $G_{BE-undrained}$ equation for determination from the conventional triaxial test without bender element system is :

$$G_{BE-undrained} = (1-0.1817\gamma^{0.32})G_{int,BE} + 0.1817\gamma^{0.32}G_{sec} \quad (4.30)$$

According to Figure 4.35, the degradation curves of both $G_{BE-undrained}$ measured from bender element system and $G_{BE-undrained}$ with various confining pressure of 150 kPa, 225kPa, and 300 kPa from Equation (4.30) was compared. A small strain zone $0.001 \leq \gamma \leq 0.1$, a small variation of $G_{BE-undrained}$ calculation were observed. For $\gamma > 0.1$, $G_{BE-undrained}$ obtained based on calculation with various confining pressure is more variation. It is implied that at a larger strain zone, $\gamma > 0.1$, η value is suitable to predict the $G_{BE-undrained}$.

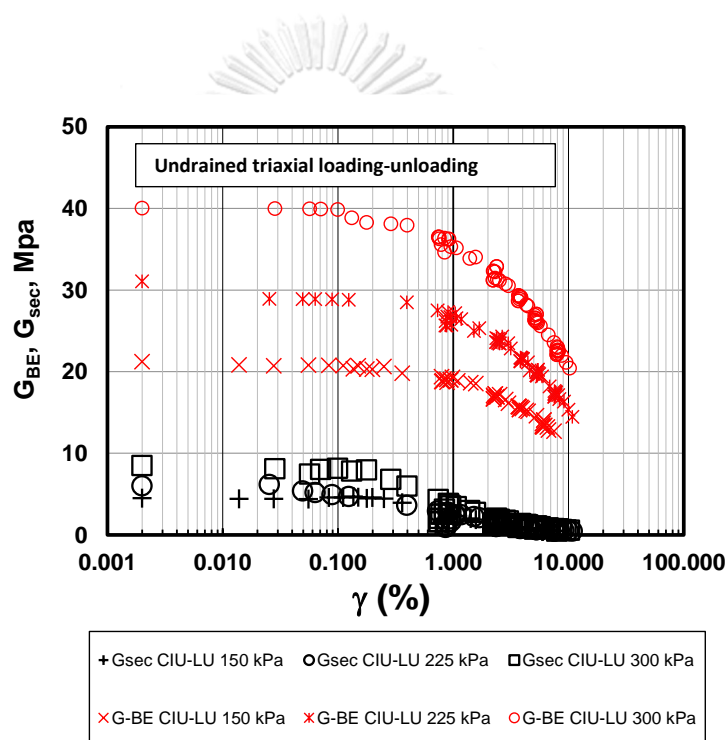


Figure 4.35 Relationship between G_{BE} and G_{sec} various shear strain under undrained tests

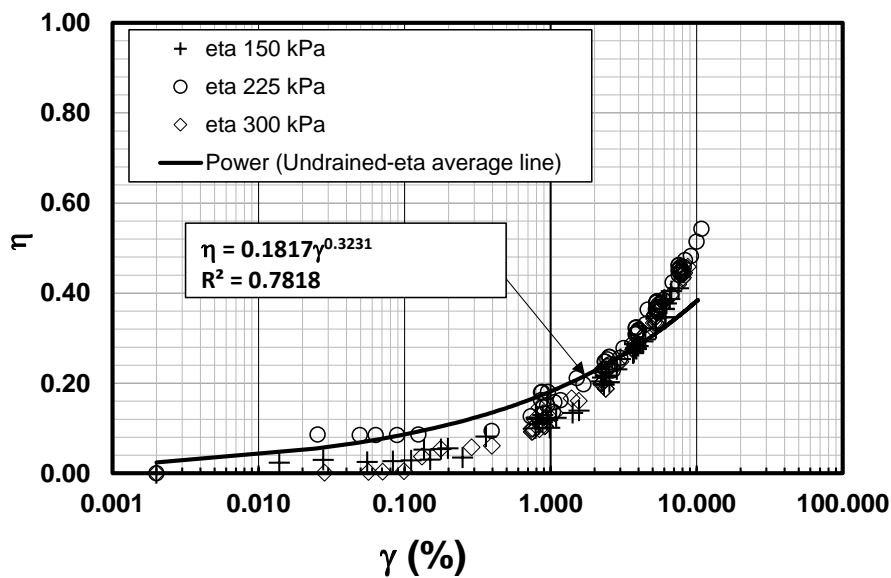


Figure 4.36 Relationship between η and various shear strain of undrained tests

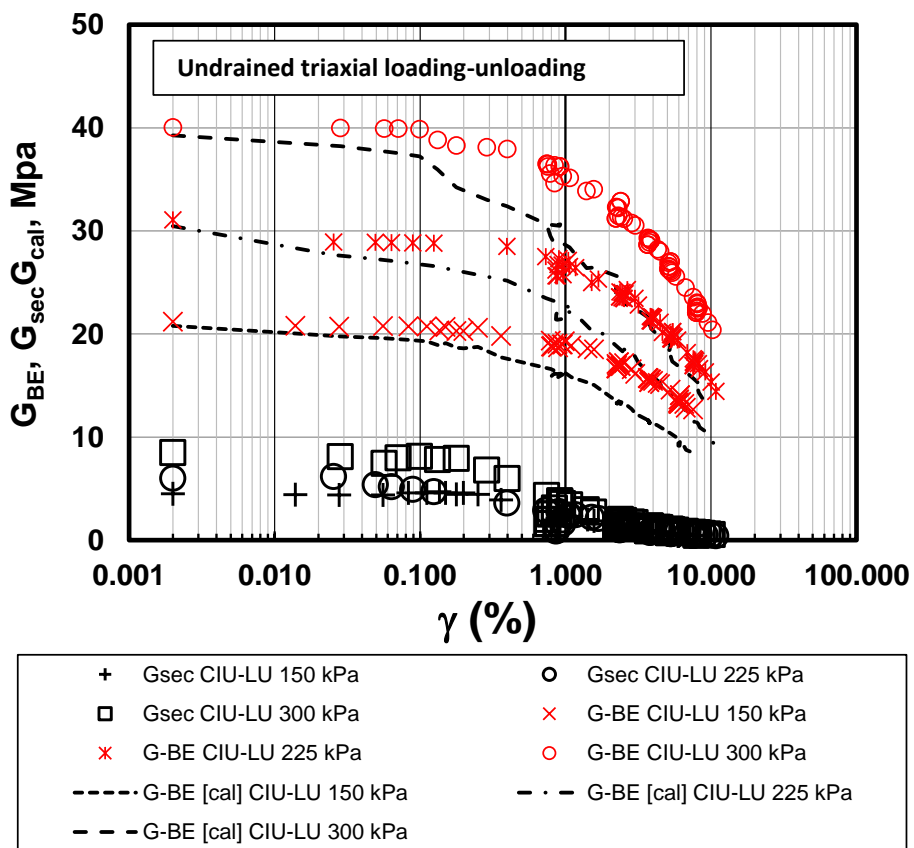


Figure 4.37 Comparison between G_{BE} , G_{sec} and G_{cal} various shear strain of undrained tests

4.4.2 Drained G-bender element with G-secant

According to the degradation curve of both G_{sec} and G_{BE} under drained monotonic triaxial loading test and drained small loading-unloading tests with bender element measurement is represented in Figure 4.38 and Figure 4.40. The results indicated that is more variation between G_{sec} and G_{BE} along the path during shearing specimens. To predict G_{BE} in drained condition, the $\eta_{drained-mono}$ strain function and the $\eta_{drained-LU}$ strain function as various confining computed by equation (4.31) and equation (4.24), respectively. The paths between $\eta_{drained-mono}$ and $\eta_{drained-LU}$ with various shear strain γ at function as various confining pressure 150 kPa, 225 kPa, and 300 kPa are plotted in Figure 4.39 and Figure 4.42. The strain function from the curve fitting under drained monotonic triaxial tests and drained small loading-unloading triaxial tests are

$$\eta_{drained-mono} = 0.0147\gamma + 0.0469 \quad (4.31)$$

$$\eta_{drained-LU} = 0.0186\gamma + 0.0490 \quad (4.32)$$

Consequently, when $G_{BE-drained}$ prediction function is need. The $G_{BE-drained}$ condition can be replaced $\eta_{drained}$ to given new $G_{BE-drained}$ function. The new equation can be rewritten as follows:

$$G_{BE-drained\ mono} = [1-(0.0147\gamma + 0.0469)]G_{int, BE} + [0.0147\gamma + 0.0469]G_{sec} \quad (4.33)$$

whereas

$$G_{BE-drained\ LU} = [1-(0.0186\gamma + 0.0490)]G_{int, BE} + [0.0186\gamma + 0.0490]G_{sec} \quad (4.34)$$

The $G_{BE-drained\ mono}$ under monotonic drained tests determined from equation (4.33) among various γ in Figure 4.40 as confining pressure of 150 kPa, 225 kPa, and 300 kPa were presented. The results showed that at strain $0.001 \leq \gamma \leq 1$, a small

variation of $G_{BE\text{-drained}}$ under monotonic calculation were illustrated. At $\gamma > 1$, $G_{BE\text{-drained}}$ obtained based on calculation with various confining pressure is more variation. Consequently, the new equation to predict G_{BE} under drained condition is applicable to predict $G_{BE\text{-drained}}$ under conventional triaxial tests.

Similarly, the results from these studies of $G_{BE\text{-drained-LU}}$ under drained small loading-unloading tests determined from equation (4.34) among various γ in Figure 4.43 as confining pressure of 150 kPa, 225 kPa, and 300 kPa were illustrated. The results indicated that at strain $0.001 \leq \gamma \leq 1$, a small variation of $G_{BE\text{-drained-LU}}$ under drained small loading-unloading calculation were illustrated. At $\gamma > 1$, $G_{BE\text{-drained}}$ obtained based on calculation with various confining pressure is more variation. In conclusion, a simplified function was proposed to help predict the $G_{BE\text{-drained-LU}}$, which also helped to solve geotechnical problems.

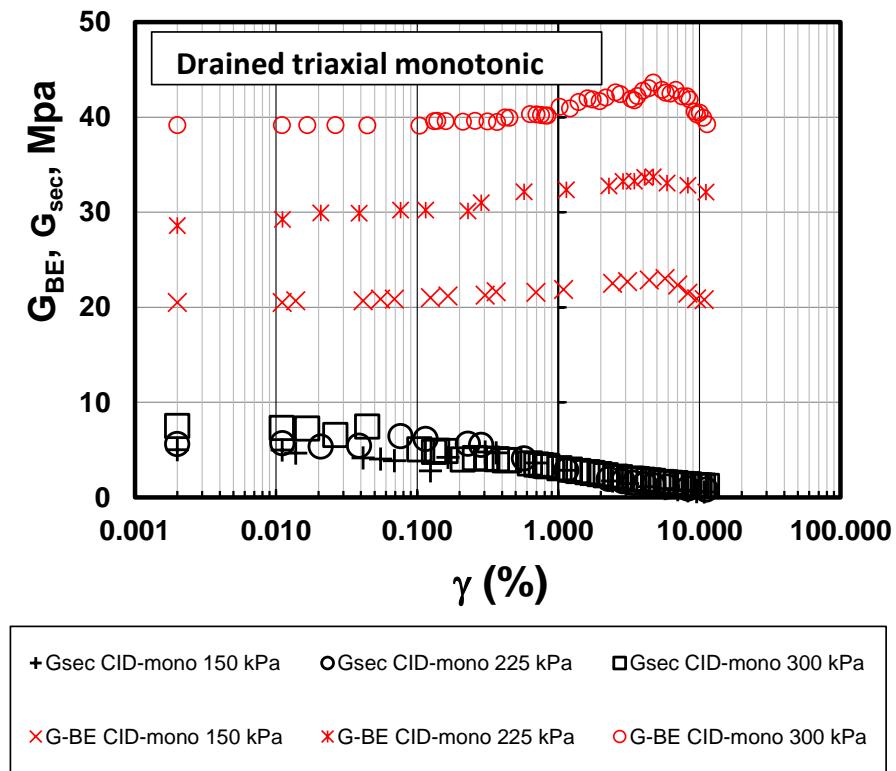


Figure 4.38 Comparison between G_{BE} and G_{sec} various shear strain of drained tests

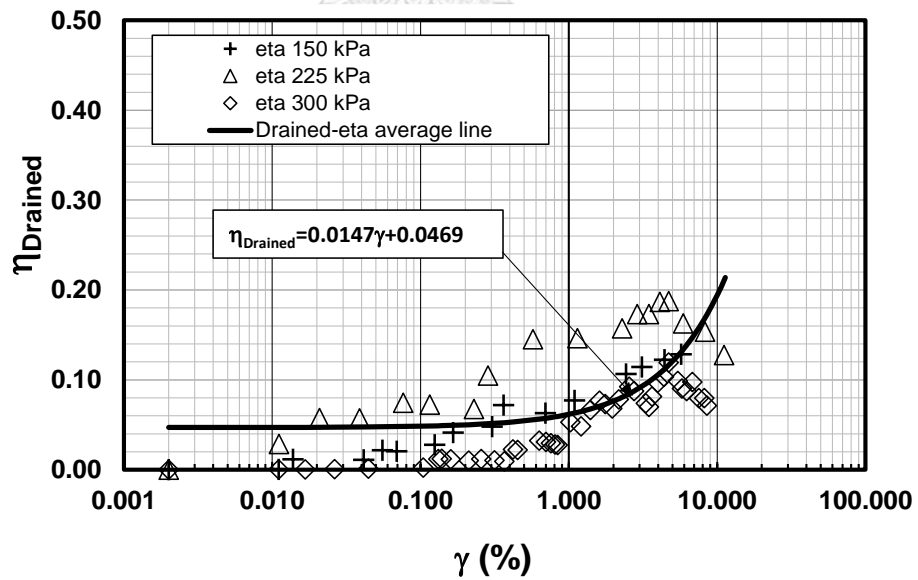


Figure 4.39 Relationship between η and various shear strain of drained monotonic tests.

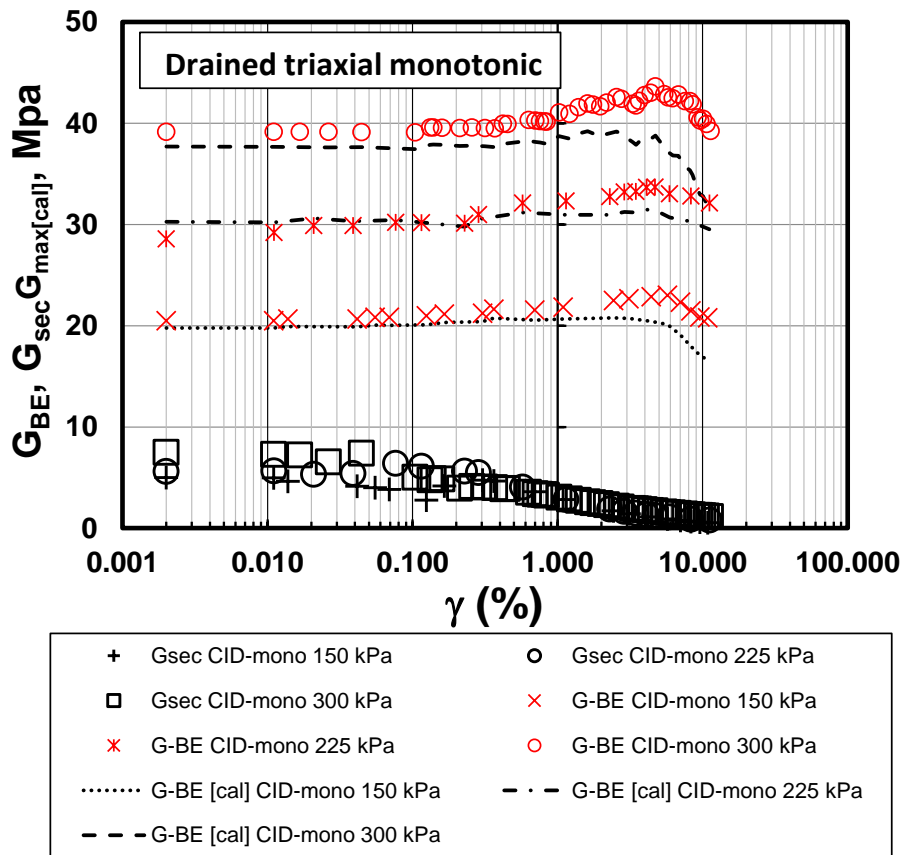


Figure 4.40 Comparison between G_{BE} , G_{sec} and G_{cal} various shear strain of drained tests

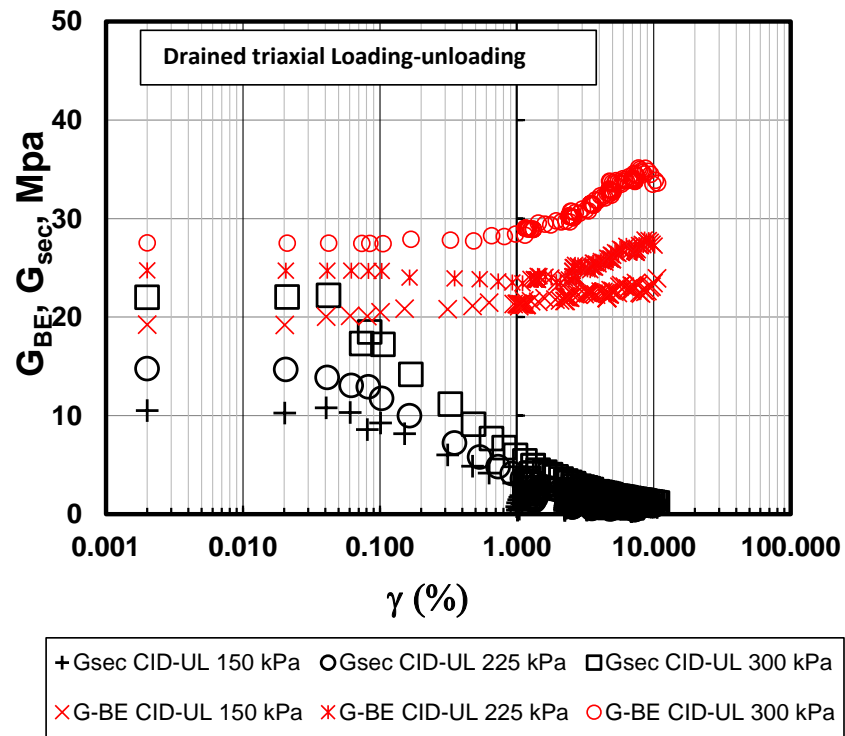


Figure 4.41 Comparison between G_{BE} and G_{sec} various shear strain of drained loading- Unloading tests.

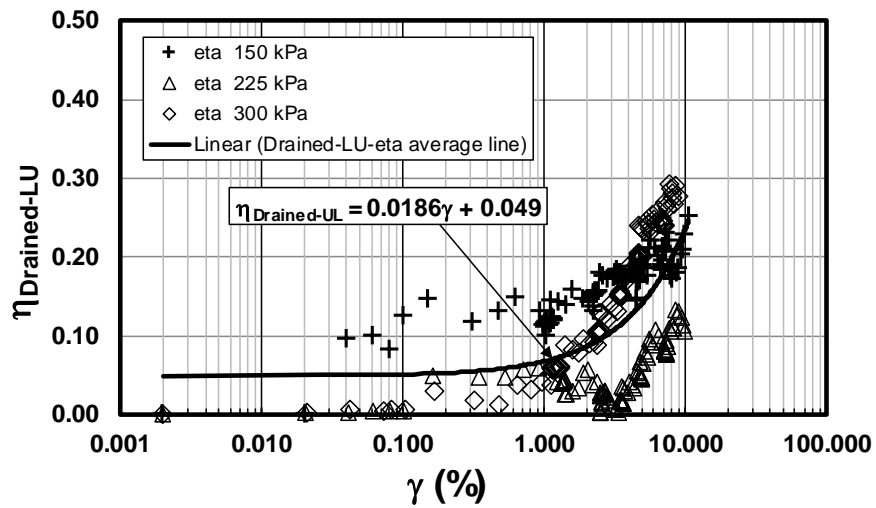


Figure 4.42 Relationship between η and various shear strain of loading- Unloading tests.

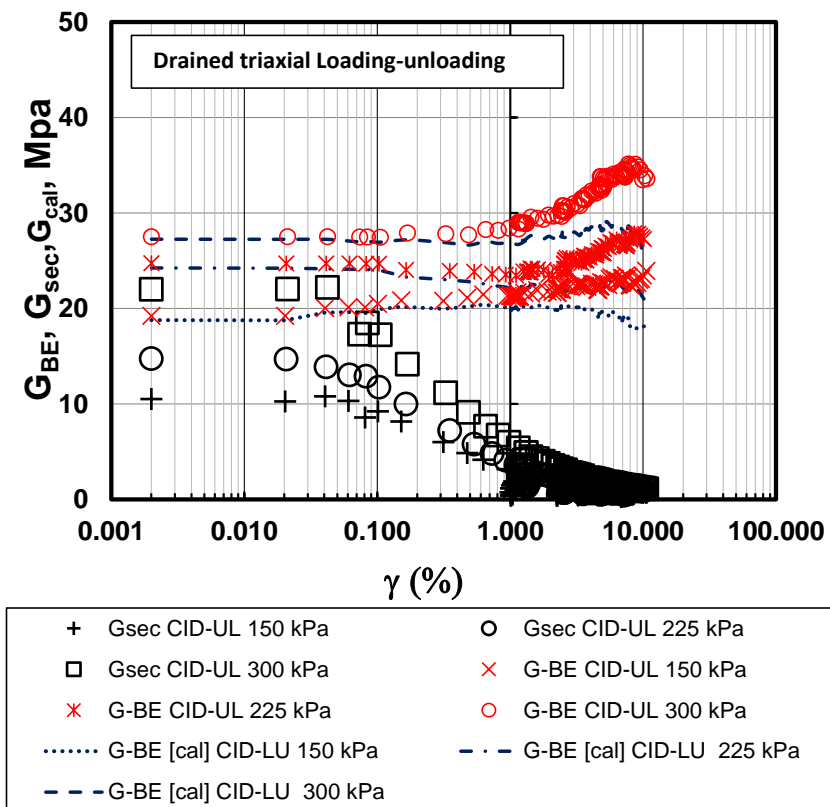


Figure 4.43 Comparison between G_{BE} , G_{sec} and G_{cal} various shear strain of drained loading- Unloading tests.

4.5 Relationship between G-Bender undrained and G-Bender drained

The correlation between G_{BE} in drained triaxial testing and G_{BE} drained monotonic tests (CID-mono) computed as shown in Figure 4.44. When considering the variation of elastic shear modulus G_{BE} bender element measurement with elastic shear modulus G_{BE} calculation as various same confining pressure 150 kPa, 225 kPa and 300 kPa, the results indicated that variation of the elastic shear modulus G_{BE} at shear strain at 0.001-1% was very small while the shear strain more than 1%, the variation elastic shear modulus G_{BE} measurement from bender element compared with G_{max} calculation was more variation. It may due to the clay soil sample change from elastic state to elastoplastic state.

The method to obtain G_{max-BE} drained monotonic condition from the triaxial undrained test was proposed by using the strain function of the ratio between G drained bender elements and G undrained bender element for both conditions. The scatter of the data of strain function of ratio between G drained bender elements and G undrained bender element various shear strain, γ during shearing was almost linear. The author processes that ratio between G drained bender element and G undrained bender element against shear strain, γ can be plotted to give a linear best-fitted function as following:

$$G_{max-drained}/G_{max-undrained} = 0.1207\gamma + 1.1014 \quad (4.35)$$

To determined $G_{BE-drained}$ can be calculated from the function Equation (4.27). $G_{BE-drained}$ of clay related to $G_{BE-undrained}$. When $G_{BE-drained}$ plotted with shear strain, γ , the results provided a similar trend. The predicting G_{BE} various confining pressure 150 kPa 225 kPa and 300 kPa was given the same paths in a range of small level when compared with drained triaxial test at the small strain level. It is implied that the correlation method can be used for approximation of the $G_{BE-drained}$ condition when η function and G_{BE} undrained triaxial tests were known.

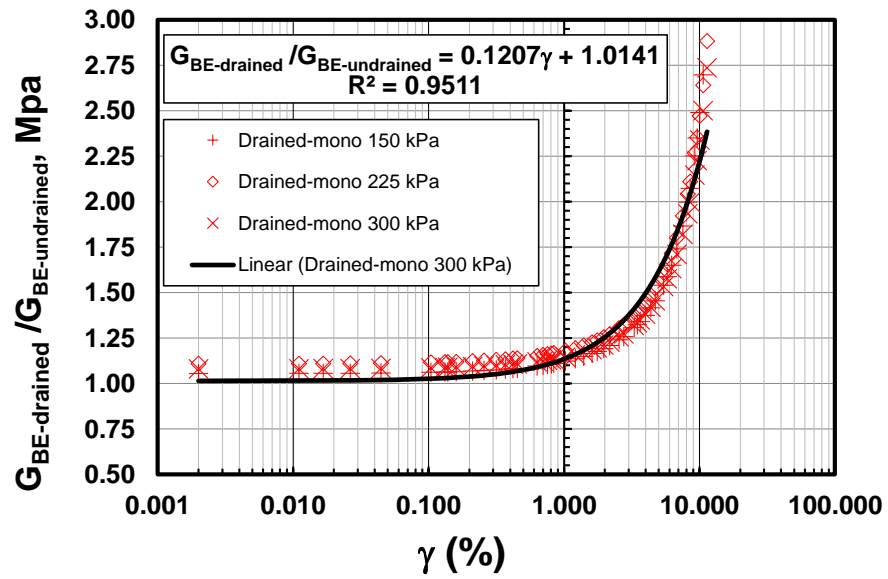


Figure 4.44 The relationship of ratio between G_{BE} drained and G_{BE} undrained various shear strain



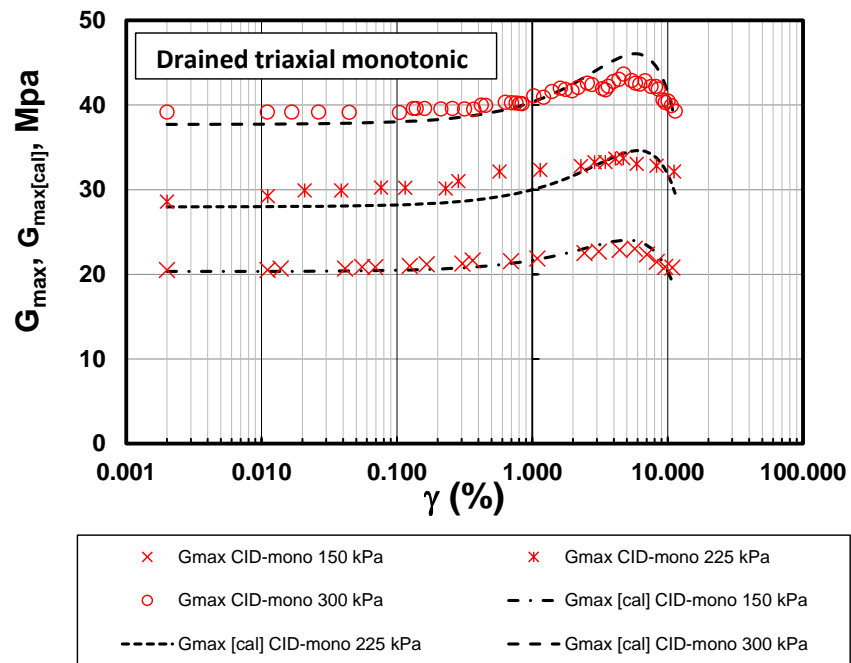


Figure 4.45 Comparison between G_{max-BE} and $G_{max-cal}$ various shear strain of drained tests.



4.6 Application of proposed methodology in calibrating shear modulus undrained condition into the drained condition

This section presents an application of the proposed methodology in calibrating shear modulus undrained conditions into drained conditions. According to Kok-hooi C. and Boonyatee, 2007, the G_{\max} bender element measured under undrained triaxial test can be computed by using the value of G_{secant} with various shear strain. The strain function equation (4.27) from previous studied was adopted to develop the new strain function under the average three confining pressure of 150, 225 and 300 kPa respectively. The new G_{\max} measured from bender element of undrained condition tests for determining the G_{\max} bender element without bender element measurement system in equation (4.30) was proposed.

For example, the shear modulus under drained condition with $\gamma=0.01$ percent shears strain was required to design the retaining wall. The effective confining pressure $p'400$ kPa and $E_{\text{sec}} = 36$ MPa from undrained triaxial test at $\gamma=0.01$ were employed to elaborate calibrating shear modulus undrained condition into drained condition procedures. The determination of G_{sec} at $\gamma=0.01$ can be calculated from $E_u/3$, while G_{sec} at $\gamma=0.01$ was given by input the value of effective confining pressure in equation (4.30) Thus, The G_{\max} bender element drained from undrained triaxial laboratory test can be calculated as:

- (a) Determined G_{sec} at $\gamma = 0.01$ percent from undrained triaxial test data.

When E_{sec} at $\gamma = 0.01$ is equal to 36 Mpa

$$\begin{aligned} G_{\text{sec}} &= E_u/3 && \text{MPa} \\ &= 36/3 && \text{MPa} \\ &= 12 && \text{MPa} \end{aligned}$$

(b) Determined $G_{int, BE}$ from empirical equation (4.17)

effective confining pressure $p' = 400$ kPa

$$G_{max} = 0.451p'^{0.78} \quad \text{MPa}$$

$$G_{max} \text{ or } G_{int, BE} = 0.451(400)^{0.78} \quad \text{MPa}$$

$$= 44.43 \quad \text{MPa}$$

(c) Determined G_{BE} from empirical equation (4.30)

$$\begin{aligned} G_{BE-undrained} &= (1-0.1817\gamma^{0.32})G_{int, BE} + 0.1817\gamma^{0.32}G_{sec} \\ &= (1-0.1817(0.01)^{0.32})(44.43) + 0.1817(0.01)^{0.32}(12) \\ &= 39.03 \quad \text{MPa} \end{aligned}$$

(d) Determined G_{BE} drained condition using empirical equation (4.35)

$$\begin{aligned} G_{max-drained}/G_{max-undrained} &= 0.1207\gamma + 1.1014 \\ G_{max-drained} &= G_{max-undrained} [0.1207\gamma + 1.1014] \\ &= 39.03 [0.1207(0.01) + 1.1014] \\ &= 43.03 \quad \text{MP} \end{aligned}$$

CHAPTER V

CONCLUSIONS AND RECOMMENDATIONS

5.1 Conclusions

The characteristics of shear wave velocity, V_s and also elastic shear modulus, G_{max} of clayed soil with various stress paths by using bender element technique were investigated in multiple conditions from triaxial testing of clay, i.e. triaxial undrained Load-unload test (CIU-LU), monotonic drained triaxial compression test (CID-mono), drain triaxial Load-unload test (CID-LU), triaxial stress control test (CIDS), drained triaxial extension (CIDE), and undrained triaxial extension (CIDE). The essential results of this research are as follow;

- (a) The characteristics of shear wave velocity and elastic shear modulus along with the whole paths of drained and undrained triaxial conditions revealed that the shear wave velocity and elastic shear modulus were dependent on the stress-strain state together with the change of void ratio. The mean effective stress was found to be more favorable to identify the entire paths of shear wave velocity and elastic shear modulus.
- (b) According to test results of CIU, CID, CIDS, CIUE and CIDE, an empirical equation, $G = \rho 1.29 p^{1.3}$ or $G = F(e) 12.42 p^{0.44}$ are applicable to predict the shear wave velocity paths and elastic shear modulus of clay at small strain to large strain levels. Note that the axial strain 0-10 % is appropriated.
- (c) The variation of shear wave velocity and elastic shear modulus under loading-unloading conditions are small variables. Since the state of specimens along path of testing is elastic state.
- (d) For undrained triaxial test and drained triaxial test, G_{max} -bender element can be computed through G-secant data from convention triaxial test without bender element system. Besides, a similar methodology to identify G-bender element and G-secant under undrained isotropic

consolidation triaxial test and drained isotropic consolidation triaxial test was proposed.



- (e) The G drained-bender element can be computed by G-Bender from undrained triaxial test. A small strain level ($0.001 \leq \gamma \leq 0.1$), the G_{\max} drained-bender element correlated from undrained triaxial tests had highly accuracy.

5.2. Recommendations

- (a) It is recommended to identify shear wave velocity, V_s and elastic shear modulus of clayed soil with various stress path might be investigated in anisotropic consolidation.
- (b) Due to the restrain of bender elements from the epoxy coating, install method, and soil stiffness, a future researcher should select the self-monitoring circuit method to install a couple of bender elements.
- (c) The travel time from a pair of bender elements should select an appropriate, method to determine the travel time between transmitting and receiving bender elements.

REFERENCES

- Bartake, P., Patel, A., & Singh, D. (2008). Instrumentation for bender element testing of soils. *International Journal of Geotechnical Engineering*, 2(4), 395-405.
- Brignoli, E. G., Gotti, M., & Stokoe, K. H. (1996). Measurement of shear waves in laboratory specimens by means of piezoelectric transducers. *Geotechnical Testing Journal*, 19(4), 384-397.
- Bui, M. T., Clayton, C., & Priest, J. A. (2010). The universal void ratio function for small strain shear modulus.
- Chan, K.-H. (2007). DETERMINATION OF STRAIN DEPENDENCY OF SHEAR MODULUS OF SOFT CLAYS USING BENDER ELEMENT. *A Dissertation for the Degree of Doctor of Philosophy Program in Civil Engineering Chulalongkorn University, Thailand.*
- Chuan Gu, e. (2012). Effects of loading history on small-strain shear modulus of saturated clays. *Chinese Journal of Geotechnical Engineering*, 34(9), 1654-1660.
- Dano, C., Hareb, H., & Hicher, P.-Y. (2003). *Characterization of Loire river sand in the small strain domain using new bender-extender elements.*
- Dano, C., & Hicher, P.-Y. (2002). *Evolution of elastic shear modulus in granular materials along isotropic and deviatoric stress paths.*
- Dyvik, R., & Madshus, C. (1985). *Lab Measurements of G_m vs σ_v Using Bender Elements.* Paper presented at the Advances in the art of testing soils under cyclic conditions.
- Escribano, D., & Nash, D. (2015). Changing anisotropy of G_0 in Hostun sand during drained monotonic and cyclic loading. *Soils and Foundations*, 55(5), 974-984.
- Flores-Guzmán, M., Ovando-Shelley, E., & Valle-Molina, C. (2014). Small-strain dynamic characterization of clayey soil from the Texcoco Lake, Mexico. *Soil Dynamics and Earthquake Engineering*, 63, 1-7.
- Hardin, B. O., & Black, W. L. (1968). Vibration modulus of normally consolidated clay. *Journal of Soil Mechanics & Foundations Div.*
- Hardin, B. O., & Richart Jr, F. (1963). Elastic wave velocities in granular soils. *Journal of Soil Mechanics & Foundations Div*, 89(Proc. Paper 3407).

- Ishihara, K. (1996). Soil Behaviour in Earthquake Geotechnics. *Oxford Engineering Science Series (Book 46)*, 360.
- Iwasaki, T., & Tatsuoka, F. (1977). Effects of grain size and grading on dynamic shear moduli of sands. *Soils and Foundations*, 17(3), 19-35.
- Iwasaki, T. T., F. and Takagi, Y. (1978). Shear moduli of sands under cyclic torsional shear loading. *Soils and Foundations*, 17(3), 19-35.
- Jamiolkowski, M., Lancellotta, R., & Lo Presti, D. (1995). Remarks on the stiffness at small strains of six Italian clays. *Pre-failure deformation of geomaterials*, 2, 817-836.
- Jovicic, V., Coop, M.R., and Sicmic, M. (1996). Objective criteria for determining G_{max} from bender element tests. *Géotechnique*, 46, 357-367.
- Ku, T., & Mayne, P. W. (2015). Directional properties of small strain shear stiffness in soils. *Geomechanics and Geoengineering*, 10(1), 68-81.
- Kumar, J., & Madhusudhan, B. (2010). Effect of relative density and confining pressure on Poisson ratio from bender and extender elements tests. *Géotechnique*, 60(7), 561-567.
- Lee, J.-S., & Santamarina, J. C. (2005). Bender elements: performance and signal interpretation. *Journal of geotechnical and geoenvironmental engineering*, 131(9), 1063-1070.
- Leong, E. C., Yeo, S. H., & Rahardjo, H. (2005). Measuring shear wave velocity using bender elements. *Geotechnical Testing Journal*, 28(5), 488-498.
- Lings, M., & Greening, P. (2001). A novel bender/extender element for soil testing. *Géotechnique*, 51(8), 713-717.
- Mitchell, J. K., & Soga, K. (2005). *Fundamentals of soil behavior* (Vol. 3): John Wiley & Sons New York.
- Oh, T.-M., Bang, E.-S., Cho, G.-C., & Park, E.-S. (2017). Estimation of undrained shear strength for saturated clay using shear wave velocity. *Marine Georesources & Geotechnology*, 35(2), 236-244.
- Patel, A., & Singh, D. (2009). A generalized relationship for estimating shear wave velocity in soils. *International Journal of Geotechnical Engineering*, 3(3), 343-351.

- Ratananikom, W., Likitlersuang, S., & Yimsiri, S. (2013). An investigation of anisotropic elastic parameters of Bangkok Clay from vertical and horizontal cut specimens. *Geomechanics and Geoengineering*, 8(1), 15-27.
- Roesler, S. K. (1979). Anisotropic shear modulus due to stress anisotropy. *Journal of the Geotechnical Engineering Division*, 105(7), 871-880.
- Santamarina, J. C., Klein, K., & Fam, M. (2001). Soils and Waves: Particulate Materials Behaviour, Characterisation and Process Monitoring. In: Chichester: John Wiley & Sons.
- Senetakis, K., Anastasiadis, A., & Ptilakis, K. (2012). The small-strain shear modulus and damping ratio of quartz and volcanic sands. *Geotechnical Testing Journal*, 35(6), 964-980.
- Shirley, D. J., & Hampton, L. D. (1978). Shear-wave measurements in laboratory sediments. *The Journal of the Acoustical Society of America*, 63(2), 607-613.
- Teachavorasinskun, S., & Akkarakun, T. (2004). Paths of elastic shear modulus of clays. *Géotechnique*, 54(5), 331-333.
- Teachavorasinskun, S., & Amornwithayalax, T. (2002). Elastic shear modulus of Bangkok clay during undrained triaxial compression. *Géotechnique*, 52(7), 537-540.
- Teachavorasinskun, S., & Pongvithayapanu, P. (2016). Shear wave velocity of sands subject to large strain triaxial loading. *Geomechanics and Engineering*, 11(5), 713-723.
- Teachavorasinskun, S., Thongchim, P., & Lukkunaprasit, P. (2002). Shear modulus and damping of soft Bangkok clays. *Canadian Geotechnical Journal*, 39(5), 1201-1208.
- Thakur, V. (2007). Strain localization in sensitive soft clays. *NTNU, Trondheim*.
- V. SIVAKUMAR, P. M., J. ZAINI, and P. CAIRNS. (2010). Effectiveness of filters in reducing consolidation time in routine laboratory testing. *Géotechnique*, 60 Issue 12, 949-956.
- Viggiani, G., & Atkinson, J. (1995). Stiffness of fine-grained soil at very small strains. *Géotechnique*, 45(2), 249-265.
- Yu, P., & Richart Jr, F. (1984). Stress ratio effects on shear modulus of dry sands. *Journal*

of Geotechnical Engineering, 110(3), 331-345.





จุฬาลงกรณ์มหาวิทยาลัย
CHULALONGKORN UNIVERSITY

VITA

NAME Sirichai Pethrung

DATE OF BIRTH 11 May 1985

PLACE OF BIRTH Suratthani Province

INSTITUTIONS ATTENDED 1.B.eng, Kasetsart University Kamphaeng saen campus in 2009
2.M.eng Chulalongkorn University in 2011

HOME ADDRESS 50 Moo 4, chaiya,
Suratthani 84110, Thailand

